Microscopic Simulation Model for Mixed Traffic of Connected Automated Vehicles and Conventional Vehicles on Freeways

By

Punyaanek Srisurin
M.S., University of Hawaii at Manoa, 2013
B.Eng., Chulalongkorn University, 2010

Submitted to the graduate degree program in Civil Engineering and the Graduate Faculty of the University of Kansas in partial fulfillment of the requirements for the degree of Doctor of Philosophy.

_____

Chair: Dr. Alexandra Kondyli

_____

Dr. Huazhen Fang

_____

Dr. Thomas E. Mulinazzi

_____

Dr. Steven D. Schrock

_____

Dr. Dan Tran

Date Defended: 28 July 2020

The dissertation committee for Punyaanek Srisurin certifies that this is the approved version of the following dissertation:

Microscopic Simulation Model for Mixed Traffic of Connected Automated Vehicles and Conventional Vehicles on Freeways

Chair: Dr. Alexandra Kondyli

Date Approved: 10 August 2020

ABSTRACT

This study developed mixed-traffic simulation models of connected automated vehicles (CAVs) and manually-driven vehicles (MDVs) at the full-spectrum of mixed penetration rates on a freeway segment by incorporating the car-following and lane-changing models via a conditional linkage to investigate the sensitivities in highway capacity and travel time. The car-following models for CAVs and MDVs were modified from the full-velocity difference (FVD) car-following model, while the lane-changing logic was adopted to regulate the lane-changing decisions for both CAVs and MDVs. The desired speeds of each MDVs were determined on the basis of stochasticity to represent various desired speeds taken by human drivers, while the uniform desired speed was employed for CAVs. The stochastic gap acceptance was applied for MDVs to replicate the stochasticity of the gaps accepted by human drivers, whereas the static gap acceptance was adopted to establish the safe decision-making thresholds for CAVs prior to performing lane changes. Two algorithms were proposed separately for governing the movements of CAVs and MDVs in the traffic simulation models. The proposed algorithms, along with a 3-to-2 virtual freeway lane drop, were coded in JAVA to develop a simulation platform, prior to calibrating the default model with field data. Eleven mixed traffic scenarios were simulated in the developed platform, along with parallel simulation in VISSIM, to generate and validate the resultant speed-flow diagrams.

The results were then analyzed and compared to determine the changes in highway capacity and travel time with respect to the variations in CAV penetration rate. The resultant vehicular trajectories in the scenarios of interest were also analyzed to perceive the impact of CAVs on the trajectories and speeds of the interacting vehicles in traffic. The results showed increase in capacities in the range of 25.9 – 26.9 percent, while travel time decreased by up to 55.4 percent, as the CAV penetration rate shifted from 0 to 100 percent. The trajectory analysis indicated that CAVs have an influence on guiding the smoother speed and acceleration rates of MDVs while an MDV is following a CAV. The results suggest that although headways increased with increasing CAV penetration rate, capacity also increased; however, there should be an optimal headway that maximizes the capacity.

ACKNOWLEDGEMENTS

I would like to express my gratitude and appreciation to my doctoral advisor, Professor Alexandra Kondyli, for her indispensable supervision and support throughout my doctoral work. Her insightful critiques and suggestions were always delivered with experience and wit, which greatly influenced the direction of this work. Without her excellent guidance, this dissertation would never be accomplished.

I am very grateful for having a splendid advisory committee and wish to thank Professor Steven D. Schrock, Professor Thomas E. Mulinazzi, Professor Dan Tran, and Professor Huazhen Fang for reviewing this dissertation and providing helpful comments, which led to a great improvement in this dissertation.

I would like to express my deepest appreciation to my parents, Wasunt Srisurin and Jarunee Srisurin, for their unconditional love and encouragements. I am very grateful to them for providing me an opportunity to pursue a doctoral degree with their own savings. Without their love, supports, and faith; my education here would never have been possible. I am also grateful to my grandmother, Nalinee Srisurin, and my younger sister, Piyaporn Srisurin, whose supports and encouragements always helped me get through my hard times. I would also like to thank all my friends; especially Walaipan, Pornlert, and Jack, for their friendships and supports as always.

Last but not least, I would like to dedicate this dissertation to my deceased beloved paternal grandparents who brought me up with love and great patience – Suthep Srisurin (1930 – 2008) and Nalinee Srisurin (1934 – 2019), who had been waiting in hope for this day to come until the last breaths of their lives. I would also like to dedicate this work to my deceased lovely maternal grandparents, Sanya Visarat (1936 – 2010) and Somjai Visarat (1938 – 2015), for their love and kindnesses.

"Gone yet not forgotten. Although we are apart, your spirits live within me, forever in my heart."

Punyaanek Srisurin

TABLE OF CONTENTS

LIST OF FIGURES

LIST OF TABLES

CHAPTER 1 INTRODUCTION

1.1 Background

Connected Automated Vehicles (CAVs) are an emerging technology which is speculated to supersede the human-driven vehicle technologies on the roadways in the near future. They are expected to improve the efficiency and capacity of the roadways, reduce non-productive vehicle-occupancy time that passengers need to spend traveling in vehicles, as well as enhance traffic safety (Naumann et al., 1998; Zhao and Sun, 2013; Le Vine et al, 2015; Lefèvre et al., 2015). So far, twenty-nine states and Washington D.C. have already enacted legislations related to automated vehicles to prepare for this upcoming change (National Conference of State Legislature, 2019). However, it is still uncertain when exactly CAVs will penetrate the roadways and to what extent they will improve traffic operations since this type of vehicle has neither fully developed nor physically been implemented on roadways in real life yet.

There are two major technologies in vehicles: automation and connectivity. Automated vehicles (AVs) operate using on-board sensors and have at least one aspect of a safety-critical control function performed without direct driver input required (Schubert et al., 2010; Luettel et al., 2012; Zhao and Sun, 2013; Talebpour and Mahmassani, 2016). Vehicles are classified by the Society of Automobile Engineers (SAE) into six levels of automated driving, based on the degree of automation. Vehicles categorized at levels 0-2 require full or partial monitoring from human driver, whereas vehicles at levels 3-5 apply automated driving system to monitor the driving environment (SAE, 2014). In addition, vehicles at levels 0-3 require a licensed driver to be present in the vehicle; while levels 4 and 5 allow for a completely driverless operation (Litman, 2018). Level 2 automated vehicles employ adaptive cruise control (ACC) system, which enables automatic car-following in the longitudinal direction to enhance comfort and safety for drivers (Ioannou and Stefanovic, 2005).

Connected vehicles (CVs) use wireless connection systems to communicate with other vehicles and the roadside infrastructure (USDOT, 2019). Based on the type of connectivity, CVs are often classified into three types: vehicle-to-vehicle (V2V), vehicle-to-infrastructure (V2I), and

vehicle-to-everything (V2X) (Dimitrakopoulos, 2011; UK Department for Transport, 2016; Patel et al., 2017). CV technology is expected to improve driver efficiency and response, along with enhanced safety and mobility, by providing real-time information on traffic conditions and the decisions from traffic management centers (Dimitrakopoulos, 2011; Tientrakool et al., 2011; Knorr and Schreckenberg, 2012; Tang et al., 2014; Xie et al., 2014; Talebpour et al., 2015; Talebpour and Mahmassani, 2016).

Vehicles that function with both of these aspects are called automated and connected vehicles (CAVs). Vehicles that do not include any of these two functions are referred to as Manually-Driven Vehicle (MDV) (Li et al., 2015; Patel et al., 2017). CAV technology is expected to maximize the capability of vehicles to safely operate in all traffic conditions, roadway geometry, and weather conditions (UK Department for Transport, 2016). In addition, CAV technology is speculated to improve the efficiency and mobility of the connected vehicles to a greater extent since these vehicles can fully operate without drivers, as well as improve traffic safety and increase capacity of highways (Fernandes and Nunes, 2010; Milanes et al., 2011; Gong et al., 2016; Li et al., 2016; Talebpour and Mahmassani, 2016; Zhang et al., 2016; Rios-Torres and Malikopoulos, 2017). An example of CAV technology is cooperative adaptive cruise control (CACC), which is adaptive cruise control (ACC) equipped with V2X communication (Zhao and Sun, 2013; Gong et al., 2016; Patel et al., 2017; Ramezani et al., 2017).

Various levels of mixture between AVs and MDVs in traffic streams are expected to yield varying performance under different traffic conditions (Michael et al., 1998; Ioannou and Stefanovic, 2005; Tientrakool et al., 2011; Knorr and Schreckenberg, 2012; Bierstedt, 2014; Bekiaris-Liberis et al., 2016; Levin and Boyles, 2016; Shi and Prevedouros, 2016; Talebpour and Mahmassani, 2016; UK Department for Transport, 2016; Wang et al., 2016; Chen et al., 2017; Fountoulakis et al., 2017; Ghiasi et al., 2017; Ramezani et al., 2017; Shi and Prevedouros, 2017). In addition, AVs are expected to have different car-following characteristics from MDVs. Various combinations of different types of leading and following vehicles could produce different car-following and platooning characteristics that affect highway capacity (Fernandes and Nunes, 2010; Knorr and Schreckenberg, 2012; Zhao and Sun, 2013; Tang et al., 2014; Li et al., 2016; Wang et al., 2016; Chen et al., 2017; Fountoulakis et al., 2017; Ghiasi et al., 2017; Ramezani et al., 2017). Lane-changing maneuvers also play an important role in highway capacity. Lane-changing

behavior and frequency were found to contribute to capacity drop, traffic congestion, and collisions between vehicles (Lv et al., 2013; Xie et al., 2014; Talebpour et al., 2015; You et al., 2015). Lane-changing characteristics in mixed-traffic streams could lead to complex scenarios that produce different levels of impact on the highway capacity due to complex interactions between different types of vehicles. AVs are expected to operate with shorter headways than MDVs and, therefore, increase highway capacity (Bose and Ioannou, 2003; Fernandes and Nunes, 2010; Zhao and Sun, 2013; Levin and Boyles, 2016; Shi and Prevedouros, 2016; Ramezani et al., 2017; Rios-Torres and Malikopoulos, 2017; Shi and Prevedouros, 2017). However, recent studies rebutted that higher CAV penetration rates and platooning intensities do not necessarily lead to greater mixed traffic capacity (Chen et al., 2017; Ghiasi et al., 2017). Consequently, further studies are required to address the effects of these four types of vehicles in mixed traffic streams at various penetration rates under different traffic flow conditions, considering both car-following and lane-changing characteristics.

Previous studies predicted that the freeway capacity could be increased by 200 percent as traffic shifted from 100-percent MDVs to 100-percent CAVs (Shi and Prevedouros, 2016; Olia et al., 2018). However, several recent studies suggested more conservative improvements in freeway capacity of 32 – 149 percent when taking into account more practical parameters, such as larger space headways for safety and passenger comfort reasons (Devore, 2019; Fan and Liu, 2019; Morgan et al., 2019). A recent study suggested that the increase in capacity could be translated into shorter space headways, which trades off safety and stress of the passengers for the efficiency of the roadway facilities (Morgan et al., 2019).

Although the possible impacts of CAVs on the driving environment have been investigated by several researchers, most of the models did not distinguish between CVs and AVs in the traffic stream (Talebpour et al., 2016). Furthermore, previous studies focused on automation of the longitudinal driving task; and only a few studies took into account the effects of automated lateral vehicular interactions, such as lane changing and transient maneuvers on human behavior (Hoogendoorn, 2014). In addition, no previous works were found to incorporate both longitudinal and lateral movements of multiple vehicle types simultaneously in a mixed-traffic model (Lv et al., 2013; Wang et al., 2015). Also, as suggested by Ghiasi et al. (2017), most of the studies in capacity analysis were conducted based on assumed deterministic time headways; however, time

headways between consecutive vehicles are greatly stochastic in reality. Finally, although various control lane-changing algorithms were proposed for AVs (Schubert et al., 2010; Xie et al., 2014; Talebpour et al., 2015; Wang et al., 2015; You et al., 2015; Wang et al., 2016; Letter and Elefteriadou, 2017), complex interactions between different vehicle types when performing lane-changing maneuvers have not been investigated.

1.2 Dissertation Objectives

This study aims to develop a realistic simulation model of mixed traffic flow of CAVs and MDVs at various penetration rates on freeways by incorporating both longitudinal and lateral vehicular interactions altogether to investigate the sensitivity in highway capacity. This study also attempts to quantify a relationship between the penetration rates of various types of vehicles in mixed traffic and the corresponding capacity, based on the simulation results. In addition, a prototype of a microscopic traffic simulation platform for freeway traffic scenarios via JAVA is also developed.

CHAPTER 2 LITERATURE REVIEW

The literature review was conducted by compiling the related previous studies to summarize the findings and identify the shortcomings that could be addressed in this work. The explored recent studies were classified into three categories: traffic simulation and modeling, car-following models, and lane-changing models.

2.1 Traffic Simulation and Modeling

2.1.1 Modeling and Simulation of Mixed Traffic

Michael et al. (1998) presented a methodology for quantifying per-lane capacity of an Automated Highway System (AHS), in which both the vehicles and the roadside infrastructure operate with automation, as a function of vehicle capabilities and control system information structure. AHS was assumed to be used by fully AVs only. A single-lane highway segment without entrances and exits was adopted in this study. The authors also assumed that the capacity was constrained by the minimum longitudinal spacing between AVs necessary for safe operation. Two safety criteria were assumed: 1) the following vehicle should be able to stop without colliding with the leading vehicle if maximum braking was applied until it comes to a stop and 2) the relative velocity at initial impact of collision should be small if the leading vehicle applies maximum braking and the following vehicle collides with it. Three vehicle classes were defined based on the level of cooperation for individual vehicles: 1) automated, 2) low cooperation, and 3) high cooperation. A state vector with dynamics was used to capture the car-following characteristics. The longitudinal spacing, which is a function of the vehicle braking capability, operating speed, and control loop delays, was applied to determine the capacity for a given mix of vehicle classes. The effectiveness of four distinct AHS designs was analyzed in terms of their corresponding maximum achievable per-lane capacity. The sensitivity analysis of the capacity was performed with regard to the degree of inter-vehicle cooperation, speed limits, vehicle mix (passenger cars, buses, and trucks), platoon length, lane utilization policies, vehicle braking capability, and dynamic safe-spacing adjustment. The results showed that the highway capacity increases as the level of inter-vehicle cooperation increases or as the platoon length increases. Also, capacity peaks and then drops as highway speed increases. In addition, capacity drops as the vehicle mix loses its

homogeneity or as intra-platoon spacing increases. Finally, the online estimation of the vehicle braking capabilities for adjusting vehicle spacing was found to increase capacity.

Bose and Ioannou (2003) performed macroscopic analysis of mixed traffic flow to examine the resultant fundamental flow–density diagrams and shockwaves via simulation. They assumed that semi-automated vehicles have shorter time headways than the average time headway of conventional vehicles. A linear follow-the-leader human driver model was adopted to model the random characteristics of manually-driven vehicles in a single lane, whereas the responses of semi-automated vehicles were modeled in deterministic fashion due to the use of computerized longitudinal controllers. The authors found that the flow rate increased with the presence of semi-automated vehicles in the traffic stream. In addition, shockwaves were found to be dissipated faster in mixed traffic than in conventional traffic. The authors concluded that semi-automated vehicles can increase the traffic flow rate and traffic density.

Ioannou and Stefanovic (2005) evaluated the effect of ACC to examine microscopic lane changing characteristics and the sensitivity of benefits induced by the ACC technology. Simulation and experimental approaches were applied to perform the evaluation, based on variables such as ACC vehicles penetration rate and level of traffic disturbances. The results disproved the claim that large gap between the ACC vehicle and the leading vehicle created by high-acceleration maneuver generates greater level of disturbances. The authors concluded that the smooth response of the ACC vehicle technology not only has a positive effect on the environment, in terms of fuel consumption and emissions, but the disturbances in traffic flow due to high-acceleration maneuvers, lane cut-ins, and lane exiting are also alleviated. These benefits vary with the levels of the disturbance in a traffic stream, the position of the ACC vehicle in the platoon, and the market penetration of ACC vehicles.

Tientrakool et al. (2011) used an analytical approach to explore whether V2V applications and sensors for collision avoidance increase highway capacity. Their objective was to compare capacity for the cases when vehicles are equipped with sensors and when vehicles are equipped with both sensors and C2V communication. The results indicated that both V2V communication and sensor technologies can increase highway capacity. The authors concluded that capacity increases to a greater degree as the proportion of vehicles equipped with both sensors and V2V

communication increases, whereas the capacity improves linearly as the proportion of vehicles equipped with only sensors increases.

Zhao and Sun (2013) proposed a simulation framework for modeling vehicle platooning and car-following characteristics of a mixed traffic composed of: MDVs, single ACC vehicles, and CACC vehicles or CACC platooning. The aim of this study was to establish a procedure to model a CACC platoon by implementing microscopic platooning maneuvers such as joining, splitting, forming, adjusting, and dismissing maneuvers in VISSIM, which is a standard microscopic traffic simulation platform. The authors assumed that ACC technology produces a more favorable time headway, while CACC technology decreases the perception-reaction time. Wiedemann's driver behavior model was assumed for MDVs. Also, it was assumed that the leader in a CACC platoon commands action sequences that should be simultaneously followed by the following vehicles in the platoon. The algorithm was set such that the leader CACC vehicle in traffic is responsible for forming a platoon and transferring information to the platoon members. Also, a CACC requests to join a platoon by notifying the platoon leader via the nearest member. The leader then responds to the request, recalculates the parameters, and informs the readjusted operation sequences to the platoon members. When a CACC vehicle opts to split from a platoon, it requests to cancel the communication and return to a free-control mode. However, the simulation was done based on an assumption that vehicles, including CACC, do not perform lateral movements in the 2-lane freeway scenario. The microscopic characteristics of the mixed traffic was implemented in VISSIM as a C++ DLL (Dynamic Link Library) plug-in, which works as an External Driver Model (EDM) and interfaces with the VISSIM external driver during the simulation, as illustrated in Figure 2-1. The EDM decides the acceleration/deceleration rates, lane changing maneuvers, and trajectories of automated vehicles based on the x-y axis of the vehicles. The results illustrated that the lane capacity substantially increased as the market penetration rate of CACC vehicles increased. However, the platoon size was found to create little impact on the highway capacity. Automated vehicles were found to require special infrastructure and dedicated lanes since the capacity of a highway could be substantially increased only when the market penetration rates of these types of vehicles is sufficiently high in a traffic stream.

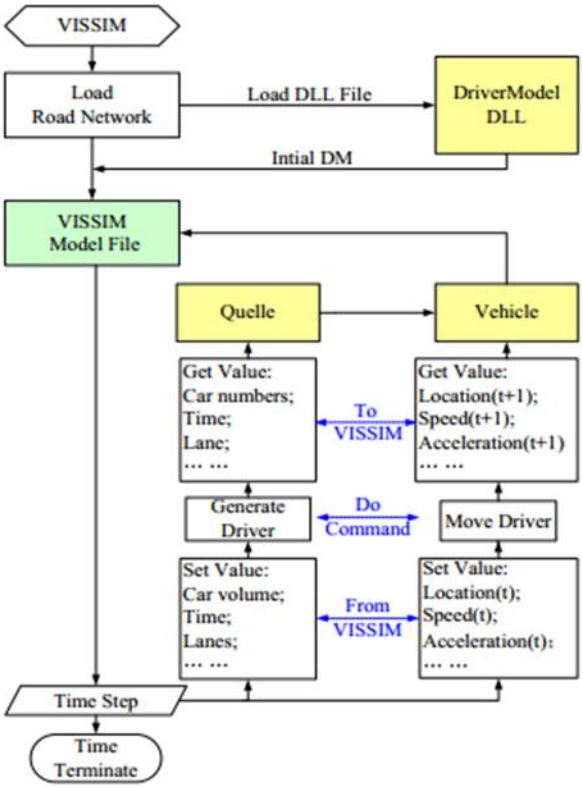

Figure 2-1 The interchanges between DriverModel and VISSIM (Zhao and Sun, 2013)

Bierstedt (2014) investigated the potential effects of AVs on travel demand, highway capacity, and congestion over time. The use of exclusive freeway lanes was speculated by the authors to be implemented in the introductory stage (between 2025 and 2030); followed by the use of mixed freeway lanes and AV-dominated arterials, during 2030-2035 and 2035-2040, respectively. The concept of multimodal streets and intersections was anticipated by the authors by 2040. VISSIM was adopted as a simulation tool to analyze the potential changes in vehicle miles of travel (VMT) and highway capacity. The analysis showed that the roadway capacity substantially increased only on freeways when the fleet mix is at least 75 percent automated. The authors concluded that AVs would either have no impact or degrade highway capacity during the introductory stage since vehicle densities and flow could be reduced as a result of the conservative programming of vehicle speeds and headways to prioritize safety. On the other hand, traffic operational quality could be improved when AVs reach almost full penetration of the fleet and when V2V communication technology is fully developed to negotiate merging and intersection right-of-way. In addition, the VMT is expected to increase as the market penetration of AVs grows.

Hoogendoorn et al. (2014) summarized existing studies on AVs to review the potential influences of automation on traffic flow efficiency and behavior of the drivers and address gaps for future research. Traffic flow efficiency was defined in terms of capacity, capacity drop, and traffic stability. This literature review found that recent studies mainly focused on the longitudinal control; without any considerations to lane changing. Recent studies did not consider behavioral adaptations of the MDVs when interacting with AVs. In terms of driver behavior, it was found that the recent simulation studies predominantly considered the direct adaptation effects, which are the effects in driving behavior caused by the functional specification of the automated vehicles themselves, by assuming smaller headways for AVs than MDVs. It was also found that automation may affect driver behavior by increasing the reaction time due to a reduction in situation awareness and attention.

Levin and Boyles (2016) developed a multiclass cell transmission model (CTM) that allows variations in highway capacity and backward shockwave speed in response to mixed traffic scenarios of MDVs and AVs. The objective of this study was to develop a dynamic traffic assignment (DTA) to minimize delays and travel time for the mixed traffic case. A constant acceleration model was adopted in this study, based on an analytical approach, to predict highway capacity and wave speed as a function of the proportion of each vehicle class in traffic. A collision avoidance car-following model with various reaction times was developed to predict highway capacity and backward shockwave speed for multiclass scenarios. A single intersection and a traffic network in the downtown Austin City, Texas were used as a case study. Two control algorithms were applied to implement the reservation-based controls: 1) movements across the intersection for MDVs require available capacity for all possible turning movements since the communications between vehicles and the intersection controller are not available and 2) space for all possible turning movements must be assured when a space reservation for AVs is accepted. The empirical results indicated that intersection controls were a major bottleneck in the model. The results from the case studies suggested that the use of reservation-based controls decreased the intersection delay linearly with the increase in proportion of AVs; however, the reservation-based controls did not overcome the use of signal control optimization until AV penetration reached 80 percent or greater.

Talebpour and Mahmassani (2016) proposed a framework that employs different models to simulate mixed traffic streams to examine the effects of CAVs in the future driving environment. Three types of vehicles were distinguished: MDVs, CVs, and AVs. Both analytical and simulation-based analyses of the string stability of mixed traffic streams were performed. The results showed that oscillation and collision thresholds increased when the platoon size decreased, or when the market penetration rate increased. In addition, the authors found that the throughput increased as market penetration rates of AVs and CVs increased.

Large scale impacts of CAVs on traffic flow were investigated by the UK Department for Transport (2016) to assess the expected average delay and travel time of the roadway network under various levels of mixed traffic of CAVs and MDVs using VISSIM. The study applied normal car-following behavior for the case when a CAV follows an MDV, whereas a shorter gap was modeled for the case when a CAV follows another CAV. Two traffic settings were adopted for the simulation models: urban road network and strategic road network (SRN). The results indicated that average delay and travel time decreased as the CAV penetration rate increased from the base condition to the upper bound condition. The author concluded that high penetration of CAVs, at least between 50 percent – 75 percent, is required to achieve significant improvement in these performance measures.

Shi and Prevedouros (2016) presented a macroscopic methodology for estimating performance measures for freeways under two types of mixed traffic scenarios: 1) mixed traffic of AVs and MDVs and 2) mixed traffic of CAVs and MDVs, at various market penetration rates. The aim was to propose an analytical assessment for the potential capacity enhancement and LOS improvement based on the Highway Capacity Manual (HCM 2010) methodologies for basic freeway and weaving segments. The study found that the capacity increased by 200 percent as the traffic shifted from 100-percent MDV to 100-percent CAV. The authors concluded that driverless cars would provide low or no impacts on LOS under low density conditions, whereas they might significantly improve LOS under high density conditions. However, market penetration rates of CAV below 2 percent are unlikely to improve performance measures.

Shi and Prevedouros (2017) investigated traffic operations at a single-lane roundabout considering MDVs and AVs considering the HCM 2010 analytical roundabout method. AVs were expected to operate with shorter headways than MDVs at both roundabout entries and within

roundabouts. The adjusted critical and follow-up headways were estimated as the weighted average between the expected headway of MDVs and expected headway of the AVs, based on the proportion of each type of vehicle in the traffic stream. The authors concluded that the presence of AVs might increase capacity of single-lane roundabouts due to the expected improvements in driver familiarity and aggressiveness.

Fountoulakis et al. (2017) developed a microscopic simulation-based methodology for estimating performance measures in mixed traffic scenarios of CVs and MDVs, in which only speed measures stemming from CVs and a limited number of flow measures were employed. The scenarios of various penetration rates of CVs in mixed traffic streams were simulated under both congested and free-flow conditions on a highway stretch that contained a number of on-ramps and off-ramps via AIMSUN. A Kalman filter was applied to estimate the traffic state of the network. Two cases of CV characteristics were simulated: (1) car-following characteristics of CV and MDV are identical and (2) CV has different car-following characteristics from MDV due to ACC. The authors concluded that the ramp flow estimation is more sensitive to the choice of the filter parameters, whereas the density estimation is relatively less sensitive.

Ramezani et al. (2017) investigated traffic flow characteristics and proposed analytical models of mixed AV and MDV traffic on arterials in urban transportation networks. The authors pointed out that the differences between longitudinal driving of AVs and MDVs, along with the complexity of car-following dynamics within various traffic compositions of these two types of vehicles, contribute to the complex resultant performance measures. Four possible headways between two successive vehicles were assumed in this study: MDV-MDV, MDV-AV, AV-MDV, and AV-AV. These four possible headways were used as inputs to estimate the theoretical expected headway of the mixed traffic stream via theoretical and analytical approaches, based on a binomial distribution. Microsimulation data were used to validate the resultant headways. Four scenarios were adopted to analyze the performance measures at a signalized two-lane arterial: 1) mixed lanes, (2) one dedicated lane for each of AVs and MDVs, (3) one mixed lane and one AV lane, and (4) one mixed lane and one MDV lane. The authors suggested that the expected headway of a mixed platoon depends on the relative positions of AV in the platoon. The study speculated that the smallest headway is induced by AV-AV due to CACC technology. The results indicated that

the delays for scenario 2 and scenario 3 are similar at 0 percent AV penetration rate. In addition, delays for scenario 2 and scenario 4 are similar at 100 percent AV penetration rate.

Ghiasi et al. (2017) developed an analytical model to quantify highway capacity for mixed traffic of MDVs and CAVs using a Markov chain to represent the spatial distribution of heterogeneous and stochastic headways. An analytical stochastic formulation for mixed traffic highway capacity was proposed as a function of three critical factors: CAV penetration rate, CAV platooning intensity, and mixed traffic headway settings. The authors pointed out that most of the studies of capacity analysis were conducted based on assumed deterministic time headways in a specific technology scenario; however, time headways between consecutive vehicles are greatly stochastic in reality. This finding cautioned that CAV is not a sole factor to guarantee the increase in highway capacity since it also heavily depends on the assumed headways. Furthermore, the authors also suggested that apart from the market penetration rates, another important factor is the CAV platooning intensities. The impact of different CAV technology scenarios on mixed traffic capacity was also investigated in this analytical model. This model was developed on a one-lane highway segment, without considering lateral movements. The authors concluded that the proposed numerical analysis shed some lights on how the key parameters affect the optimal CAV lane solution and the corresponding optimal capacity.

Chen et al. (2017) proposed an analytical approach to investigate the operational capacity (defined as the maximum sustainable flow) in mixed traffic of AVs and MDVs, under the assumed equilibrium state of traffic. The authors pointed out that the formulation of lane capacity was overly simplified in recent studies since the interaction between platoons and the distribution of AVs across different lanes were not considered. As a result, the proposed capacity formulations considered three factors: (1) AV penetration rate, (2) microscopic and mesoscopic characteristics of AVs and MDVs, such as platoon size and spacing characteristics, and (3) lane policies to accommodate AVs, such as exclusive lanes for AVs or MDVs and mixed-use lanes. Four different critical spacing levels, based on the vehicle pairing, were identified: AV-AV, AV-MDV, MDV-MDV, and MDV- MDV. The authors concluded that a strict lane policy to segregate AVs and MDVs can lead to lower capacity, while the mixed-use lane policies offer higher capacities. It was also found that feasible domains of AV distributions shrink as demand increases and converge to

a unique solution that is controlled by the AV penetration rate and efficiency gain via AV platooning.

Olia et al. (2018) conducted a study to predict capacity of the mixed traffic between various types of AVs and MDVs. This research applied an analytical approach to quantify and evaluate the impacts of AVs on the capacities of highway systems based on the microscopic traffic simulation point of view. The results showed that an increase in traffic capacity of 200 percent, or a maximum lane capacity of 6,450 veh/h/ln, could be achieved as the traffic shifted from 100-percent MDVs to 100-percent CAVs.

Devore (2019) created VISSIM models to investigate the capacity of a 4.5-mile freeway segment on I-35W in Minnesota under various CAV penetration rates for a dedicated CAV-only lane. The study assumed a decrease in distance and headway between vehicles, less variability and oscillation in speed, communication between vehicles, and smaller reaction time for CAVs. The author found that CAVs would provide significantly greater benefits in a separated lane than in mixed traffic situations due to the restriction in interactions, such as lane change, between CAVs and MDVs. The results showed that the capacity of the dedicated CAV-only lane was expected to be increased from 2,000 – 2,200 veh/h/ln to 3,000 – 3,300 veh/h/ln, or increased by 50 percent, as the CAV penetration rate in the lane shifted from 0 percent to 100 percent.

Fan and Liu (2019) investigated the impact of CAVs on freeway capacity by developing guidelines and providing recommendations on estimating the freeway capacity in mixed traffic of CAVs, AVs, and human-driven vehicles. VISSIM was adopted as a simulation tool to simulate four different freeway segments adopted from Caltrans Performance Measurement System (PeMS). The study employed 20-percent increment rate of CAVs, AVs, and MDVs to simulate mixed traffic scenarios on each selected freeway segment. The results showed that, as the CAV penetration rate shifted from 0 percent to 100 percent in the mixed traffic of CAVs and MDVs, the capacity of freeway increased by 70 – 149 percent.

Morgan et al. (2019) conducted a study using microscopic traffic simulation in realistic networks to predict the capacities of mixed traffic of CAVs and MDVs on freeways for 14 DOTs to use in planning decisions. Mixed traffic simulation models were performed by adopting the FHWA algorithm to replicate the behavior of CAVs on basic, merge, and weaving freeway segments. The study concluded that CAVs have potential to increase capacity and reduce

bottlenecks; however, the anticipated improvements are not as aggressive as suggested in the previous studies for two reasons. Firstly, most of the recent CAV studies were tested in a controlled and isolated environment. These models were developed based on single-lane facilities and not at the bottleneck locations; therefore, the results are less important and relevant for agencies. Secondly, the headways applied in the previous studies were too close for passenger comfort and safety. The study pointed out that the current average headway between vehicles is 46 m when traveling at 112 km/h; however, to increase the capacity by 200 percent (three times), the space headway must be only 15 m, which could increase the stress level of the passengers. Moreover, the tire traction, roadway conditions, and braking system of the vehicles may be additional obstacles for CAVs to achieve the speculated capacities in recent studies. The simulation results indicated that capacity increased by 32 – 82 percent as the traffic composition shifted from 100-percent MDVs to 100-percent CAVs, with the maximum capacity available of 3,200 veh/h/ln. In other words, the study suggested that CAVs would increase capacity due to the connectivity between vehicles and the capabilities to discard distractions; however, the degree of improvement tended to be at a more conservative rate. In addition, the authors suggested that bottlenecks could be significantly improved and congestion could be mitigated via the application of CAVs in traffic.

2.1.2 Modeling and Simulation of CAV Traffic

Naumann et al. (1998) developed a traffic management strategy for AVs at intersections by implementing coordination between vehicles to increase safety and mitigate congestion. The idea of the strategy was to enable coordination for AVs traversing conflict points at an intersection via wireless connections to avoid collisions and improve traffic flow. The strategy consisted of three components: the vehicle model, the collision avoidance algorithm, and the fairness-by-priority strategy. The vehicle model dealt with both continuous and discrete systems. The continuous system accounted for the lateral and longitudinal controls of the vehicular dynamics; while the discrete system took into account the communications, along with information-sharing between vehicles to assign appropriate velocities and routes for conflicting vehicles at the intersection. When an AV entered a sphere of influence, its discrete system received the geometry information of the intersection and the management strategy from a traffic signal control. Next, its surrounding vehicles are detected via sensors and wireless communication to recognize its inertial position in the sphere. Permission to traverse the intersection was individually assigned to each

vehicle, simultaneously with the calculation of its reference velocity. The controller of the continuous system then collected velocity and position values, which were feedbacked to the strategy when assigning permissions for the next vehicles to enter the intersection. The collision avoidance algorithm worked by permitting only one vehicle to occupy a region of a radius (r) around each conflict point at a time to avoid potential collisions. The system worked by having the whole set of data transferable among vehicles in the sphere of influence.

Fernandes and Nunes (2010) developed an approach to increase the roadway capacity, as well as to eliminate the stop-and-go characteristics in urban traffic, by reducing the longitudinal spacing between CAVs in a platoon. The constant-spacing platooning method with inter-vehicle communications (IVC) was analyzed and simulated. Simulation was performed via SUMO (Simulation for Urban MObility) software (Behrisch et al., 2011) to test this concept. The platoon leaders were assigned to be controlled by an external application, and the simulation platform was performed at the sub-second level. The study analyzed only the longitudinal control of vehicles, without any lateral movements considered. In addition, the study assumed flawless communications between vehicles. The study also assumed that no packet collisions occurred within a platoon.

Milanes et al. (2011) developed an automated on-ramp merging system to automatically merge vehicles from a minor road to a major road under congested conditions. The research objectives were: 1) to minimize congestion at the merge zone by automatically guiding the merging vehicle to smoothly enter the major road and 2) to maintain the speed of vehicles on the main road by minimizing effects of the conflicts at the merge zone. Wireless V2I communication was proposed to exchange data between vehicles. A decision algorithm was developed to determine a target gap for each vehicle to perform a smooth transition between the position of the merging vehicle on the on-ramp and the final merging point. A fuzzy longitudinal controller was developed to automatically command the longitudinal control of vehicles via throttle and brake pedals to guide the merging vehicle to merge into the main road as precisely as possible to the suggested gap determined by the decision algorithm. The results showed that the system was capable of guiding the vehicle to smoothly merge into the main road using an appropriate gap under congested conditions. The results also indicated that the speeds of the vehicles involved in the merging maneuver were automatically adjusted prior to the occurrence of the maneuver.

Li et al. (2013) used VISSIM's EDM to model the automated control of urban traffic (ACUTA), which is a reservation-based intersection control system for automated intersections. The proposed system applies a centralized control strategy, using an intersection manager (IM) for communications between vehicles, for organizing fully AVs at an intersection on the first-come-first-serve (FIFO) basis. ACUTA was modeled at a four-leg intersection with three lanes per direction. Each lane was built as a separate link to simplify the simulation model to eliminate the lane changes since it was assumed that vehicles can turn from any lane. Capacity was measured as the maximum throughput among all demand conditions, while the volume was directly obtained from VISSIM's output for that specific demand condition. The authors found that the results obtained from the use of ACUTA showed significantly reduced delays, higher capacity, and lower volume-to-capacity (V/C) ratios under various demand levels at the intersection; compared to the results obtained from the normal optimized signalized control.

Zhang et al. (2016) developed a decentralized optimal control framework to yield real-time optimal acceleration and deceleration rates for CAVs traversing urban intersections to minimize fuel consumption. Hamiltonian analysis was applied to formulate the analytical solution and online implementation of the decentralized problem. The proposed solution was validated in VISSIM, considering two adjacent intersections located in downtown Boston. The FIFO queuing system was adopted to govern the service for CAVs at each intersection. When a vehicle entered a control zone, a unique identity (i, j) is assigned to the vehicle by the coordinator. These two intersections in the model were considered to be interdependent since potential congestion on the connecting roadway can affect the overall traffic flow. The algorithm was found to enable vehicles to traverse the intersections without the use of signal control, without creating impacts of congestion on the connecting roadways, and without collisions between vehicles, as restricted by the strict safety constraint proposed. It was concluded that the coordination of CAVs can significantly reduce both average fuel consumption and travel time for CAVs crossing intersections in urban setting.

Rios-Torres and Malikopoulos (2017) investigated the optimal vehicle coordination for CAVs at a merging roadway, in terms of fuel consumption under a constraint of collision avoidance, and derived a solution to optimize the traffic flow by eliminating the stop-and-go characteristics. In this study, an analytical online closed-form solution using Hamiltonian analysis and an optimization framework for the online coordination of vehicles at a merging zone were

proposed in a centralized fashion. Simulation was employed to validate the effectiveness of the proposed solution. The authors developed an algorithm to formulate the queuing characteristics of the CAVs at the merging zone by assuming a dynamic FIFO queuing manner. The results showed that the coordination of vehicles at the merging zone could substantially reduce the travel time and fuel consumption of vehicles.

2.1.3 Modeling and Simulation of AV Traffic

Fiosins et al. (2011) used multi-agent simulation in AIMSUN to model AVs in urban traffic, based on assumptions that these vehicles attempt to reach their destinations as quickly as possible and act individually with regard to their own characteristics. Two stages of the planning process for an automated vehicle agent were presented: strategic planning for selecting the optimal route (SP) and tactical planning for optimizing travel time when traversing a street (TP). The study analyzed the vehicle routing as a stochastic shortest path problem with imperfect knowledge about the network conditions, while the tactical planning was performed as a function of collaborative communications between adjacent vehicles. Planning algorithms for both stages were presented, and interactions between these stages were illustrated in this study. For the strategic planning process, vehicles were assigned to plan their routes independently, based on the historical and real-time information about travel time of the roadway link. For the tactical planning process, AVs were assigned to plan their cooperative decisions with other adjacent vehicles, on which speed change and lane change were adopted as their functions, to minimize travel time of the whole group. The results showed that application of integrated strategic and tactical planning offered the greatest effectiveness since the average travel time was reduced by 10 percent.

Asplund et al. (2012) illustrated how a vehicular coordination problem for AV traffic can be formalized via a constraint specification language called the Satisfiability Modulo Theories (SMT) solver. The authors found that setting up a central controller at all intersections would not be a cost-effective alternative; therefore, a fully distributed approach was adopted. An intersection collision avoidance (ICA) scenario, which is a case study for a distributed coordination problem, was modeled to evaluate the feasibility of the proposed approach. The system was modeled that each vehicle has its own control and dynamics automation that works interdependently with the network, coordination protocol, surrounding vehicles, and environment. A basic four-leg intersection scenario was modeled and validated to demonstrate the applicability of this approach.

The results showed that the proposed model was found to capture continuous time and space, along with an unbounded number of vehicles and messages. The authors concluded that the proposed approach to perform distributed coordination was an appropriate approach to formalize the system safety at intersections.

2.1.4 Modeling and Simulation of CV Traffic

Dimitrakopoulos (2011) proposed the concept of an internet of vehicles (IoV) as the IP-based connections between a vehicle and other vehicles in its vicinity, and between vehicles and objects of the transportation infrastructure, to exchange information for enhancing safety and efficiency of traffic; yet promoting green transportation. Four basic components of the IoV solution are: the autonomic management algorithms, the internet of vehicles as enablers of future green ITS, the IoV architecture fundamental functional blocks, and the scenario-driven approach. In order to achieve this concept, the autonomic management algorithms for vehicles needs to be established to provide a modeling and evaluation chain to model the status of vehicles and environment, which shall be interpreted and distributed in real-time. In addition, an integration between vehicles and the internet needs to be pursued via a properly designed and developed system to establish an appropriate platform for the IoV. Finally, the author suggested that the concept of IoV could resolve several issues of transportation; and lead to safer, more efficient, and eco-friendly driving environment.

Wang et al. (2014) conducted research to propose a radio-frequency-identification-based (RFID) vehicle positioning approach to facilitate the applications of CVs. The system was designed by providing a series of RFID tags on the road surface, while each vehicle is equipped with an on-board RFID antenna and RFID reader, connected by a cable. RFID tags were designed to contain position information, such as distance to a reference point, lane number, and direction of the roadway. The system works when a vehicle passes above an RFID tag embedded on the road surface, the RFID reader and antenna carried by a vehicle activates the RFID tag and reads the accurate position information from it. However, at locations without RFID coverage, the vehicle position is estimated from the most recent tag location using a kinematics integration algorithm until the updates from the next RFID tag are available. A calibration algorithm was proposed to mitigate positioning errors due to the speed changing of vehicles when traversing roadway segments without RFID coverage. It was found that RFID-based positioning offered high

accuracy for vehicular tracking. The authors concluded that the use of RFID positioning is a promising approach for facilitating the applications of CVs due to its low cost and reasonable accuracy.

2.2 Car-Following Models

2.2.1 Car-Following Models for MDVs

A car-following model is a mathematical model developed to describe the longitudinal interaction between vehicles in the same lane in a traffic stream. Car-following is an essential component of microscopic simulation modeling. In recent years, the importance of the car-following model has increased since it formed a basis for the development of AV technologies. According to Brackstone and McDonald (1999) car-following models were categorized into five types: Gazis-Herman-Rothery (GHR), Collision Avoidance models (CA), linear (Helly) models, psychophysical or Action Point models (AP), and fuzzy logic-based models.

1) The GHR model, which was initially developed in late 1950s, applies a stimulus-response type function that a driver's acceleration was proportional to the relative speed between vehicles and deviation from a following distance, as shown in Equation (2-1). Due to the miss-match between the macroscopic relationship obtained from the microscopic equation, the model has been calibrated and validated to yield the more realistic results by defining the best combination of *m* and *l* in the equation. However, the authors commented that the exact values of *m* and *l* might not be obtainable since car-following characteristics are likely to vary with traffic flow conditions and the empirical studies often took place at relatively lower speeds than the actual traffic.

$$a_n(t) = cv_n^m(t)\frac{\Delta v(t-T)}{\Delta x^l(t-T)} \tag{2-1}$$

A sub-category of the stimulus-response models is the Optimal Velocity Model (OVM) resolves limitations of these models, based on the perspective that each vehicle has an optimal velocity as a function of the space headway, $V(s)$. The form of the OVM is presented by Bando et al., as presented by Equations (2-2).

$$dv_{n+1}(t)/dt = \kappa\,[V(s) - v_{n+1}(t)] \tag{2-2}$$

Where κ = sensitivity constant

$V(s)$ = calibrated optimal velocity as a function of the space headway

The value of $V(s)$ was then calibrated using empirical data by Helbing and Tilch (1998) to yield the realistic acceleration and deceleration profiles of a vehicle, as displayed by Equation (2-3). Note that all the values were calibrated in the metric system.

$$V(s) = V_1 + V_2 \tanh [C_1(s - LS) - C_2] \quad (2\text{-}3)$$

Where LS = length of the vehicles (5 meters)

V_1 = 6.75 m/s

V_2 = 7.91 m/s

C_1 = 0.13 m^{-1}

C_2 = 1.57 m^{-1}

However, the OVM was found to yield a relatively high acceleration rate, while the deceleration rate produced by the model was discovered to be unrealistically low. Consequently, the model was once again improved and called the General Force Model (GFM) by Helbing and Tilch. The model was proposed by including a term on the right-hand-side of the OVM equation to account for the negative interaction force between the pair of vehicles. Therefore, the negative velocity difference ($-\Delta v$) was added to Equation (2-2). In addition, the sensitivity constant (κ) was recalibrated and the value of 0.41 s^{-1} was suggested, as presented by Equation (2-4).

$$dv_{n+1}(t)/dt = \kappa [V(s) - v_{n+1}(t)] + \lambda \boldsymbol{\Theta}(-\Delta v)(\Delta v) \quad (2\text{-}4)$$

Where $\boldsymbol{\Theta}$ = Heaviside function, which can only yield the value of 0 or 1

κ = 0.41 m^{-1}

Later, researchers discovered that when the leading vehicle is moving at a much faster speed, the follower does not have the tendency to decelerate even if the space headway between the vehicles is smaller than the safe distance (Treiber et al., 1999).

Jiang et al. (2001) developed a car-following model that simultaneously takes the positive velocity difference (Δv) and negative velocity difference ($-\Delta v$) between the subject vehicle and its leader into account. The reason was that the velocity difference affects the acceleration rate of the follower not only when the velocity of the follower is larger than the leader, but also when the

velocity of the follower is smaller than the leader. Therefore, the positive Δv factor was added to the equation of GFM to yield a new car-following model called Full Velocity Difference (FVD) Model. The main equation of the FVD model is presented by Equation (2-5), while the value of $V(s)$ is adopted from Equation (2-6) in the OVM model.

$$dv_{n+1}(t)/dt = \kappa\,[v_m - v_{n+1}(t)] + \kappa\,[V(s) - v_m] + \lambda\boldsymbol{\Theta}(-\Delta v)(\Delta v) + \lambda\boldsymbol{\Theta}(\Delta v)(\Delta v) \quad (2\text{-}5)$$

Where v_m = maximum longitudinal velocity allowed on the roadway (speed limit)

κ = 0.41 m^{-1}

$\lambda = \begin{cases} 0.5, & s \le s_c \\ 0, & s > s_c \end{cases}$

s_c = 100 m

$$V(s) = V_1 + V_2 + \tanh\,[C_1(s - LS) - C_2] \quad (2\text{-}6)$$

Where LS = length of the vehicles (5 meters)

V_1 = 6.75 m/s

V_2 = 7.91 m/s

C_1 = 0.13 m^{-1}

C_2 = 1.57 m^{-1}

Accordingly, the FVD model can be rewritten using all the calibrated parameters as presented in Equations (2-7). The units used in this model are in metric.

$$dv_{n+1}(t)/dt = 0.41[V(s) - v_{n+1}(t)] + \lambda\boldsymbol{\Theta}(-\Delta v)(\Delta v) + \lambda\boldsymbol{\Theta}(\Delta v)(\Delta v) \quad (2\text{-}7)$$

Where $\lambda = \begin{cases} 0.5, & s \le 100\ m \\ 0, & s > 100\ m \end{cases}$

$V(s) = 14.66 + \tanh\,[0.13\,(s - 5) - 1.57]$

It was also suggested that the smaller sensitivity constant (κ) produces the greater value of delay time of motion and the smaller value of jam density. Furthermore, the authors pointed out that the effect of a positive Δv on traffic dynamics is not included in the GFM model; therefore, the delay time of motion and jam density produced are not accurate (Jiang et al., 2001).

In 2019, Yu et al. recalibrated the FVD model with the NGSIM trajectory data (FHWA, 2008) to create a more realistic model called the confined Full Velocity Difference Model (c-FVD

Model). The form of the original FVD model's equation was still applied; however, the calibrated parameter values of the original FVD model (V_1, V_2, C_1, and C_2) and the sensitivity parameter (λ) were revised. The parameters V_1 and V_2 were recalibrated as 14.300 m/s and 15.997 m/s, respectively; while C_1 and C_2 were modified as 0.066 m^{-1} and 1.508 m^{-1}, respectively. Besides, the sensitivity constant (κ) and the sensitivity parameter (λ) were revised as 0.895 and 0.3405, respectively. The study found that the maximum acceleration rate in the original FVD model was 18 m/s^2, which was extremely high; therefore, the authors also bounded the acceleration rate in the C-FVD model to be 3.4 m/s^2 for producing the milder vehicular trajectories (Yu et al., 2019; Qu et al., 2019).

2) The collision avoidance model (CA) uses the basic Newtonian equations of motion to identify a safe car-following distance, within which a collision would be inevitable, if the driver of the leading vehicle were to act unpredictably, as shown in Equation (2-8). The model, which was initially formulated in 1959, was further modified by Gipps in 1981 to account for mitigating factors such as additional safety reaction time, maximum braking rate that the driver of the following vehicle desires to use, and maximum braking rate of the leading vehicle that the driver of the following vehicle estimates (Gipps, 1981). The Gipps model has been adopted in various simulation platforms such as CARSIM, INTRAS, and AIMSUN.

$$\Delta x(t-T) = \alpha v_{n-1}^2(t-T) + \beta_l v_n^2(t) + \beta v_n(t) + b_0 \quad (2\text{-}8)$$

3) The Linear (Helly) model is a car-following model which is similar to the GHR model, but it includes additional terms for the adaptation of the acceleration regarding whether the leading vehicle and the second vehicle in front were braking, as shown in Equation (2-9). It was noticed that the time delay in the relationship with the speed of the leading vehicle tends to decrease each time a run is made in the model. This indicates that some form of anticipation occurs in the model. The model also suggests that the driver considers the behavior of any two out of the three vehicles ahead as a justification for car-following decisions.

$$a_n(t) = C_1\Delta v(t-T) + C_2\big(\Delta x(t-T) - D_n(t)\big); \quad D_n(t) = \alpha + \beta v(t-T) + \gamma a_n(t-T) \quad (2\text{-}9)$$

4) Psychophysical or action point models (AP) are perception-based car-following models that were developed based on the concept that drivers would initially be able to realize they were approaching a leading vehicle by perceiving relative velocity through changes on the visual angle

subtended by the leading vehicle. Once a space-based threshold is exceeded, the driver of the following vehicle will decelerate until any relative velocity can be no longer perceived. If the threshold is not re-exceeded while the two vehicles are maintaining their speeds, the actions of the driver of the following vehicle will depend on whether any changes in spacing with the leading vehicle can be perceived. The individual properties of these two thresholds were integrated into a complete working simulation model by Widemann in 1986. This type of model has been adopted by various simulation platforms such as PARAMICS-CM and VISSIM.

5) Fuzzy logic-based models represent the next logical step in explaining driver behavior by dividing the inputs of the model into a number of overlapping fuzzy sets, each of which describes how adequately a variable fits the description. Once defined, it is possible to incorporate these fuzzy sets via logical operators (such as AND, IF, and THEN) to equivalent fuzzy output sets, with the actual course of action being assessed from the modal value of the output set.

2.2.2 Car-Following Models for CAVs

Tang et al. (2014a) developed a new microscopic car-following model for vehicles with inter-vehicle communication (IVC) technology to investigate driver behavior under an accident. The proposed car-following model was developed by modifying the FVD model (Jiang et al., 2001) so that drivers can adjust their acceleration rates based on the traffic in front of them. To illustrate, an accident in traffic can be perceived by CV drivers ahead of their sight distances and they can adjust their acceleration rates immediately as the information is sent. Euler forward difference was applied to discretize the FVD model to be a multi-regime model. The time-step of 1 second was adopted. The simulation results showed that during an accident, the deceleration rate of each CV in the proposed model was greater than the deceleration rate of each vehicle in the FVD model under the same condition. On the other hand, after the accident was cleared and before the queue was dissipated, the acceleration rate of each CV in the proposed model was greater than the acceleration rate of each vehicle in the FVD model under the same condition. The authors concluded that the proposed car-following model for CV traffic can capture the effects of IVC on speed, acceleration, trajectory, and headway of a connected vehicle during an accident. It was also found that the model can overcome the shortcoming of the FVD model that collisions occur under an accident.

Tang et al. (2014b) extended the modified FVD car-following model considering IVC (Tang et al. 2014a) to explore the influences of the reliability of IVC technology on the driving behavior of CVs, along with their corresponding fuel consumption rates and exhaust emissions. To take into account the effects of the failure of IVC technology on some vehicles in a traffic stream, a probability parameter (p) was added to the proposed model to represent the probability that each vehicle successfully receives the traffic information via IVC. The study assumed that any vehicle that fails to receive the traffic information will have a randomly produced vehicle trajectory. The results showed that the vehicles that were unable to receive the information provided by IVC might produce an abrupt deceleration when approaching an incident. It was also found that the vehicles which failed to be connected, had lower speeds than those that received the information via IVC during the dissipating process. The authors found that IVC technology enabled vehicles to reduce their speeds, fuel consumption rates, and tailpipe emissions during the braking process. On the other hand, the technology was found to enhance speeds and, thus, increase the corresponding fuel consumption rates and tailpipe emissions of the CVs during the acceleration process.

Lefèvre et al. (2015) developed a learning-based approach for the longitudinal control of AVs in the traffic stream to propose a system controller that operates vehicles in a comfortable and safe manner. The authors mentioned that although the current AV technology applies the system architecture which has been successfully used in the field of terrestrial robotics, AVs have an additional constraint for passenger comfort, which makes their system architecture different from the one for robotic applications. The authors developed a driver model designed to work in a machine-learning basis to imitate the driving characteristics from the drivers it learns from. The output of the driver model is the acceleration sequences which are as close as possible to the characteristics that drivers would have performed. A combination of Hidden Markov Model and Gaussian Mixture Regression (HMM+GMR), a non-parametric regression method, was used for acceleration prediction in the driver model. The proposed system works when the driver model is fed with real driving data in order to reproduce the driver behavior. Then the model predictive controller is fed with acceleration inputs from the driver model to create appropriate commands for the trajectory of the vehicle. The model predictive controller was designed to be bounded by safety constraints, such as collision avoidance. By solving the optimization constraints for the model predictive controller, the control inputs applied to the AVs were ensured to satisfy the safety

criteria. The system was validated via an experiment by implementing and testing the system in car-following scenarios under dangerous driving situations using artificial obstacles. The results showed that the proposed system can reproduce different human driving characteristics for AVs under safety constraints. It was found that the driver model can learn continuously in machine-learning manner to be evolved with the changes in driving characteristics.

Gong et al. (2016) developed a car-following control scheme for a platoon of CAVs on a straight highway segment based on constrained optimization and distributed vehicular coordination via an analytical approach. The authors pointed out that the conventional CACC technologies primarily focus on mobility and safety requirements of individual vehicles; however, this may have negative impacts on the platoon performance. They suggested that traffic constraints such as physical limitations, safety concerns, and driving comfort need to be considered to achieve desired platoon performance. In addition, the distributed coordination system is more favorable than the centralized coordination system when implementing an automated platoon control since the centralized system is considered infeasible based on a topological point of view. The vehicular platoon was modeled as an interconnected multi-agent dynamic system subjected to acceleration, speed, and safety constraints. The global information structure, in which each vehicle exchanges information with all the other vehicles, was adopted for vehicular coordination. The car-following control scheme consisted of transient dynamics and asymptotic dynamics. The aim of the transient dynamics was to maintain a desired safe spacing between two consecutive vehicles in a platoon and reduce traffic flow oscillations in terms of spacing and speed changes; while the aim of the asymptotic dynamics was the relative distance of two consecutive vehicles should be asymptotically stable and converge to a constant spacing. Car-following characteristics of vehicles in a platoon were modeled according to three categories of constraints: 1) control constraint, in which acceleration and deceleration rates of vehicles were taken into account; 2) speed constraint, in which longitudinal speeds of vehicles were considered; and 3) safety distance constraint, which was inequality based on a kinematic analysis. The efficiency of the proposed algorithms was validated via numerical simulation. The results from the numerical simulation showed that the proposed control scheme effectively reduced the propagation of traffic oscillation in the platoon. The authors concluded that the proposed car-following control scheme for CAV outperforms CACC in a platoon.

Li et al. (2016) proposed a microscopic car-following model that takes into account the effect of electronic throttle with opening angle to capture the characteristics of CAVs in traffic flow. The opening angle of the electronic throttle of the leading vehicles allows the following vehicle in the platoon to react accordingly to the leading vehicle by adjusting its electronic throttle in an automated fashion to avoid a potential collision. CAVs are equipped with electronic throttle control (ETC), which is a core controller of the vehicle, to command the automated functions of the vehicles such as cruise control, stability control, traction control, and pre-crash systems. The authors realized that the opening angle of the ETC affects the vehicle characteristics at a microscopic level. Therefore, the characteristic of the opening angle of the electronic throttle was integrated into the FVD model based on an assumption that the information of the electronic throttle dynamics is shared among vehicles in the traffic via the V2V communications. This model was referred to as the throttle-based FVD (T-FVD) model. The proposed model leverages the automated capability of the vehicles to capture the characteristics of CAVs so that information from the electronic throttles of all CAVs in a platoon can directly be accessed and promptly be adopted as input by the surrounding vehicles. The stability analysis of the proposed car-following model was performed based on the perturbation method to obtain the stability condition. An assumption was made that the initial state of the vehicular traffic flow is steady, in which all vehicles in the traffic stream travel at the optimal velocity under the identical space headway. To analyze the traffic flow characteristics of the proposed model, numerical experiments were performed, which showed that the proposed car-following model has a larger stable region than the FVD model. The theoretical analyses and numerical experiments indicated that the inclusion of the electronic throttle dynamics improved the smoothness and stability of the FVD model.

Wang et al. (2016a) designed a variable speed limit (VSL) and car-following control system that connected a traffic controller with in-vehicle controllers via V2I communication to resolve stop-and-go waves in traffic. CAVs were used as main actuators for traffic control systems in this concept. An open-source microscopic traffic simulator named MOTUS was adopted to test the effectiveness of the proposed control system. In the proposed control system, the link-level traffic controller regulated traffic speeds which minimized stop-and-go waves via VSL gantries; while the acceleration/deceleration rates of the CAVs were controlled by the local in-vehicle controllers. The in-vehicle controllers were linked with traffic controller to command the vehicle propulsion and brake systems for optimizing their trajectories. These two-level controllers were

connected via DSRC. The car-following algorithm used by the vehicle controller was designed for two modes: 1) car-following mode and 2) cruising mode. These two modes were distinguished by a gap between vehicles (s) and a gap threshold (s_f). In the cruising mode ($s>s_f$), the car-following algorithm minimized driving efficiency and comfort costs in its objective function; while safety, efficiency, and comfort costs were minimized in the objective function for the car-following mode ($s<s_f$). The gap threshold was determined by a user-defined maximum desired time gap in the car-following mode, the desired speed, and the minimum gap between vehicles at a standstill condition. The optimal acceleration rates were recalculated at every vehicle control cycle. The gap and speed differences with the leading vehicle were perceived by the vehicle's on-board sensors only. The proposed control system was tested via simulation, and it was found that the connected VSL and vehicle control system improved both traffic efficiency and sustainability.

Wang et al. (2016b) developed controllers and implementable car-following control (CFC) algorithms for AVs and CAVs under a receding horizon control framework. Two CFC algorithms were designed separately for AVs and CAVs. An automated CFC system was developed to control vehicle acceleration for optimizing the vehicle's own trajectory, whereas a cooperative CFC (C-CFC) system was developed to coordinate accelerations of cooperative vehicles for optimizing the joint situation in a platoon. The decentralized algorithm was proposed for the CFC controller, whereas the distributed algorithm was adopted for the C-CFC controller. It was assumed that the lane change decisions of both the CFC and C-CFC vehicles were made by human drivers, and lane change maneuvers were performed by human drivers through steering wheels. A C-CFC vehicle predicted the behavior of its leading and following vehicles based on the information from on-board sensors when direct neighbors are human-driven vehicles, whereas information from V2V communication was used when one or two of its direct neighbors are C-CFC vehicles. The cooperative controller was designed to compute the vehicle's acceleration to minimize its own cost subjected to the situation in front, as well as the cost of its follower subjected to the situation behind. A simulation scenario of a two-lane freeway segment with CFC/C-CFC vehicles randomly distributed was created to investigate the impacts of the proposed controllers on the dynamic traffic flow features. The results showed that C-CFC systems induced faster stop-and-go waves propagating upstream due to V2V communications. The results revealed that although a considerable proportion of AV and CAV in traffic seemed to substantially change the flow characteristics, the characteristics remain qualitatively the same as the case of 100 percent HDVs

at penetration rates of AV and CAV less than 5 percent in traffic. The authors concluded that the roadside controller was necessary for resolving stop-and-go waves at low penetration rates of AVs and CAVs.

2.3 Lane-Changing Models

Ahmed (1999) developed a microscopic model that incorporates acceleration and lane-changing to model the gap acceptance on a freeway merge. The model was estimated using the empirical microscopic data collected from real traffic. The acceleration model was designed based on two regimes of traffic flow: the car-following and the free-flow regimes. The lane-changing decision process was developed based on a sequence of three steps: conditions for lane-changing decision, choice of the target lane, and gap acceptance. According to the field data, the lead gap was in the range of 0.13 - 102.9 meters, whereas the lag gap ranged between 0.5 and 172.9 meters.

Hwang and Park (2005) designed a gap acceptance model based on the discrete choice theory. The objective of the study was to determine the lag gap, which is defined as the gap between the subject vehicle and the vehicle behind it in the target lane, for lane changing maneuvers. Driver behavior data collected during actual merging situations were used to develop the gap acceptance model. The research found that gap acceptance is significantly affected by congestion, as drivers have a tendency to accept smaller gaps to avoid delays under congested conditions. The results showed that the lag gap accepted for lane change during non-congested conditions was 32.70 meters, while the lag gap of 28.71 meters was accepted for lane change during congested conditions (Hwang and Park, 2005).

Lee (2006) developed a freeway lane-changing model to capture the gap acceptance behavior of drivers that merge from a ramp into a congested freeway. The model applied the single critical gap function, which incorporateed explanatory variables that capture all three types of merging behavior: normal, forced, and cooperative lane changing. Trajectory data collected on two freeway sections in California were used in this study. The gap acceptance model was affected by traffic conditions such as average speed in the mainline, the interactions between the subject vehicle and its lead and lag vehicles, and urgency of the merge. The results showed that the median lead critical spacing ranged from 1.5 to 49.2 meters.

Ben-Akiva et al. (2006) conducted research to summarize several enhancements that were made to the generic lane changing model in order to improve its realism and identify limitations. The observed enhancements in lane-changing model are: 1) integration of mandatory and discretionary lane changes in a single framework, 2) inclusion of explicit target lane choice in the model, and 3) incorporation of various types of lane changing maneuvers, such as cooperative and forced lane changes. A mandatory lane change (MLC) occurs when a driver must change lane to follow a path; while a discretionary lane change (DLC) occurs when a driver changes to a lane that is perceived to offer better traffic conditions. These model enhancements were implemented and validated in MITSIMLab, a microscopic traffic simulator. The authors found that integrating MLC and DLC into a single utility model captured the need of drivers to be in the correct lanes, the relative speed advantages, and ease of driving in the current lane and in the lanes to the right and to the left. In addition, the model with explicit target lane choice on multi-lane roadway facilities was found to match the observations. Furthermore, the model that integrated cooperative and forced merging with gap acceptance was found to capture transitions from one type of merging to the other and improved fit to both microscopic and macroscopic traffic flow characteristics.

Schubert et al. (2010) developed an automatic system that can perceive the vehicle's surrounding environment, assess the traffic situation, and recommend appropriate occasions for lane-changing maneuvers. The algorithm behind the proposed lane-changing control was presented with the image processing for lane and vehicle detection, Kalman Filtering for parameters estimation and tracking, and a Bayesian Network (BN) approach for automatically dealing with maneuvering decisions under uncertainty. The experiment of the prototypical automatic lane-changing maneuvers using the concept vehicle was also performed on a highway. The prototype vehicle equipped its front bumper with a 77-GHz long-range radar (LRR), while two 24-GHz short-range radars (SRRs) were installed at its rear end, for collision avoidance. Since lanes needed to be perceived by the vehicle prior to performing automatic lane-keeping and lane-changing maneuvers; two gray-scale cameras with video graphics array (VGA) resolution were installed to cover the frontal and the rear-end areas of the vehicle. The vehicle was equipped with an internal controller area network (CAN) to perceive its motion information, which can be exchanged with other vehicles. Finally, a decision on the appropriate maneuver was made and passed as a recommendation to the driver via a human–machine interface (HMI). The Unscented Kalman Filter (UKF) was applied for estimating the motion of the subject vehicle and the

surrounding vehicles, as well as quantifying a mathematical description of the lane. Bayesian Network (BN) was applied for both the situation assessment and the decision-making algorithms since its main feature was the capability to perform probabilistic reasoning that can be used to handle situations under uncertainties. Situation parameters, represented by random variables, were defined to account for surrounding conditions such as a dashed or solid lane border, the status of a certain lane with respect to its occupancy, and the feasibility of a lane-changing maneuver to the left or right. Likelihood evidence parameters were defined to account for the probability distributions if certain actions are considered safe. The expected utility (EU) was adopted for the decision-making process in the algorithm. The alternative with the greatest EU is considered the optimal decision.

Sun and Elefteriadou (2010) proposed a framework for modeling lane-changing maneuvers in urban traffic based on the empirical driver-behavior data obtained through focus groups and from instrumented vehicle experiments. The focus group study categorized drivers into four types based on aggressiveness: a) type A, drivers who would not change lanes in most situations; b) type B, drivers who seek to get a better position or speed advantage under lower-risk situations; c) type C, drivers who seek to get a better position or speed advantage under higher-risk situations; and d) type D, drivers who always try to get a better position or speed advantage without hesitation. The authors developed a binary logistic regression model that predicted the probability of changing lanes. The model consisted of two components: 1) lane-changing component, in which driver's decision on each lane-changing reason was taken into account, and 2) gap acceptance component, which contained gap acceptance models for various driver types and various types of lane-changing (such as free, cooperative/competitive, and forced maneuvers). The proposed lane-changing model was implemented in CORSIM microscopic simulation platform and was calibrated and validated using real-world data. The results of the proposed model and the original lane-changing model embedded in CORSIM were compared and the authors concluded that the observed traffic under different levels of congestion was better replicated by the proposed model.

Sun and Kondyli (2010) developed a lane-changing model that takes into account the vehicle interactions during a lane-changing maneuver on arterial streets by using the negotiation procedure in computer communications. Conditions were established to distinguish three lane-changing types: free lane changes, forced lane changes, and competitive/cooperative lane changes.

A lognormal model was applied to estimate the duration of lane change (t_{LC}). A sequence of "hand-shaking" negotiations, based on the "TCP/IP" protocol in computer network communications, was designed to model the competition and cooperation among vehicles in the lane-changing process. When a lane-changing request was sent from the subject vehicle (*S*1) to the potential lagging vehicles in the target lane (*T*2), it was a cooperative lane change if the request was accepted by the potential lagging vehicles in the target lane; otherwise, it was a competitive lane-changing maneuver. Under the cooperative lane-changing maneuver, the potential lagging vehicles in the target lane decelerated to allow the subject vehicle to pull ahead of it. On the other hand, there were three scenarios under the competitive lane-changing maneuver: 1) if the potential lagging vehicles in the target lane accelerated, the subject vehicle assessed the next gap to perform the lane-changing maneuver; 2) if the potential lagging vehicles in the target lane maintained its speed, and the subject vehicle was not aggressive, the subject vehicle sought for the next gap to perform the maneuver; and 3) if the potential lagging vehicles in the target lane maintained its speed, and the subject vehicle was aggressive, a forced lane change was performed by the subject vehicle. The algorithm for modeling competitive/cooperative lane-changing maneuver is shown in Figure 2-2. CORSIM was used to implement and validate the proposed model. The simulation capabilities of the proposed and original lane-changing models were compared, based on the results produced by CORSIM. The results indicated that the observed traffic under different levels of congestion was better replicated by the proposed lane-changing model than the original model.

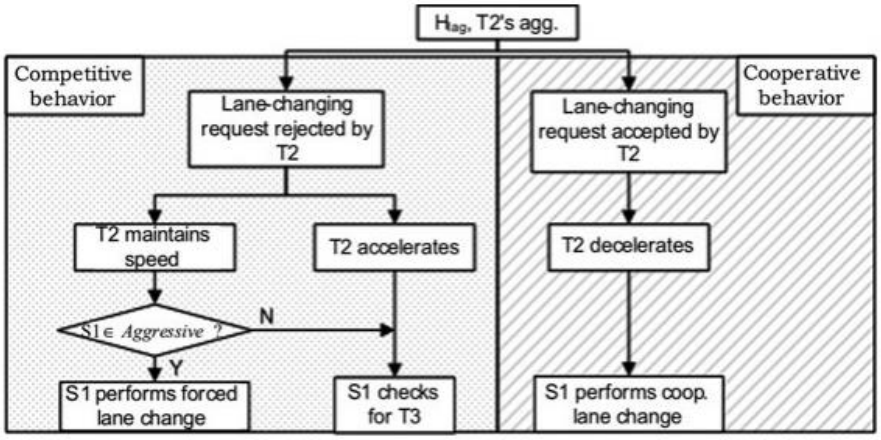

Figure 2-2 Algorithm for modeling competitive/cooperative lane changes (Sun et al., 2010)

Kondyli and Elefteriadou (2011) developed a ramp-merging model to examine how driver behavior affects traffic operations and gap-acceptance decisions at freeway-merging segments and

to determine the relationship between vehicle interactions and breakdowns, which might explain the observed variability in capacity of freeways. In-vehicle experiments were performed using an instrumented vehicle and simultaneous video recording, to observe the merging behavior of the drivers. Different types of drivers were taken into account. A gap-acceptance model under different merging conditions and a driver behavior model for predicting vehicle interactions with merging vehicles on freeway segments were developed, based on the actual data obtained from the experiments. A conceptual framework of the merging process based on gap acceptance and driver behavior was developed. The gap-acceptance model was developed based on regression analysis to predict the total accepted gaps as a function of driver type (aggressive and nonaggressive), merging maneuver type, average freeway density, location of the ramp vehicle in the acceleration lane, and acceleration of the ramp vehicle. Three types of merging maneuvers were defined in this study: free, cooperative, and forced merges. Probability models were developed to determine the probability that any vehicle on freeway would decelerate when encountering a cooperative or forced merging situation. A merging turbulence model that analyzed the effect of vehicle interactions on traffic flow was also proposed. The results showed that the merging turbulence increases before the breakdown and could be used as an indicator for the breakdown events.

Gurupackiam and Jones (2012) conducted a study to observe variations in gap acceptance and lane change duration on arterials under recurrent and non-recurrent traffic congestion. Hypothesis testing via Mann-Whitney U-Test was performed and found that the means of accepted gaps and lane change durations were significantly different between the congested and non-congested traffic conditions. The results showed that the accepted gaps under the recurrent traffic congestion ranged between 1.60 and 7.80 seconds, with the mean of 4.04 seconds; whereas the mean accepted gap for the non-recurrent congestion was 3.52 seconds. The lane-changing durations under the recurrent traffic congestion ranged between 2.60 and 6.00 seconds, with the mean of 4.19 seconds; while the mean lane-changing durations for the non-recurrent congestion was 4.71 seconds. The study concluded that drivers tend to accept smaller gaps, while spending longer lane changing durations under non-recurrent congested traffic conditions.

Lv et al. (2013) proposed a microscopic lane-changing process (LCP) model by simplifying the lane-changing process to the single car-following framework via simulation to imitate the realism that a lane-changing maneuver was a continuous process than an instantaneous action.

Specifically, this study focused on the lane-changing process and the impact of lane changing on the following cars on different lanes. Jiang's FVD model (Jiang et al., 2011) was selected as the basic car-following model in the simulation, with the adoption of the optimal velocity function proposed by Helbing and Tilch (Helbing and Tilch, 1998). The lane-changing characteristics in the simulation model were developed considering two criteria: 1) the incentive criterion, which is a good reason for a driver to change lane, such as changing lane to maintain high speed or avoid congestion, and 2) the security criterion, in which a driver perceives that the changing lane is safe before performing the maneuver. The authors concluded that the lane-changing maneuvers might strengthen velocity variation at medium density and weaken velocity variation at high density.

Hill et al. (2015) conducted research on freeway lane changing based on driver behavior to find the fitted distributions for various lane-changing durations and accepted gaps. The field study results suggest that the mean lag gap accepted under uncongested conditions was 26.60±13.76 meters and was gamma-distributed; whereas the mean lag gap accepted under congested conditions was 13.92±9.44 meters, and was gamma-distributed as well. In addition, the DLC duration for uncongested conditions followed a normal distribution, with the mean of 5.28±1.00 seconds. Furthermore, the mean uncongested and congested DLC and MLC accepted lag gap was 24.70±13.96 meters, with a gamma distribution. The mean uncongested and congested DLC and MLC lead gap accepted was found to be 34.66 ±42.85 meters, with a Johnson SL distribution.

Xie et al. (2014) proposed an optimization-based on-ramp control strategy and developed a simulation model to investigate the potential benefits of collaborative merging behaviors enabled by CV technology. In addition, an empirical gradual speed-limit control strategy was proposed. The proposed nonlinear optimization model employs accelerations of all vehicles in traffic as the decision variables for maximizing the total speed of all vehicles over the upcoming short time period, as defined in the objective function. To ensure traffic safety, a constraint was also set, so that when a vehicle arrived at the merging point, the distance headways between the vehicle and adjacent vehicles were greater than a minimum value. Freeway vehicles were modeled to slow down, accelerate, or shift to the left lane when approaching an on-ramp merge. The proposed model assumed that vehicles are connected via Dedicated Short-Range Communications (DSRC). The model also assumed that as freeway and ramp vehicles approach a 500-meter radius ahead of the on-ramp gore, the vehicles strictly followed the instructions received from a central traffic

controller. An integrated modeling framework was developed to simulate traffic operations at freeway on-ramps via VISSIM. The VISSIM simulator and the add-on Car2X module were applied to capture the accelerations, speeds, and positions of vehicles in the model (Figure 2-3). Next, this information was fed into an optimization module coded in MATLAB. Finally, the optimal strategies were sent back to the VISSIM simulator for vehicle control. The results showed that the proposed optimal control strategy can effectively coordinate all merging vehicles at freeway on-ramps and significantly improve traffic safety and efficiency on the freeway, especially under oversaturated conditions.

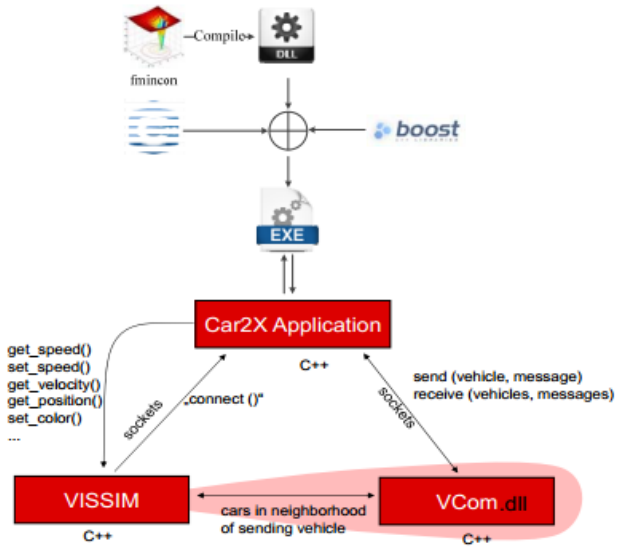

Figure 2-3 Integrated platform architecture for modeling lane changes for CV (Xie et al., 2014)

Talebpour et al. (2015) proposed a lane-changing model based on a game-theoretical approach accounting for the real-time information exchange between CVs in traffic. The objective of this study was to show that game theory may be applied to develop robust lane-changing models. A calibration approach based on the method of simulated moments (MSM) was proposed. The prediction capability of the simplified version of the proposed framework was calibrated against NGSIM data and then validated. Two game types were suggested in this model: two-person non-zero-sum non-cooperative game under complete information (Game 1), which represents lane-changing decisions in a connected environment, and two-person non-zero-sum non-cooperative game under incomplete information (Game 2), which represents lane-changing decisions in a situation that the other drivers' decisions are unknown. The model assumed that drivers play a repeated game until a Nash equilibrium is reached. Both MLC and DLC maneuvers were

considered in this study. In both cases, the subject vehicle had two strategies: change lane and wait, while the lagging vehicle had three strategies: accelerate, decelerate, and change lane. The payoff functions for a pair of subject and lag vehicles in all possible scenarios were then defined. Root Mean Square Error (RMSE) was used to validate the proposed model. The simulation model assumed that V2V communications reduced drivers' reaction time by 50 percent. The simulation results indicated that the proposed lane-changing model provides a greater degree of realism than a basic gap-acceptance lane-changing model, and was capable of predicting lane-changing behavior; however, there were still limitations that needed to be identified. For example, the authors noted that applying game theory to microscopic driving decisions modeling may induce computationally slow algorithms rendering the adopted approach to be impractical for real-time decision making.

You et al. (2015) developed a trajectory planning algorithm for automated lane change based on the cooperative vehicle infrastructure for CAVs. Two main functions of lane-changing maneuvers were considered in the model: trajectory planning and trajectory tracking. The polynomial method was applied for modeling the trajectory planning function, while the trajectory tracking function was modeled using a back stepping principle. For the trajectory planning system, the subject vehicle motion and the collision detection were incorporated into the algorithm. For trajectory tracking system, a tracking controller with global convergence property was validated based on the Lyapunov function. The cooperative trajectory planning was performed based on V2X technology to consider not only the motion of the subject vehicle, but also the driving state of the surrounding vehicles. The proposed trajectory planning algorithm and tracking controller for trajectories were then tested via simulation and experimental analysis to validate their performances. The simulation was performed for a vehicle in MATLAB/Simulink, while the experiment was conducted on a basis that vehicles are coordinated in the lane-changing scenario and enable to connect with the infrastructure. The results from the simulation models and the experiments indicated that the proposed automated lane-changing system was feasible and effective to be adopted in CAV technologies.

Wang et al. (2015) developed a jointly evaluated model of discrete lane-changing decisions and continuous car-following accelerations for AVs under a central mathematical framework. The optimal control decisions generated by the approach determined a unique and continuous trajectory

that could be adopted by the AV actuators to follow. Simultaneously, the approach anticipated lane changes and dealt with the interaction and cooperation of multiple vehicles in conflicting situations. The interactions between controlled vehicles and surrounding vehicles were captured in the cost function to correspond for undesirable future situations. The proposed model was designed to be flexible and compatible for both AV systems and CAV systems. The control objectives of the lane-changing and car-following control system (LCCS) incorporated multiple criteria of maximizing travel efficiency, minimizing risk of collision, and maximizing passenger comfort; while traffic regulations were still obeyed. The problem was formulated as a dynamic game in which controlled vehicles made decisions based on the expected behavior of other vehicles. The control decisions were updated at regular frequency to utilize the latest information regarding the state of controlled vehicles and surrounding vehicles available. An iterative algorithm based on Pontryagin's Principle was applied to solve the formulated problems. Numerical examples presented the proposed controller properties and performance at the microscopic level. The results indicated that the proposed model can produce efficient lane-changing maneuvers under safety and comfort constraints.

Letter and Elefteriadou (2017) developed a longitudinal freeway merging control algorithm for maximizing the average travel speed of CAVs. A roadside controller provided communications that allows the computation and transmission of optimized trajectories in a centralized fashion. These vehicles then carried out the computed trajectories and resume normal operation once the communication with the roadside controller was terminated. It was assumed that all vehicles in the network were fully automated and equipped with V2I communication devices. A tool was developed to simulate and determine the merging algorithm, using LINGO as an optimization software. A safe time gap constraint was defined in the algorithm to ensure that at every interval the time gap between the leading vehicle trajectory and the subject vehicle was greater than the safe time gap. A hypothetical merging segment was created and simulated in CORSIM to assess the effectiveness of the proposed merging algorithm. The performance of the merging algorithm was then compared to the performance of the conventional vehicle traffic. The results suggested that the algorithm can reduce travel time, increase average travel speed, and improve throughput during uncongested conditions. The authors also found that the capacity of the merge segment was directly related to the safe time gap selected to run in the algorithm. It was also found that once capacity was reached, queuing formed on both the ramp and mainline segments upstream of the

merge area. The authors concluded that the proposed algorithm induced safe merging operations under the congested traffic state.

2.4 Simulation Model Implementation

Several researchers have used VISSIM as a tool to evaluate different algorithms for CAVs. VISSIM is equipped with various add-on modules programming interfaces (API), in which users are allowed to integrate their own algorithm. There are two major programming interfaces in VISSIM: 1) COM interface and 2) External Driver Model Dynamic Linked Library (EDM.dll) interface. COM allows external programs to access to simulation objects. In COM interface, users can start VISSIM from other applications and access to the attributes of vehicles in the VISSIM network. The EDM DLL interface allows for replacing the internal driving behavior of vehicles by a user-defined behavior for some or all of the vehicles in the simulation. COM can be written in various programming languages such as VB, C#, C++, JavaScript, or Python, whereas the EDM interface can only be coded in C++ (Li et al., 2013; Zhao and Sun, 2013; Songchitraksa et, al., 2016; and PTV, 2018).

The user-defined algorithm of CAV can be implemented in the External Driver Model interface via C++. Next, the dynamic-link library (.dll) is generated after the code is compiled. In addition, a folder named DriverModelData is created in the same directory where the VISSIM.exe folder exists to avoid run-time error from VISSIM. The drivermodel.dll then returns the command back to the VISSIM network. Ultimately, the .dll file controls the behavior of vehicles that are using the EDM. (Zhao and Sun, 2013; Songchitraksa et, al.; 2016; and PTV, 2018).

The current state of the vehicle and its surroundings are sent by VISSIM to the .dll, in which the reaction of the vehicles from the user defined algorithm is computed. Some or all vehicles in the simulation run can be modeled with the user-defined drivermodel.dll, which can specify all driving behaviors based on the logic input (PTV, 2016).

2.5 Summary of Literature Review

Several car-following and lane-changing models have been proposed for simulating traffic scenarios; however, no previous works were found to combine these models via a conditional linkage in a mixed-traffic model. In addition, although several studies have been conducted on

testing mixed traffic scenarios, a study that covers the full spectrum of vehicle composition between CAVs and MDVs in mixed traffic has not been done yet. Also, only a few studies have considered the effects of automated lateral vehicular interactions, such as lane changing and transient maneuvers on human behavior. Finally, although various control lane-changing algorithms were proposed for AVs, complex interactions between different vehicle types have not been considered.

CHAPTER 3 THE PROPOSED ALGORITHMS

This chapter describes the proposed CAV Algorithm, in which the car-following and lane-changing models are incorporated, followed by the methods proposed for developing the microscopic mixed-traffic simulation model on a freeway segment. The proposed linkage between the car-following and lane-changing models, which was newly defined to simultaneously control the longitudinal and lateral movements of CAVs, is also presented.

3.1 The CAV Algorithm

The proposed CAV algorithm was developed to control the longitudinal and lateral movements of CAVs in a traffic stream. In this research, CAVs are assumed to be equipped with level 5 automation (fully automated). The algorithm is a combination of car-following/cruising and lane-changing models, with the conditional linkage, for supervising the decision-making of CAVs when interacting with the surrounding vehicles and the geometry of a freeway segment. A schematic of the car-following and lane-changing vehicles in the traffic stream is presented in Figure 3-1. As seen in the schematic, the order of the vehicle in the platoon in the lane where the subject vehicle is occupying is symbolized as *n*, whereas the order of the vehicle in the platoon in the adjacent lane is denoted by *m*. In addition, the middle lane is symbolized as lane *i*; while the adjacent lane on the left and right sides are designated as lane *i+1* and lane *i-1*, respectively. Therefore, the subject vehicle traversing the roadway in the middle lane is denoted by *veh(n+1, i)*, while its leader is symbolized as *veh(n, i)*. The longitudinal and lateral displacements of the vehicles in the traffic stream are designated as *x* and *y*, respectively. The space headway between a pair of vehicles, denoted by *s*, is measured as the longitudinal distance difference between the front ends of the vehicles; whereas the gap is measured as the longitudinal distance difference between the rear end of the leader and the front end of the follower.

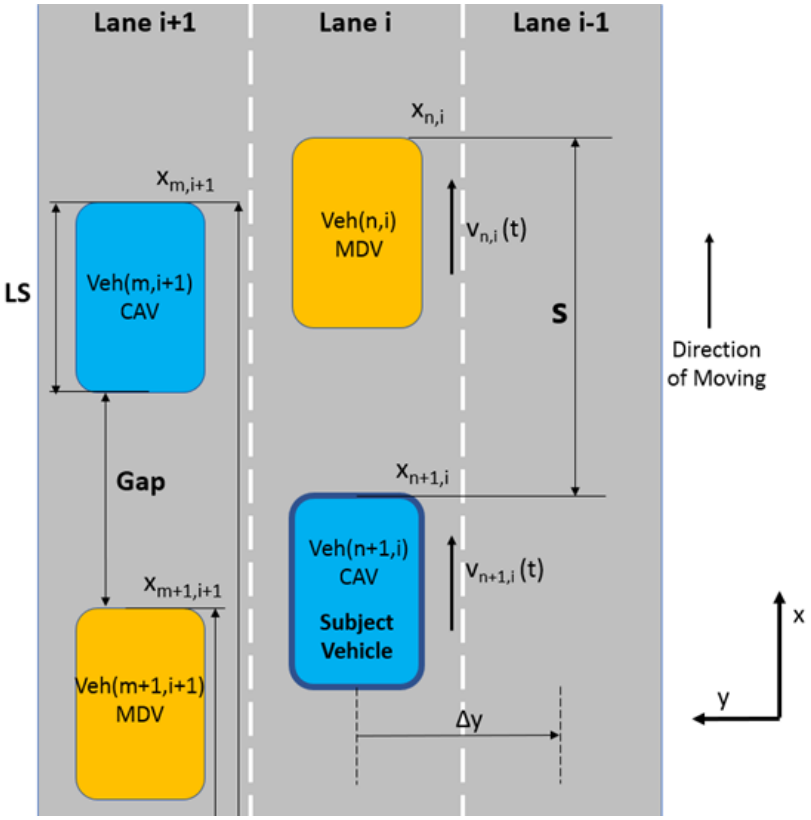

Figure 3-1 Schematic of the car-following and lane-changing vehicles in the traffic stream

The CAV algorithm is composed of two sub-algorithms: 1) Automated Car-Following/Lane-Changing Algorithm and 2) Automated Platoon-Leading/Lane-Changing Algorithm. The subject vehicle is programmed to switch between these sub-algorithms based on the current status and conditions of the vehicle. The vehicle is governed by the Automated Car-Following/Lane-Changing Algorithm when its leader is CAV or MDV, given that the space headway between the vehicle and its leader is smaller than the free-flow space headway ($s_{free\ flow}$). Otherwise, the vehicle is assigned to follow the Automated Platoon-Leading/Lane-Changing Algorithm when there is no leading vehicle ahead in that lane or when the space headway between the vehicle and its leader is greater than the free-flow space headway, as illustrated in Figure 3-2.

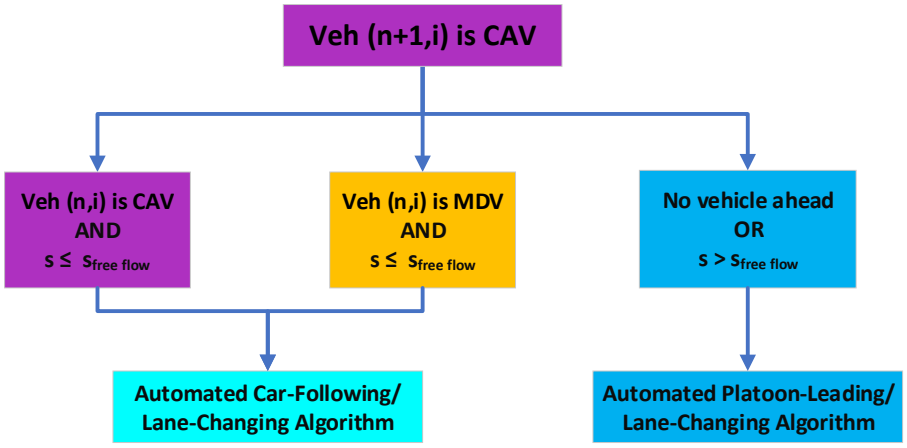

Figure 3-2 Flowchart of the CAV algorithm

The algorithm was developed to run using the time step of one second to update the real-time status and conditions of the subject vehicles and the vehicles surrounded in the traffic stream. Each sub-algorithm is composed of two main models: car-following and lane-changing models that govern the longitudinal and lateral movements of the vehicle. In addition, the linkage between the car-following and lane-changing models was established to make these two models run interchangeably in the sub-algorithm. The mechanisms behind the sub-algorithms are explained in the following section.

3.1.1 Automated Car-Following/Lane-Changing Algorithm

The Automated Car-Following Algorithm is the sub-algorithm that governs the longitudinal and lateral movements of a CAV when the vehicle is following a CAV or MDV in the traffic with the space headway of smaller than the free-flow headway ($s_{free\ flow}$). The algorithm starts by recognizing that the subject vehicle itself occupying lane *i*, denoted by *veh(n+1, i)*, is a CAV and its leader that is occupying the same lane, denoted by *veh(n, i)*, is a MDV or CAV. Next, if the current space headway between the vehicles is smaller than the defined free-flow headway, the subject vehicle will proceed to the CAV Car-Following Model. Otherwise, it is promptly switched to the Automated Platoon-Leading/Lane-Changing Algorithm.

3.1.1.1 The CAV Car-Following Model

The CAV Car-Following Model was adopted from the Full Velocity Difference car-following model (FVD) and the confined Full Velocity Difference model (c-FVD) with an adjustment in the sensitivity value (λ) from 0.5 in the original model to 0 to fit the characteristics

of CAV. The acceleration rate is based on the optimal velocity function ($V(s)$), which depends on the real-time space headway (s), without accounting for the velocity difference between vehicles. This model generates the acceleration rate of the subject vehicle based on the current space headway (s) and the velocity difference between vehicles (Δv), as shown in Figure 3-3. For any velocity difference that occurs under the current space headway greater than the critical space headway (s_c), the subject vehicle will accelerate under the cruising mode as shown in the Equation (3-1).

$$dv_{n+1}(t)/dt = \kappa\,[v_m - v_{n+1}(t)] + \kappa\,[V(s) - v_m] \quad (3\text{-}1)$$

If the current space headway is smaller than the critical space headway (s_c), the acceleration rate of the subject vehicle is determined based on the current velocity difference between the vehicles. If the current speed of the subject vehicle ($v_{n+1}(t)$) is less than the current speed of the leading vehicle ($v_n(t)$), the positive term of $\lambda\boldsymbol{\Theta}(\Delta v)(\Delta v)$ will be added to the acceleration rate of the subject vehicle to narrow the space headway between the vehicles and maintain the car-following mode. The acceleration rate of the CAV is illustrated in the Equation (3-2).

$$dv_{n+1}(t)/dt = \kappa\,[v_m - v_{n+1}(t)] + \kappa\,[V(s) - v_m] + \lambda\boldsymbol{\Theta}(\Delta v)(\Delta v) \quad (3\text{-}2)$$

If the current speed of the subject vehicle ($v_{n+1}(t)$) is greater than the current speed of the leading vehicle ($v_n(t)$), the negative term of $\lambda\boldsymbol{\Theta}(-\Delta v)(\Delta v)$ will be added to the acceleration rate of the subject vehicle to stretch the space headway and avoid collision (Equation (3-3)).

$$dv_{n+1}(t)/dt = \kappa\,[v_m - v_{n+1}(t)] + \kappa\,[V(s) - v_m] + \lambda\boldsymbol{\Theta}(-\Delta v)(\Delta v) \quad (3\text{-}3)$$

The maximum acceleration rate of 9.8 m/s^2 (1g) – which can be exceeded by some modern supercars, such as Tesla Model S and Bugatti Veyron (Murphy et al., 1982; Wojdyla, 2011; Markus et al., 2017) – is adopted for bounding the possible acceleration and deceleration rates of all vehicles in the simulation. The value of the sensitivity parameter (λ) of 0 is applied in this algorithm to reflect the proposed submissive driving characteristics of the CAV; while the critical space headway (s_c) of 30 meters and the vehicle length of 4.5 meters were applied. The sensitivity constant (κ) of 0.30 is used, and the empirical values of C_1 and C_2 are adopted from the c-FVD model in section 2.2.1 (Yu et al., 2019; Qu et al., 2019); however, the values of the calibrated parameters V_1 and V_2 are modified as 32.000 and 1.997, respectively, based on the model calibration.

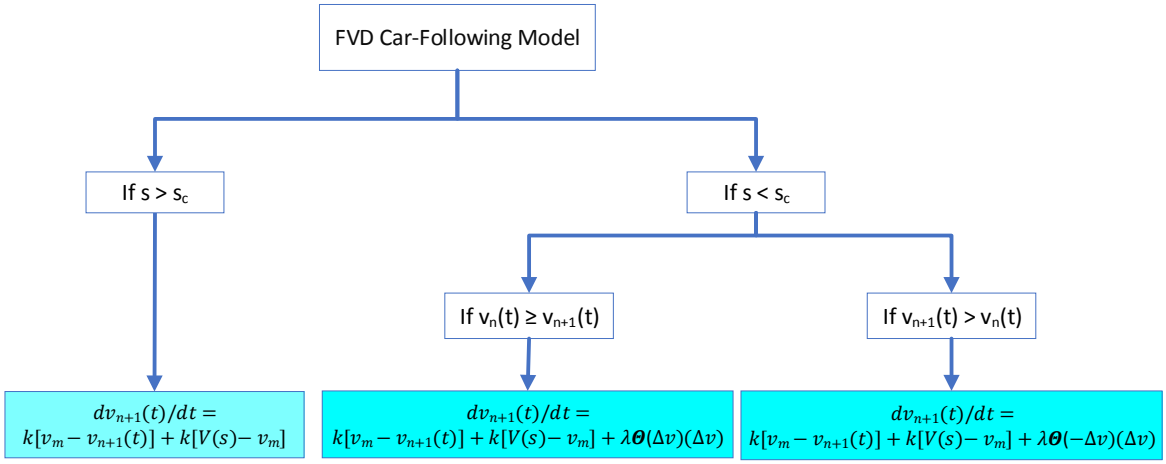

Figure 3-3 Flowchart of the car-following model

Next, after the subject vehicle accelerates based on the FVD model, the algorithm checks whether the leading vehicle still exists in the current lane (lane *i*). If the leading vehicle has just moved to the adjacent lane, the algorithm will restart to recheck the type of the leading vehicle and the instantaneous space headway between the subject vehicle and its leader. However, if the leading vehicle still exists in the current lane (lane *i*), the algorithm will check whether any vehicle from the adjacent lane is performing a lane-changing maneuver into lane *i* ahead of the subject vehicle, as illustrated in Figure 3-4.

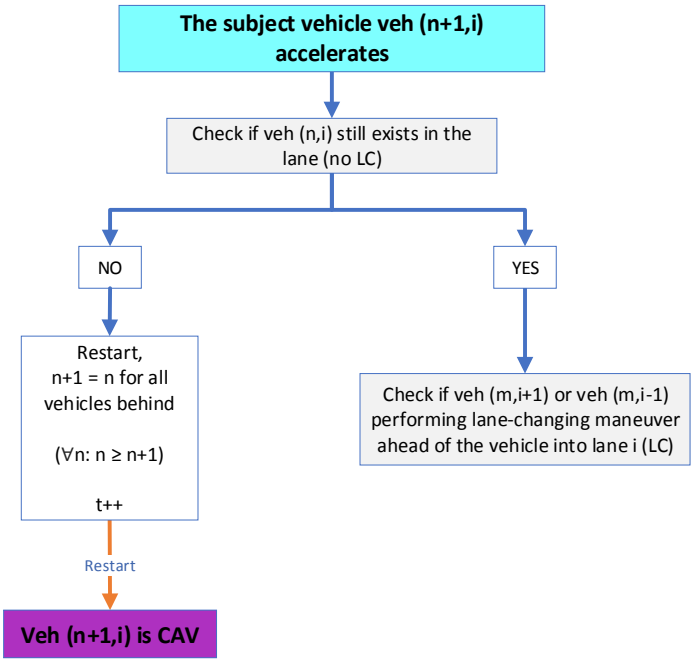

Figure 3-4 Process for checking the existence of the leading vehicle

If the leading vehicle still maintains its position in the current lane, the model will check whether a lane change is performing ahead by a vehicle from the adjacent lane (lane *i+1* or lane *i-1*). If so, the algorithm checks if the lane-changing vehicle is MDV or CAV. If the lane-changing vehicle is MDV, the algorithm restarts and the lane-changing vehicle will be the new leader for the subject vehicle. Furthermore, the order of the subject vehicle and all the vehicles behind in the platoon are moved down by one position to account for the lane-changing vehicle and the time step is counted forward by one second. If the lane-changing vehicle from the adjacent lane is CAV, the time step will also be forwarded by one second and the algorithm advances to check the longitudinal distance between the subject vehicle and the lane-changing vehicle to prepare for a gap-creation process that allows for the connected-environment lane change in the next phase. Otherwise, if no lane-changing maneuver is occurring, the algorithm checks if there is a lane drop within 0.8 km (2,640 ft), ahead of the vehicle, as seen in Figure 3-5.

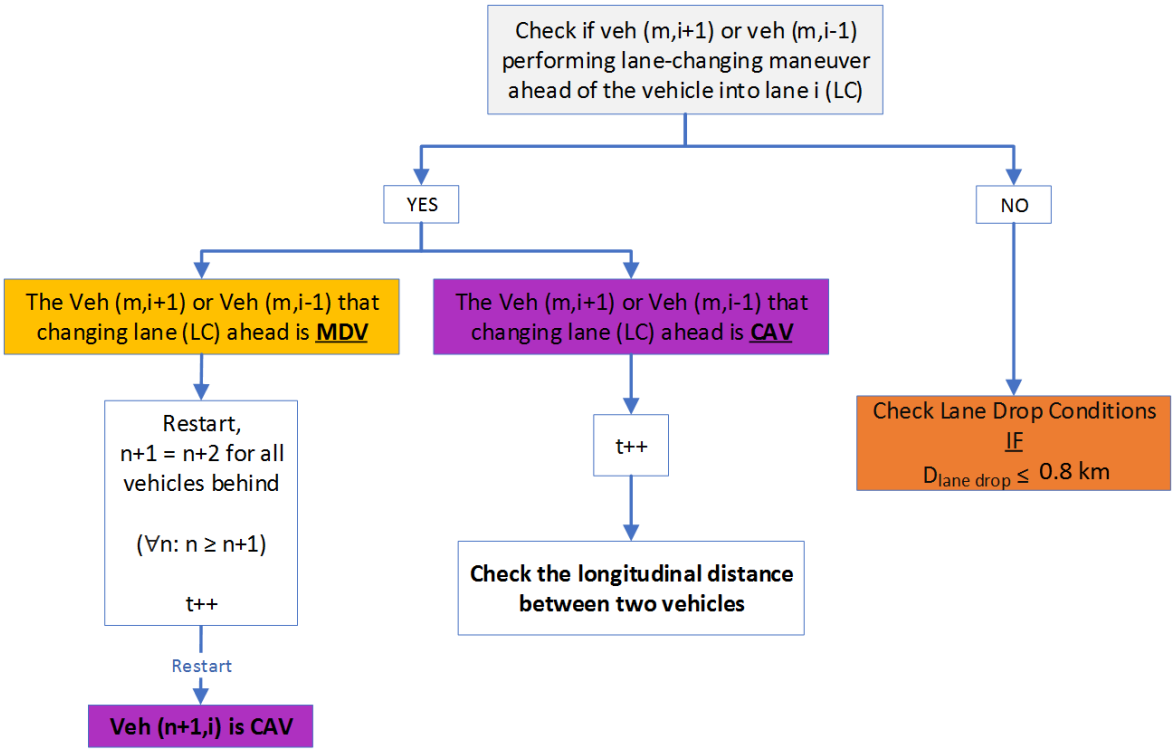

Figure 3-5 Process for checking the occurrence of lane-changing maneuver ahead of CAV

3.1.1.2 The CAV-CAV Cooperative Gap-Creation Model

If the lane-changing vehicle from the adjacent lane is CAV, the lane-changing process is programmed to occur in a cooperative manner. The algorithm checks the longitudinal distance

between the subject vehicle and the lane-changing vehicle. In this situation, there are two possible cases that can occur: case 1) the lane-changing vehicle is performing lane change from lane *i-1* to lane *i* and case 2) the lane-changing vehicle is performing lane change from lane *i+1* to lane *i*, as illustrated in Figure 3-6.

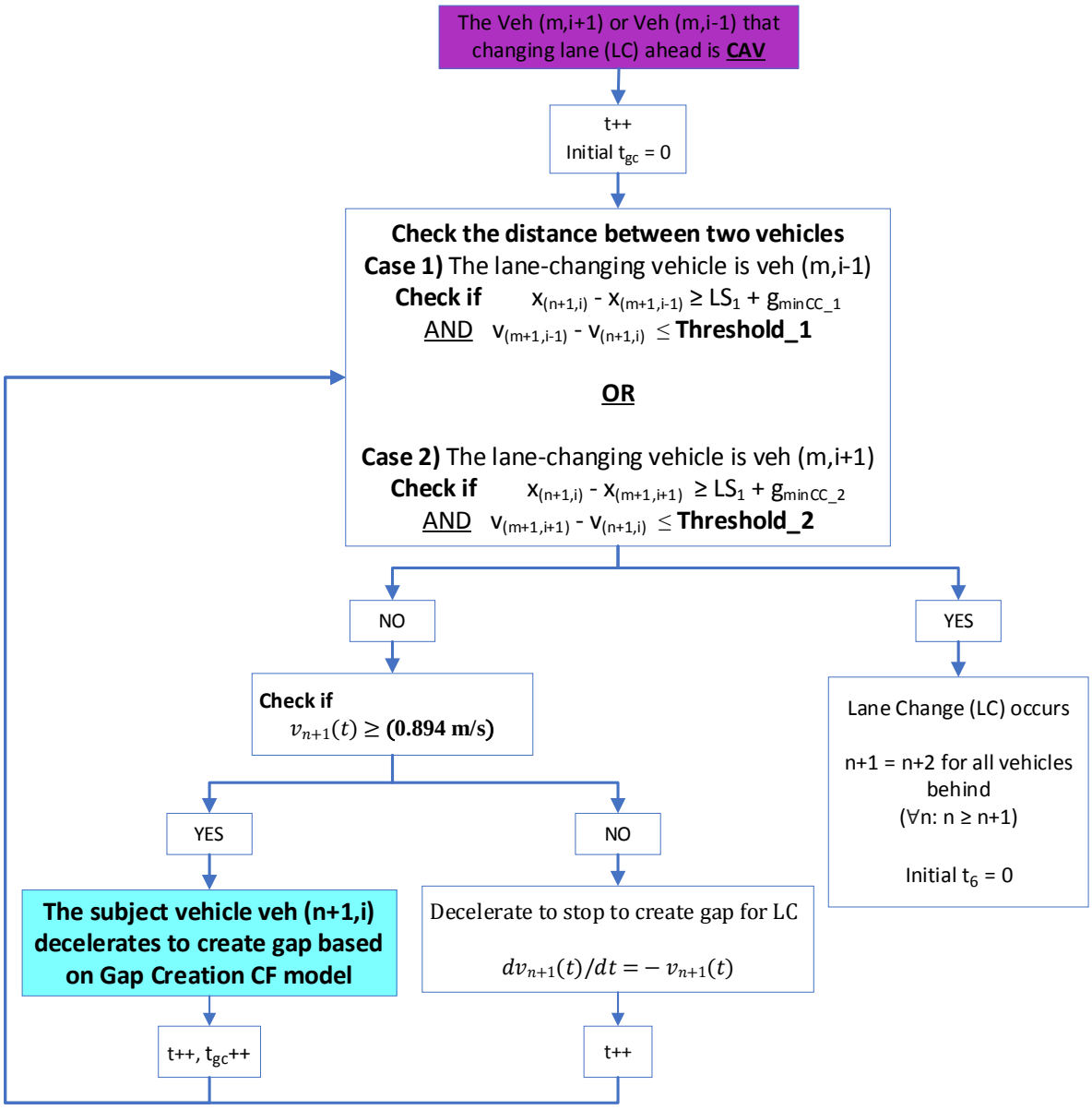

Figure 3-6 Flowchart of the CAV-CAV cooperative gap-creation model

For both cases, two conditions of longitudinal distance and velocity differences between the vehicles are checked prior to the initiation of lane change to ensure a safe and smooth lane-changing maneuver. Firstly, for the longitudinal distance difference, the algorithm examines if the

difference between the current longitudinal displacement of the lane-changing vehicle ($x_{(m+1, i-1)}$ or $x_{(m+1, i+1)}$) and the current longitudinal displacement of the subject vehicle ($x_{(n+1, i)}$) is greater than or equal to the length of the lane-changing vehicle (*LS*) plus a minimal safe constant gap (g_{min}), where $x_{(n+1, i)} \leq x_{(m+1, i+1)} \leq x_{(n+1, i)}$ or $x_{(n+1, i)} \leq x_{(m+1, i-1)} \leq x_{(n+1, i)}$, as displayed in the Equation (3-4a) and (3-4b). The values of g_{min} for the left-side and right-side lane changing in the simulation are assigned as g_{min_CC1} and g_{min_CC2}, respectively.

$$x_{(n+1, i)} - x_{(m+1, i-1)} \geq LS + g_{min}; \quad \text{for right-side lane changing} \tag{3-4a}$$

$$x_{(n+1, i)} - x_{(m+1, i+1)} \geq LS + g_{min}; \quad \text{for left-side lane changing} \tag{3-4b}$$

Secondly, for the velocity difference, the algorithm then inspects if the difference between the current velocity of the subject vehicle ($v_{(n+1, i)}$) and the current velocity of the lane-changing vehicle ($v_{(m+1, i-1)}$ or $v_{(m+1, i+1)}$) is less than or equal to a threshold, as displayed in the Equation (3-5a) and (3-5b).

$$v_{(n+1, i)} - v_{(m+1, i-1)} \geq Threshold\_1; \quad \text{for right-side lane changing} \tag{3-5a}$$

$$v_{(n+1, i)} - v_{(m+1, i+1)} \geq Threshold\_2; \quad \text{for left-side lane changing} \tag{3-5b}$$

If these two conditions are simultaneously true, the lane-changing maneuver will be triggered to occur in the next time step. The order of the subject vehicle and all vehicles in the platoon are moved down by one position to account for the lane-changing vehicle and the CAV-CAV lane change duration (t_6) of 6 seconds is initially set at zero. The CAV-CAV lane change duration was adopted from the literature (Hill et al., 2015).

However, for these two cases, if either the longitudinal distance difference and the velocity difference conditions or both turn out to be false, the algorithm will then proceed to check if the longitudinal velocity of the subject vehicle ($v_{n+1}(t)$) is greater or equal to 0.894 m/s (2 mph) prior to determining the deceleration rate of the vehicle to create a gap for the lane-changing maneuver. If the velocity of the subject vehicle is currently greater than 0.894 m/s; the vehicle will decelerate to create a gap based on the deceleration rate suggested by the gap-creation car-following model, which is discussed in the next paragraph. The time step then forwards by one second and the algorithm recalculates the longitudinal distance and velocity differences until these conditions are met. If the current velocity of the subject vehicle is smaller than 0.894 m/s, the vehicle decelerates

at the rate of $-v_{n+1}(t)$ mph. The algorithm proceeds to check the longitudinal distance difference and velocity difference conditions as a loop in the following time steps.

The gap-creation car-following model (Figure 3-7), is triggered when the current velocity of the subject vehicle is greater than 2 mph to prepare a sufficiently large gap for the lane-changing maneuver. The reason for reserving the minimum 3.22-km/h velocity for the subject vehicle in the gap-creation car-following model is to provide a safety factor for maintaining the positive velocity for the vehicle while decelerating to create gap. There are two possible cases: 1) the current leader (*veh(n, i)*) is CAV, and 2) the current leader is MDV.

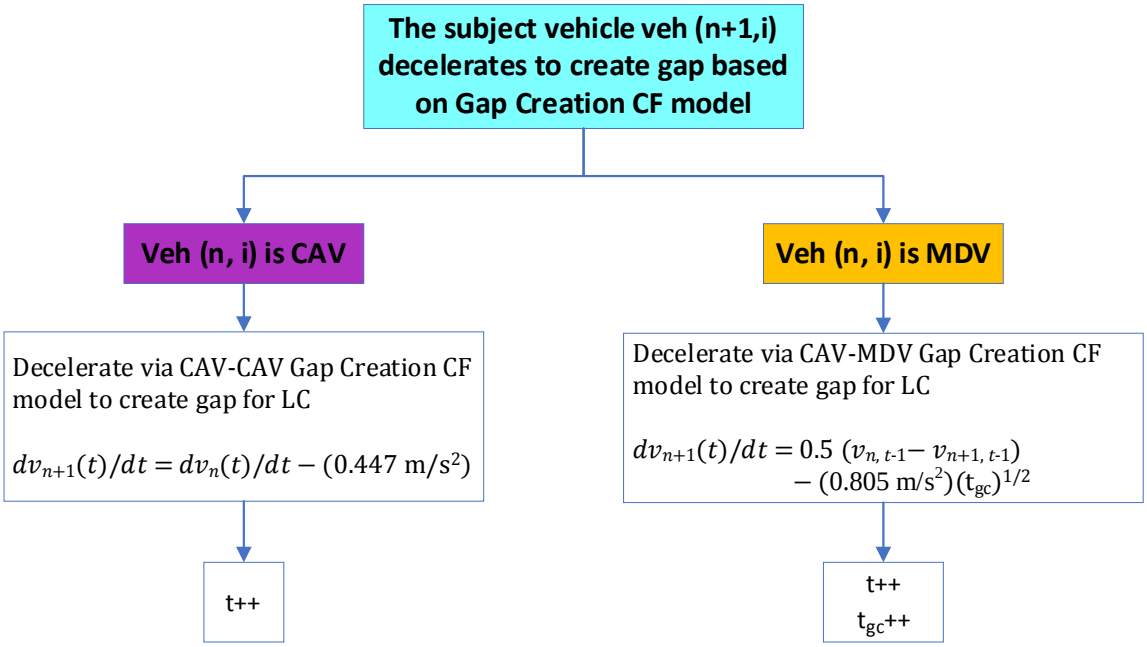

Figure 3-7 Flowchart of the CAV-CAV cooperative gap-creation model (cont.)

If the current leader is CAV, the CAV-CAV gap-creation car-following model starts by perceiving the projected longitudinal acceleration rate of its leading vehicle ($dv_n(t)/dt$) in the current time step under the connected environment. Next, it is followed by subtracting this acceleration rate by the deceleration rate of 0.447 m/s (1 mph/s) to yield the acceleration rate of the subject vehicle in that time step, according to Equation (3-6).

$$dv_{n+1}(t)/dt = dv_n(t)/dt - (0.447\ \text{m/s}^2) \quad (3\text{-}6)$$

The subject vehicle is programmed to pace at 0.447 m/s (1 mph) relatively slower than its current leading vehicle in each time step to create gap. Consequently, the additional gap of 0.447

meter multiplied by the number of time steps passed is expected to be provided when this model is applied.

If the current leader is MDV, where the connectivity between vehicles is not available, the subject vehicle is not able to precisely perceive the current longitudinal acceleration rate of its leader ($dv_n(t)/dt$) in real time. Consequently, the CAV-MDV gap-creation car-following model applies Equation (3-7) to determine the acceleration rate of the subject vehicle.

$$dv_{n+1}(t)/dt = 0.13\ (v_{n,\ t-1} - v_{n+1,\ t-1}) - (0.805\ \text{m/s}^2)(t_{gc})^{1/2} \quad (3\text{-}7)$$

where t_{gc} = the consolidated time in the gap-creation car-following model

This equation was tested and calibrated to yield similar results, in terms of longitudinal velocity and gap as a function of time, as that produced by the equation in the CAV-CAV car-following case. After this acceleration rate is applied, the time step (t) and the consolidated time in the gap-creation car-following model (t_{gc}) are counted by one second and the algorithm proceeds to recheck the updated conditions of the longitudinal distance and velocity differences between the vehicles at the beginning of this model as a loop until the conditions for the lane change are true.

If the longitudinal distance difference and velocity difference conditions simultaneously turn out to be true, as previously mentioned, the algorithm will then advance to the 6-second FVD car-following model where the new leader becomes the current lane-changing vehicle. Subsequently, the order of the subject vehicle and all the vehicles behind in the platoon are moved down by one position to account for the lane-changing vehicle and the duration for a CAV-CAV lane change (t_6) is set at zero.

This FVD car-following model is programmed to last for 6 seconds to allow the lane-changing vehicle to perform its lateral movement until it completely positions in the middle of the target lane (lane i). Same as the traditional FVD car-following model, this 6-second FVD model starts by checking the current space headway between the subject vehicle and its lane-changing vehicle. Then it checks the velocity difference between the vehicles to determine the acceleration rate for the subject vehicle in that time step, as shown in Figure 3-8.

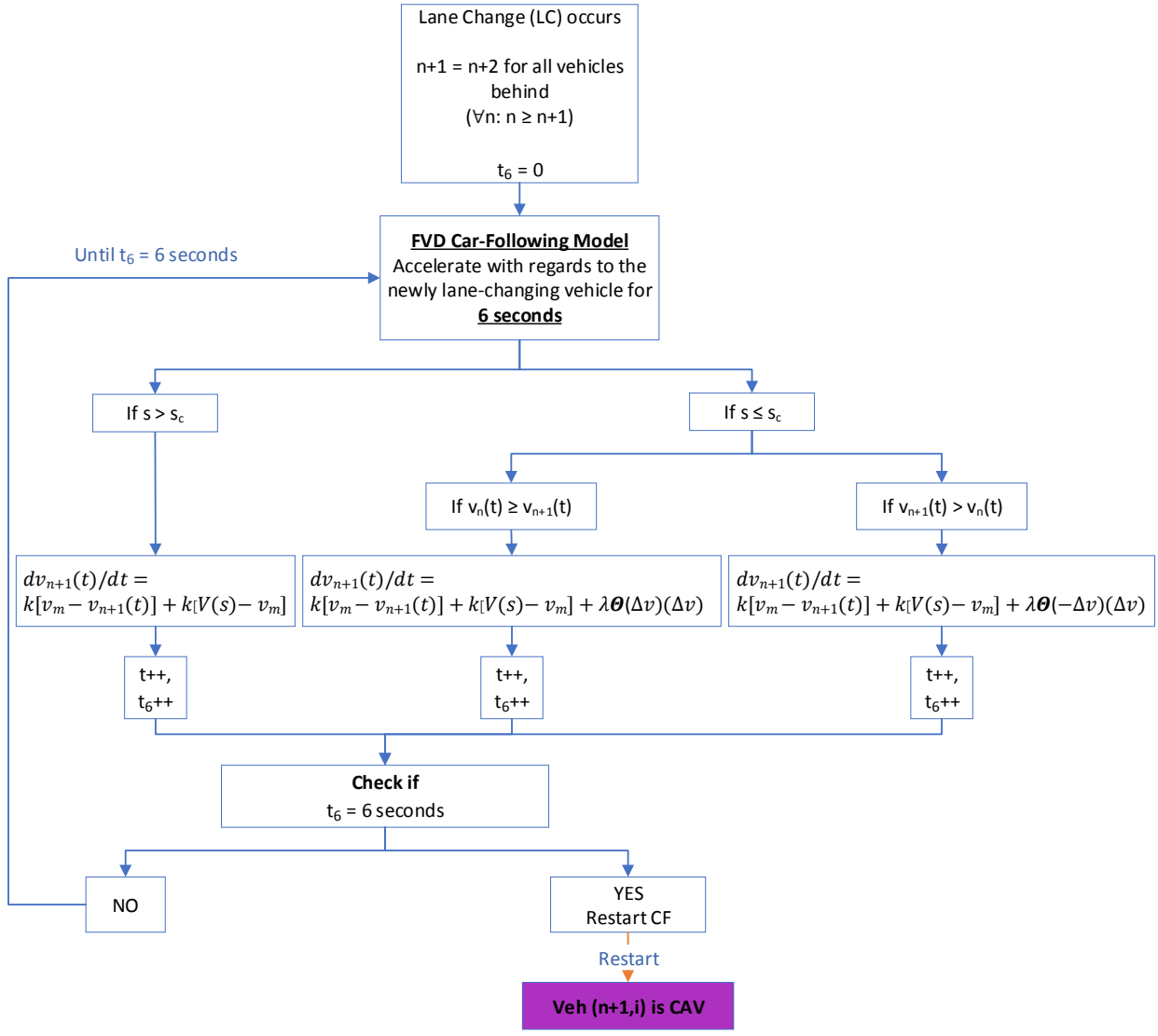

Figure 3-8 Car-following process as per the occurring cooperative CAV-CAV lane change

The acceleration rate of the vehicle in each time step is determined based on Equations (3-1), (3-2), or (3-3); depending on the car-following conditions in that time step. After the acceleration rate of the subject vehicle is determined, the time step (t) and the allowance time for a CAV-CAV lane change (t_6) are proceeded by one second. Next, the allowance time for a CAV-CAV lane change (t_6) is checked if the target of 6 seconds is reached. If so, it means that the lane-changing maneuver is completed, then the algorithm will be restarted. Otherwise, the algorithm returns back to check the current space headway (s) in this 6-second FVD car-following model as a loop until the final condition is true, as seen in Figure 3-8.

3.1.1.3 Linkage between the Car-Following and the Lane-Changing Models for CAVs

As it was shown in Figure 3-5, if there is no lane-changing maneuver, the algorithm checks if there is a lane drop within 0.8 km ahead of the vehicle. If there is no lane drop ahead, DLC conditions are examined next. However, if there is a lane drop ahead of the vehicle, the algorithm automatically performs MLC to the left. This model is considered as a linkage between the car-following and the lane-changing models.

If there is no lane drop within 0.8 km ahead of the subject vehicle, the algorithm proceeds to check the conditions for performing lane-changing to the right (slower lane). Three conditions were established to control that decision, and a lane change to the right occurs only if all three are satisfied.

Firstly, the difference between the average velocity of the current lane ($v_{AVG\ lane\_i}$) and the current velocity of the subject vehicle ($v_{n+1}(t)$) is checked. If the difference is greater than Threshold_3 shown in Equation (3-8), the output of this condition is returned as true.

$$v_{AVG\ lane\_i} - v_{n+1}(t) > Threshold\_3 \tag{3-8}$$

Secondly, if the difference between the average velocity of the current lane ($v_{AVG\ lane\_i}$) and the average velocity of the target lane on the right ($v_{AVG\ lane\_i\text{-}1}$) is greater than Threshold_4, as shown in Equation (3-9), the condition is met.

$$v_{AVG\ lane\_i} - v_{AVG\ lane\_i\text{-}1} > Threshold\_4 \tag{3-9}$$

Finally, if the difference between the current velocity of the leading vehicle in the current lane ($v_n(t)$) and the velocity of the subject vehicle ($v_{n+1}(t)$) exceeds by Threshold_5, as shown in Equation (3-10).

$$v_n(t) - v_{n+1}(t) > Threshold\_5 \tag{3-10}$$

If all of these conditions simultaneously turn out to be true, the lane-changing maneuver to the right lane (lane *i-1*) will be performed. Otherwise, the algorithm will proceed to check the conditions for performing lane-changing maneuver to the left (faster lane).

The decision for performing a lane change to the left will occur only if all three of the following conditions simultaneously turn out to be true.

Firstly, if the difference between the permitted maximum longitudinal velocity or the speed limit (v_m) and the current velocity of the subject vehicle ($v_{n+1}(t)$) is greater than Threshold_6, as seen in Equation (3-11), this condition will be returned as true.

$$v_{\mathrm{m}} - v_{n+1}(t) > Threshold\_6 \tag{3-11}$$

Secondly, if the difference between the average velocity of the target lane on the left ($v_{AVG\ lane\_i+1}$) and the average velocity of the current lane ($v_{AVG\ lane\_i}$) exceeds Threshold_7, as shown in the Equation (3-12), the condition is met.

$$v_{AVG\ lane\_i+1} - v_{AVG\ lane\_i} > Threshold\_7 \tag{3-12}$$

Finally, if the difference between the current velocity of the leading vehicle in the current lane ($v_n(t)$) and the velocity of the subject vehicle ($v_{n+1}(t)$) is less than Threshold_8, as shown in Equation (3-13), the condition is met.

$$v_n(t) - v_{n+1}(t) < Threshold\_8 \tag{3-13}$$

If all three of these conditions simultaneously turn out to be true, the lane-changing maneuver to the left lane (lane *i+1*) will be performed by the subject vehicle. Otherwise, the subject vehicle will remain in the current lane (lane *i*) and the algorithm will be restarted back to the beginning to recheck the type of the leading vehicle, as presented in Figure 3-9.

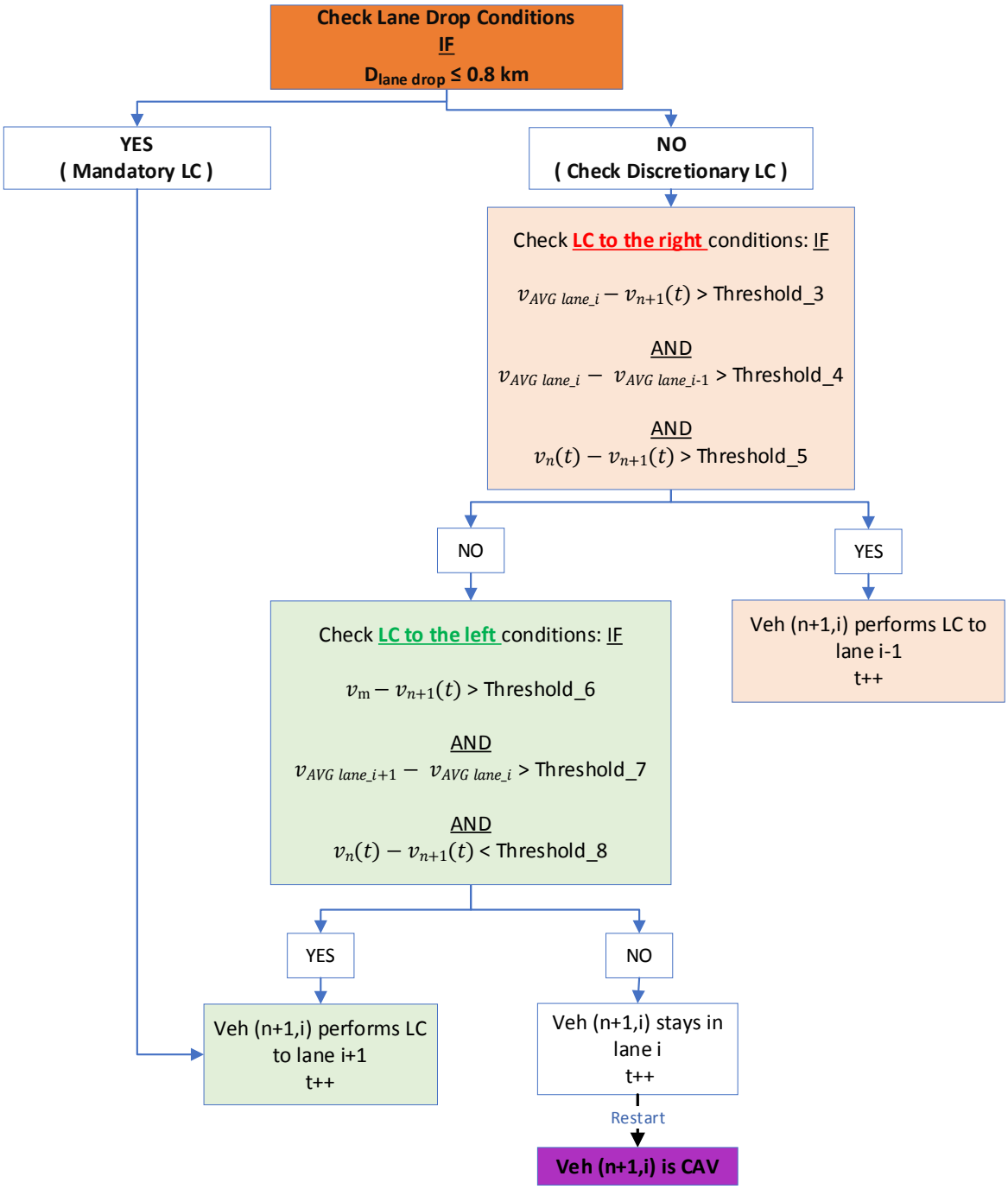

Figure 3-9 Linkage between the car-following and the lane-changing models for CAVs

3.1.1.4 The CAV-MDV Left-Lane-Changing Models

Two possible cases can occur if the subject vehicle is performing a lane change to the left: 1) the potential follower in the target lane (*veh(m+1, i+1)*) is MVD and 2) the potential follower in the target lane is CAV.

If the potential follower is MDV, the current gap on the target lane on the left (gap_{i+1}) is assessed in the next step. The current gap on the target lane on the left is defined as the difference in the longitudinal displacements between the rear-end of the potential leading vehicle ($x_{(m,i+1)}$ - LS) and the front-end of the potential follower ($x_{(m+1,i+1)}$), as displayed in Equation (3-14a).

$$gap_{i+1} = (x_{(m,i+1)} - LS) - x_{(m+1,i+1)}; \quad \text{where } x_{(m+1,\,i+1)} \leq x_{(n+1,\,i)} \leq x_{(m,\,i+1)} \tag{3-14a}$$

$$gap_{i-1} = (x_{(m,i-1)} - LS) - x_{(m+1,i-1)}; \quad \text{where } x_{(m+1,\,i-1)} \leq x_{(n+1,\,i)} \leq x_{(m,\,i-1)} \tag{3-14b}$$

There are three possible cases that can occur while the gap in the target lane is being assessed. Firstly, if the current gap in the target lane is greater than the minimum gap for free lane change ($gap_{i+1} \geq gap_{Free}$), the conditions for free lane change will be checked by the algorithm in the next step. Secondly, if the current gap in the target lane is smaller than the minimum gap for free lane change, but still greater than or equal to the length of the subject vehicle plus a minimal safe constant gap ($LS + g_{min} \leq gap_{i+1} < gap_{Free}$), the conditions for cooperative and competitive lane changes will be respectively checked in the next step. Finally, if the current gap in the target lane is smaller than the length of the subject vehicle plus a minimal safe constant gap ($gap_{i+1} < g_{min} + LS$), the subject vehicle will be made to assess the next gap and the process will be restarted, as illustrated in Figure 3-10.

Next, if the algorithm detects that the current gap on the target lane is available for a free lane change ($gap_{i+1} \geq gap_{Free}$), two conditions of longitudinal distance and velocity differences between the subject vehicle and the potential follower in the target lane will be checked prior to the initiation of lane change to ensure for a safe lane-changing maneuver.

Firstly, for the longitudinal distance difference (lag gap), the algorithm assesses if the difference between the current longitudinal displacement of the subject vehicle ($x_{(n+1,\,i)}$) and the current longitudinal displacement of the potential follower in the target lane ($x_{(m+1,\,i+1)}$) is greater than or equal to the length of the lane-changing vehicle (LS) plus a minimal safe constant gap (g_{min}), as shown in Equation (3-4b). The corresponding value of g_{min} in this case is assigned as g_{min_CM9} in the simulation models.

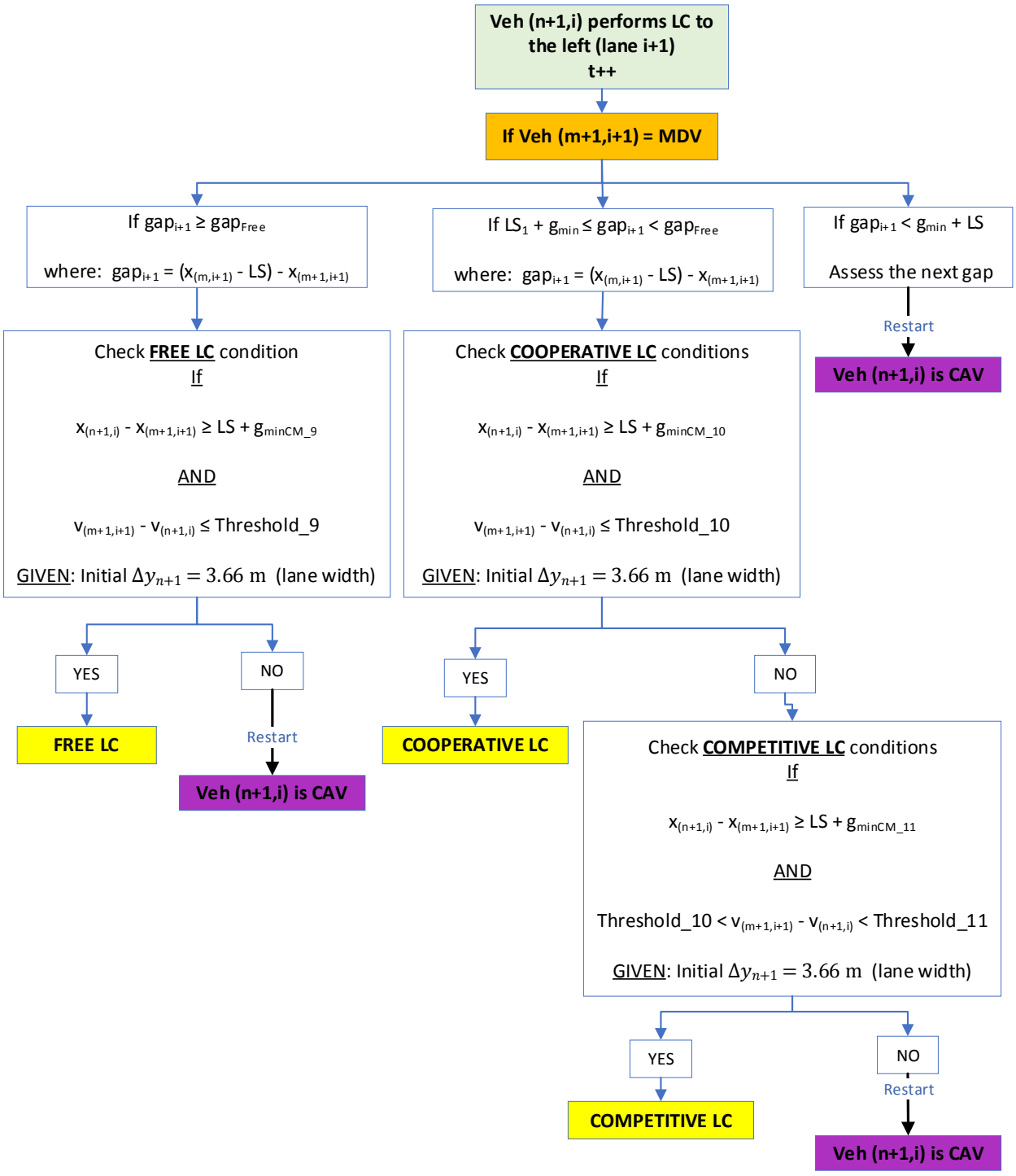

Figure 3-10 Flowchart of the CAV-MDV left-lane-changing model

Secondly, the algorithm assesses if the difference between the current velocity of the subject vehicle ($v_{(n+1,\,i)}$) and the current velocity of the potential follower in the target lane ($v_{(m+1,\,i+1)}$) is less than or equal to the threshold, as presented in Equation (3-15).

$v_{(m+1,\,i+1)} - v_{(n+1,\,i)} \le Threshold\_9$ (3-15)

If both of these conditions are true, the free lane-changing maneuver to the left will be initiated by the subject vehicle in the next step. In addition, the anticipated lateral displacement for a lane change (Δy_{n+1}) will be initiated as 3.66 m (12 ft), which is the lane width used in the model. Otherwise, the subject vehicle will assess the next gap and the process will restart, as shown in Figure 3-10. The CAV-MDV free left-lane-changing model is illustrated in Figure 3-11.

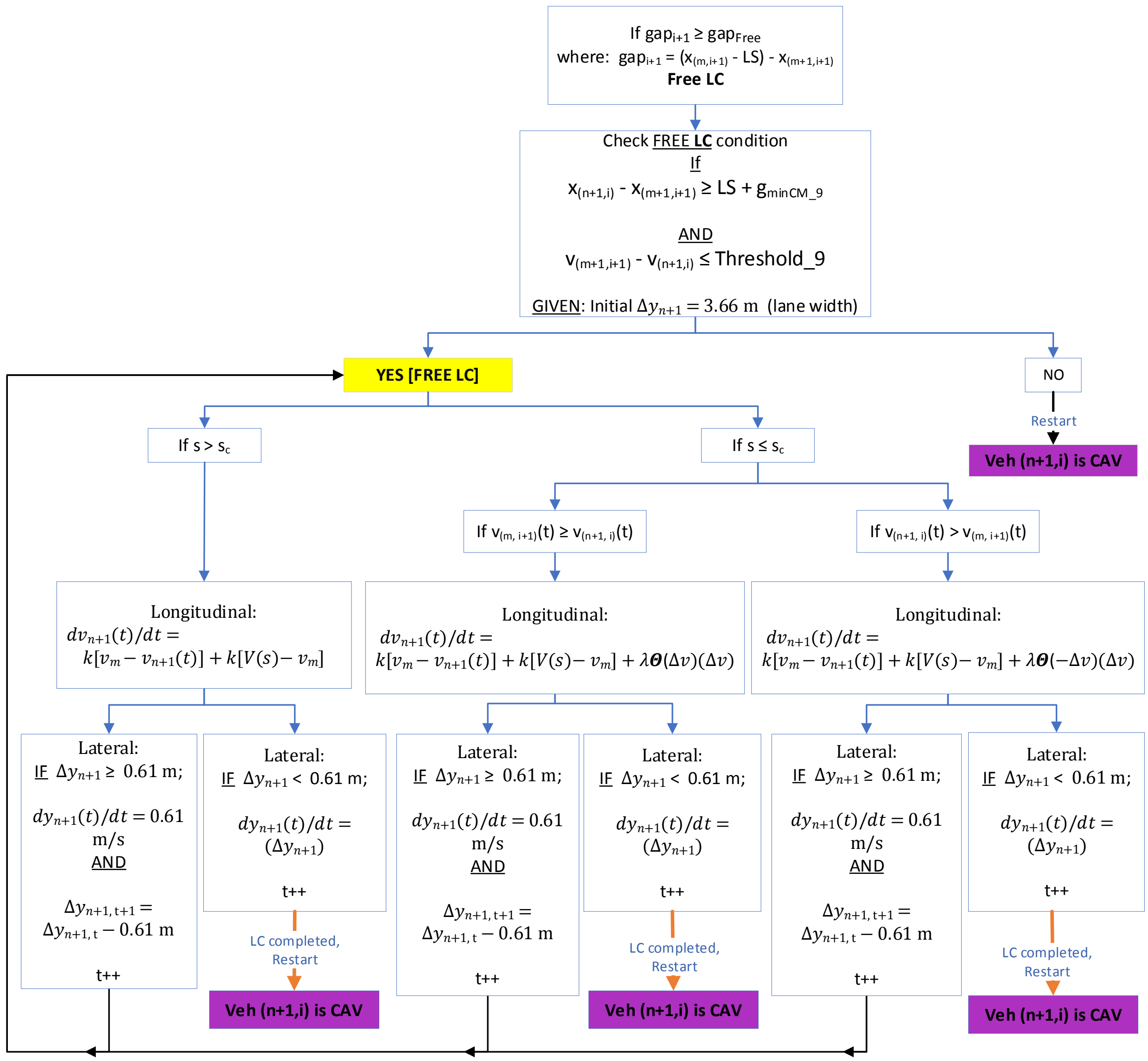

Figure 3-11 CAV-MDV free left-lane-changing model

Similarly, if the current gap on the target lane is available for a cooperative lane change ($LS + g_{min} \le gap_{i+1} < gap_{Free}$), the lag gap between the subject vehicle and the potential follower in

the target lane are assessed, as shown in Equation (3-4b). The corresponding value of g_{min} in this case is assigned as g_{min_CM10}. Secondly, the algorithm then assesses if the difference between the current velocity of the subject vehicle ($v_{(n+1,\,i)}$) and the current velocity of the potential follower in the target lane ($v_{(m+1,\,i+1)}$) is less than or equal to the threshold, as presented in the Equation (3-16).

$$v_{(m+1,\,i+1)} - v_{(n+1,\,i)} \leq Threshold\_10 \qquad (3\text{-}16)$$

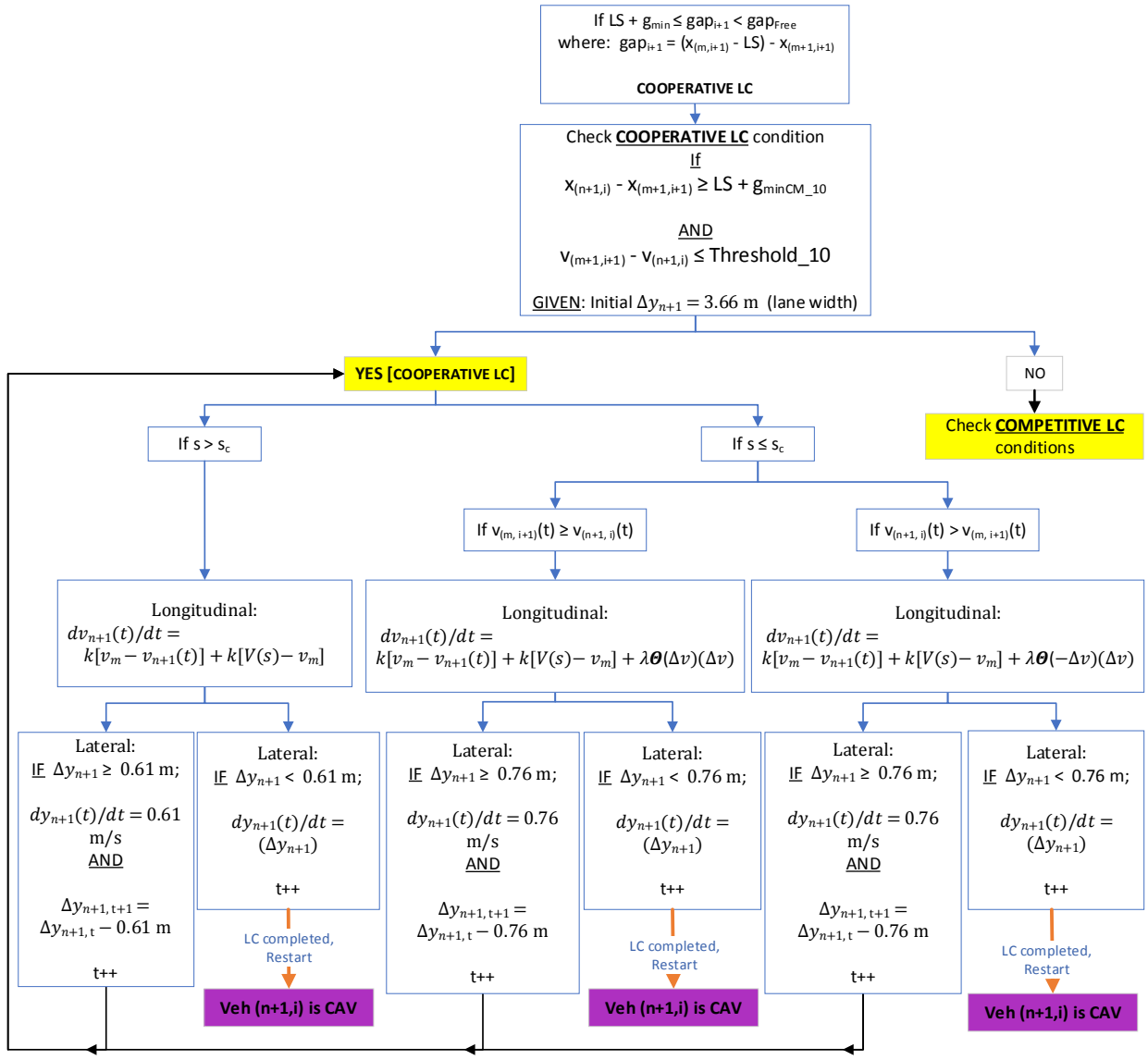

Figure 3-12 CAV-MDV cooperative left-lane-changing model

If both of these conditions simultaneously become true, the cooperative lane-changing maneuver to the left will be initiated by the subject vehicle in the next step. Otherwise, the subject

vehicle will check for the competitive lane change conditions, as presented in Figure 3-10. The CAV-MDV cooperative left-lane-changing model is shown in Figure 3-12.

The competitive lane change conditions are assessed in case the cooperative lane change conditions are false. There are two conditions of longitudinal distance and velocity differences; however, the form of the velocity difference condition is different from that in the free and cooperative lane change conditions.

Firstly, the algorithm assesses if the lag gap is greater than or equal to $LS + g_{min}$, as shown in Equation (3-4b). The corresponding value of g_{min} in this case is assigned as g_{min_CM11}. Secondly, for the velocity difference, the algorithm then inspects if the difference between the current velocity of the subject vehicle ($v_{(n+1,\ i)}$) and the current velocity of the potential follower in the target lane ($v_{(m+1,\ i+1)}$) falls between these thresholds, as presented in Equation (3-17).

$$Threshold\_10 < v_{(m+1,\ i+1)} - v_{(n+1,\ i)} < Threshold\_11 \quad (3\text{-}17)$$

If both of these conditions simultaneously are true, the competitive lane-changing maneuver to the left will be initiated by the subject vehicle in the next step. Otherwise, the subject vehicle will assess the next gap and the process will be restarted back to the beginning of the algorithm, as seen in Figure 3-10. The CAV-MDV competitive left-lane-changing model is illustrated in Figure 3-13.

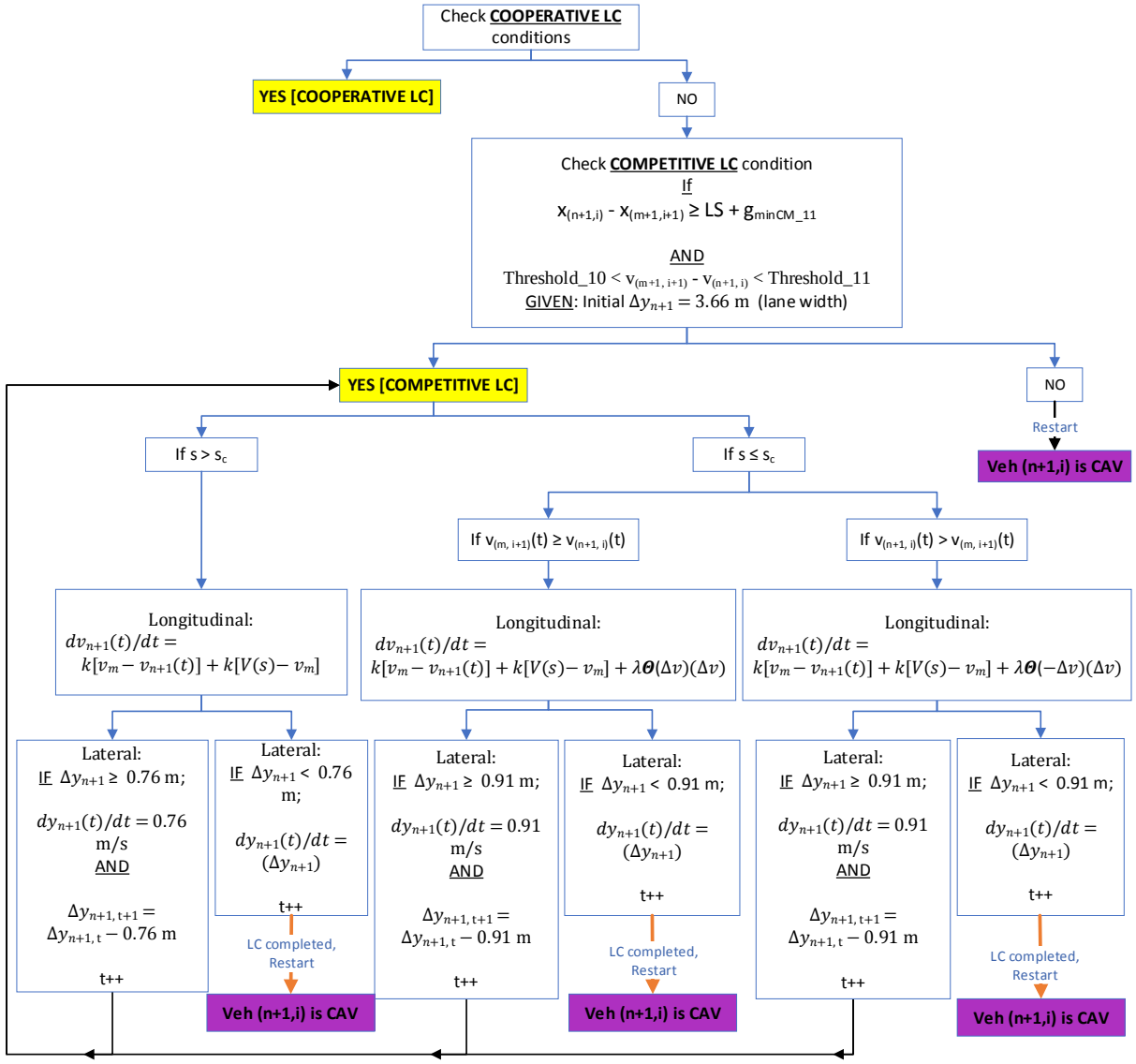

Figure 3-13 CAV-MDV competitive left-lane-changing model

The lane-changing models were developed based on the concept used in the FVD car-following model for the longitudinal movement of the subject vehicle, with the application of the lateral movement conditions to generate the two-dimensional trajectory for the vehicle. The model runs as a loop to produce the longitudinal and lateral accelerations in each time step until the lane-changing process is completed when the vehicle is settled in the middle of the target lane.

All the CAV-MDV left-lane-changing models begin with the car-following part by checking the current space headway (s) with the critical space headway (s_c), followed by assessing the longitudinal velocity difference between the subject vehicle ($v_{(n+1,\,i)}(t)$) and the potential leading vehicle in the target lane ($v_{(m,\,i+1)}(t)$), prior to determining the longitudinal acceleration for

the vehicle in the current time step. The acceleration rate of the subject vehicle in each time step is determined based on the FVD car-following model by applying Equations (3-1), (3-2), or (3-3); depending on the car-following conditions in that time step.

Since the longitudinal acceleration of the subject vehicle is calculated, the model then determines the lateral velocity of the vehicle based on the remaining anticipated lateral displacement for lane change (Δy_{n+1}), which is initially set as 3.66 m (12 ft) by the beginning of the lane-changing process. In each time step, the anticipated lateral displacement for a lane change (Δy_{n+1}) is offset by the lateral displacement that the vehicle traverses while changing lanes to yield the remaining anticipated lateral displacement for a lane change for the next time step.

If the remaining anticipated lateral displacement for a lane change in the time step is greater than or equal to α m ($\Delta y_{n+1} \geq \alpha$ m), where α is the default lateral displacement in the current case; the lateral velocity of the subject vehicle in that time step will be α m/s, as illustrated by Equation (3-18).

$$dy_{n+1}(t)/dt = \alpha \text{ m/s} \tag{3-18}$$

It means that the vehicle will be displaced in the lateral direction by α m by the end of the time step. Therefore, the remaining anticipated lateral displacement for a lane change for the next time step ($\Delta y_{n+1,\, t+1}$) will be the previous anticipated lateral displacement for a lane change ($\Delta y_{n+1,\, t}$) subtracted by the distance of α m, as displayed by Equation (3-19).

$$\Delta y_{n+1,\, t+1} = \Delta y_{n+1,\, t} - \alpha \text{ m} \tag{3-19}$$

The default lateral velocity of the subject vehicle is 0.61 m/s (α = 0.61 m/s) for all cases in the CAV-MDV free left-lane-changing model, as seen in Figure 3-11. In the CAV-MDV cooperative left-lane-changing model, the default lateral velocity of the subject vehicle is 0.61 m/s (α = 0.61 m/s) when the current space headway between the subject vehicle and its leader is greater than the critical space headway ($s > s_c$); whereas the default lateral velocity of the subject vehicle is 0.76 m/s (α = 0.76 m/s) when the current space headway is smaller than or equal to the critical space headway ($s \leq s_c$), as seen in Figure 3-12. However, in the CAV-MDV competitive left-lane-changing model, the default lateral velocity of the subject vehicle is 0.76 m/s (α = 0.76 m/s) when the current space headway is greater than the critical space headway ($s > s_c$); while the default

lateral velocity of the subject vehicle is 0.91 m/s (α = 0.91 m/s) when the current space headway is smaller than or equal to the critical space headway ($s \leq s_c$), as seen in Figure 3-13.

This loop runs until the remaining anticipated lateral displacement for lane change (Δy_{n+1}) in that time step is smaller than the default lateral displacement in the current case where the space headway and velocity difference conditions fall into ($\Delta y_{n+1} < \alpha$ m). In this phase, the calculated lateral velocity of the subject vehicle in that time step is Δy_{n+1} m/s, as displayed by Equation (3-20), so that the vehicle can complete its lane-changing maneuver by positioning in the middle of the target lane.

$$dy_{n+1}(t)/dt = (\Delta y_{n+1}) \text{ m/s} \quad (3\text{-}20)$$

3.1.1.5 The CAV-CAV Left-Lane-Changing Models

If the subject vehicle is anticipated to have a CAV as a potential follower in the target lane, the CAV-CAV left-lane-changing model will be triggered. Fundamentally, the structure of this model is similar to the CAV-MDV left-lane-changing model; however, the competitive lane-changing interaction between CAVs was not programmed to occur. The reason is that the CAV-CAV lane-changing maneuvers are expected to occur only in cooperative characteristics by utilizing the benefits of a connected environment to maximize traffic safety.

At the beginning of this model, the current gap on the target lane on the left (gap_{i+1}) is assessed by the algorithm; as determined by Equation (3-14a). The current gap is then used to identify whether the anticipated lane-changing maneuver is a free lane change ($gap_{i+1} \geq gap_{Free}$), cooperative lane change ($LS + g_{min} \leq gap_{i+1} < gap_{Free}$), or the next gap needs to be assessed prior to the emergence of the lane-changing maneuver ($gap_{i+1} < g_{min} + LS$), as shown in Figure 3-14.

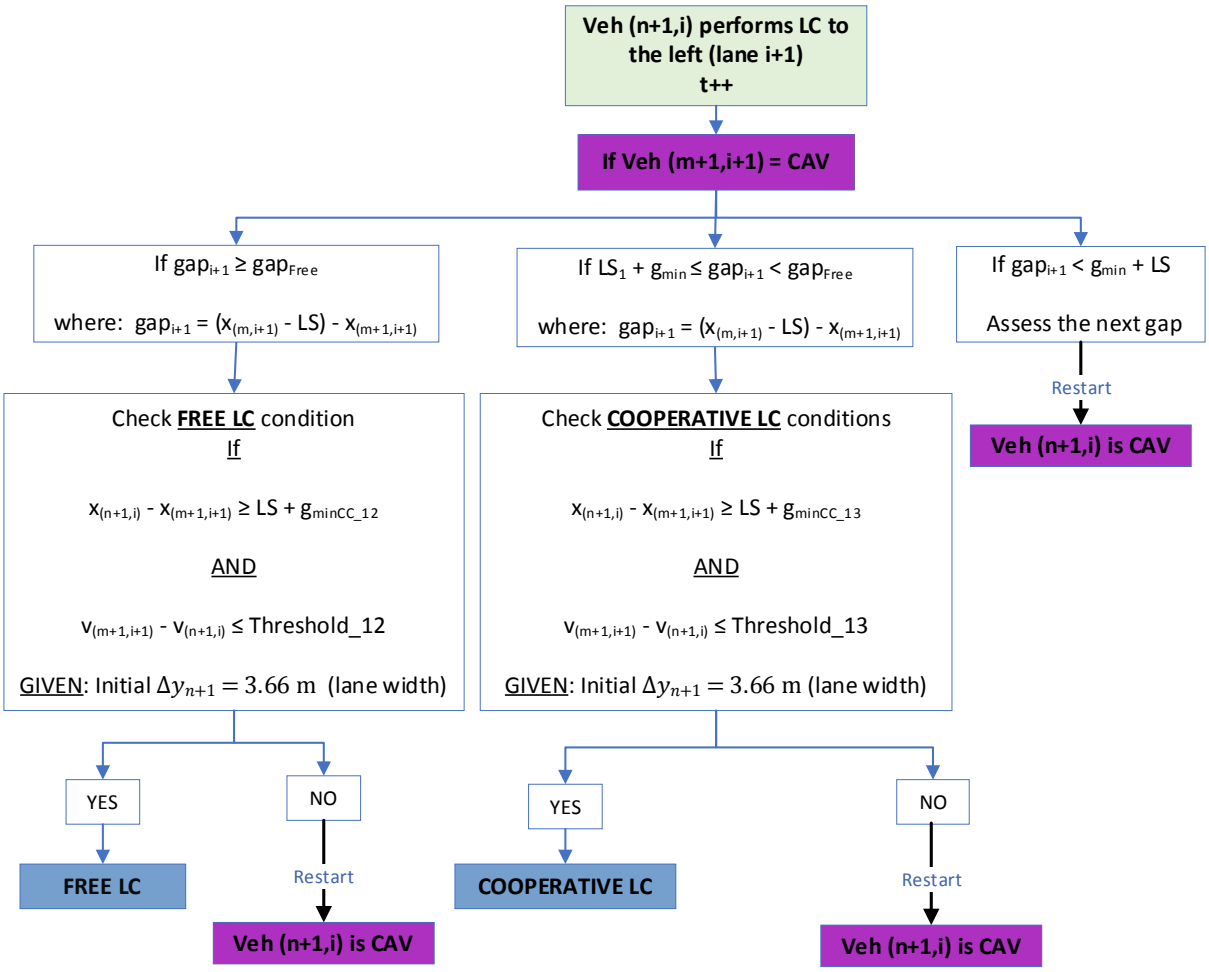

Figure 3-14 Flowchart of the CAV-CAV left-lane-changing model

In case the algorithm detects that the current gap in the target lane is available for a free lane change ($gap_{i+1} \geq gap_{Free}$), firstly, the lag gap is assessed based on Equation (3-4b). The corresponding value of g_{min} is assigned as g_{min_CC12}. Secondly, the velocity difference between the subject vehicle and the potential follower is assessed, as displayed in Equation (3-21).

$$v_{(m+1,\, i+1)} - v_{(n+1,\, i)} \leq Threshold\_12 \tag{3-21}$$

If both of these conditions simultaneously turn out to be true, the free lane-changing maneuver to the left lane (lane $i+1$) will be initiated. Otherwise, the subject vehicle will assess the next gap, as presented in Figure 3-14. The CAV-CAV free left-lane-changing model is illustrated in Figure 3-15.

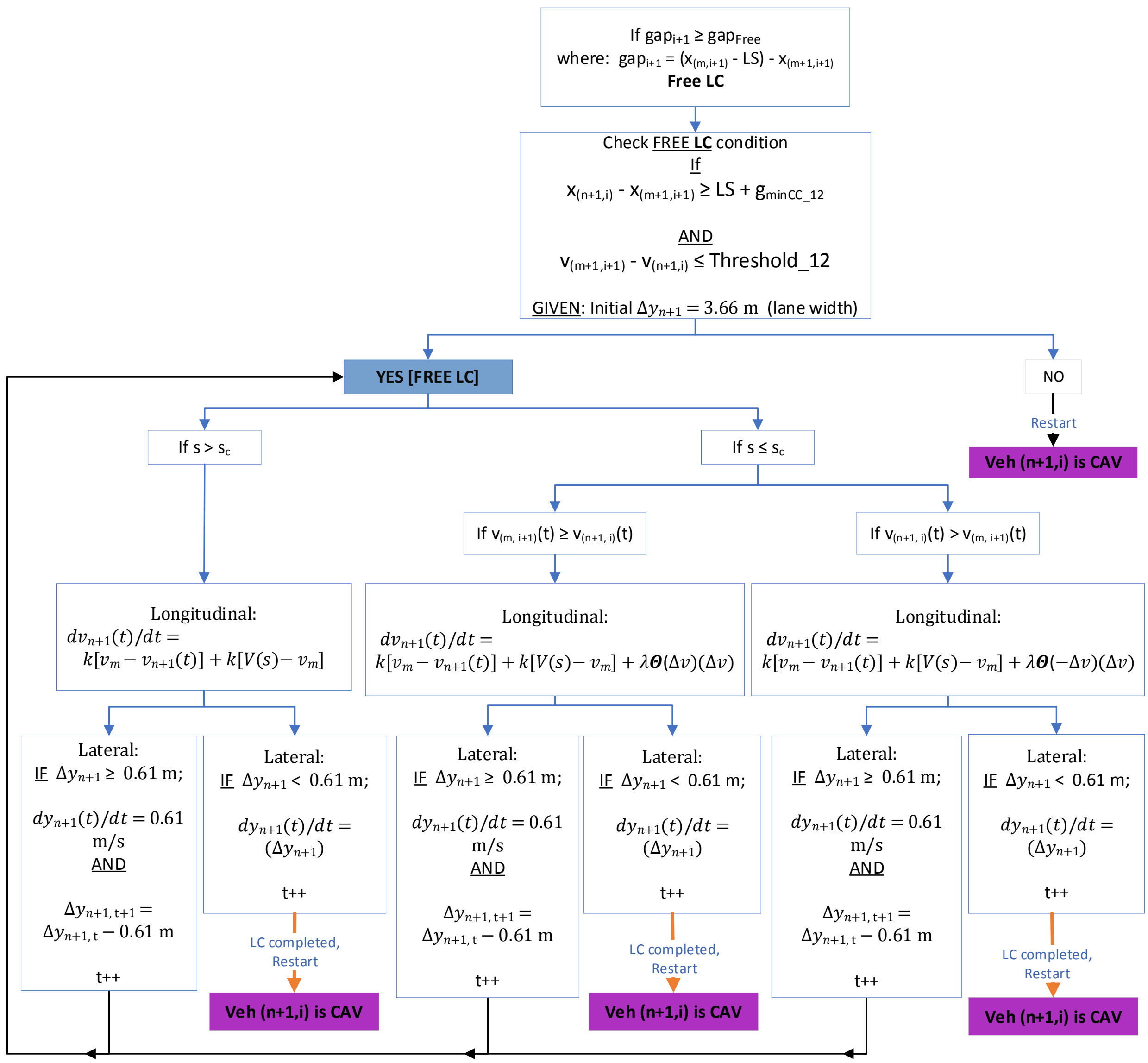

Figure 3-15 CAV- CAV free left-lane-changing model

Similarly, if the current gap on the target lane is available for a cooperative lane change ($LS + g_{min} \leq gap_{i+1} < gap_{Free}$), the lag gap will be assessed based on Equation (3-4b). The corresponding value of g_{min} in this case is g_{min_CC13}. Secondly, the velocity difference between the subject vehicle and the potential follower is examined, as presented in Equation (3-22).

$$v_{(m+1,\, i+1)} - v_{(n+1,\, i)} \leq Threshold\_13 \qquad (3\text{-}22)$$

If both of these conditions are true, the cooperative lane-changing maneuver to the left lane (lane $i+1$) will be initiated. Otherwise, the subject vehicle will assess the next gap, as illustrated in Figure 3-14. The CAV-CAV cooperative left-lane-changing model is illustrated in Figure 3-16.

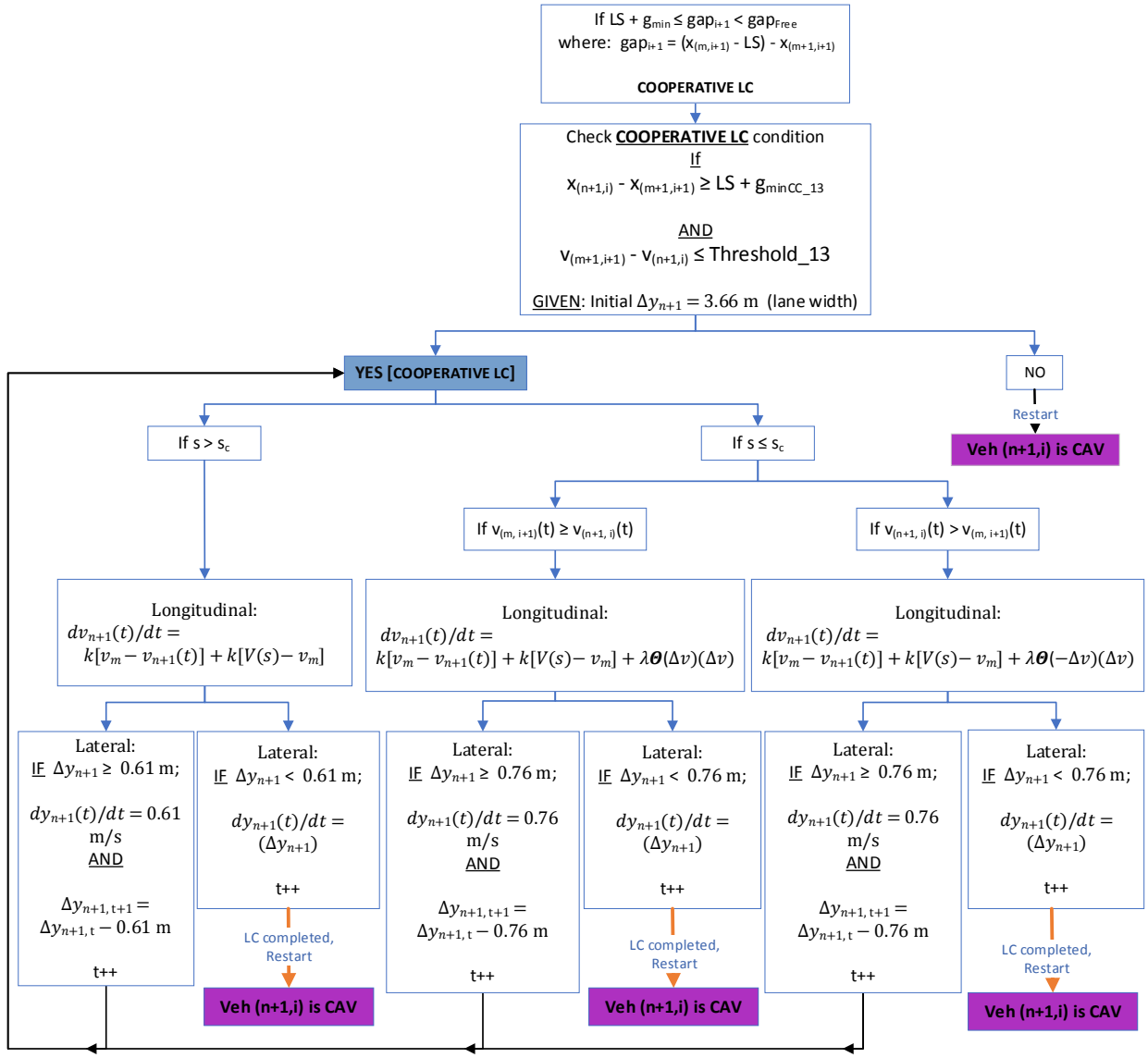

Figure 3-16 CAV- CAV cooperative left-lane-changing model

All the CAV-CAV left-lane-changing models also begin with the car-following part. The acceleration rate of the subject vehicle in each time step is also determined based on the FVD car-following model by adopting Equations (3-1), (3-2), or (3-3); depending on the car-following conditions in that time step.

Once the longitudinal acceleration of the subject vehicle is calculated, the model then determines the lateral velocity of the vehicle based on Equation (3-19). The default lateral velocity of the subject vehicle is 0.61 m/s (α = 0.61 m/s) for all cases in the CAV-CAV free left-lane-changing model, as seen in Figure 3-15. However, in the CAV-CAV cooperative left-lane-changing model, the default lateral velocity of the subject vehicle is 0.61 m/s (α = 0.61 m/s) when

the current space headway between the subject vehicle and its leader is greater than the critical space headway ($s > s_c$); whereas the default lateral velocity of the subject vehicle is 0.76 m/s (α = 0.76 m/s) when the current space headway is smaller than or equal to the critical space headway ($s \leq s_c$), as seen in Figure 3-16.

3.1.1.6 The CAV-MDV Right-Lane-Changing Models

If the lane drop condition is assessed and it turns out that there is currently no lane drop within the distance of 0.8 km ahead of the subject vehicle; the algorithm will then proceed to check the conditions for performing lane-changing maneuver to the right, which is the slower lane. Next, if three of the right-lane-changing conditions simultaneously turn out to be true, the lane-changing maneuver to the right lane (lane *i-1*) will be performed by the subject vehicle. There are two possible cases that can occur under this category: 1) the potential follower in the target lane is MVD and 2) the potential follower in the target lane is CAV, as presented in Figure 3-17.

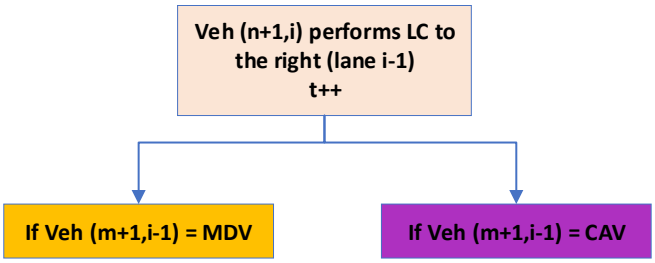

Figure 3-17 Two possible cases in the CAV-MDV right-lane-changing model

If the anticipated lane change falls into the category that the potential follower in the target lane is MDV, first of all, the current gap in the target lane on the right (gap_{i-1}) will be assessed by the algorithm in the next step based on Equation (3-14b). Next, the current gap is used to identify whether the anticipated lane-changing maneuver is a free lane change ($gap_{i-1} \geq gap_{Free}$), a cooperative and competitive lane changes ($LS + g_{min} \leq gap_{i-1} < gap_{Free}$), or the next gap needs to be assessed prior to the occurrence of the lane change ($gap_{i-1} < g_{min} + LS$), as shown in Figure 3-18.

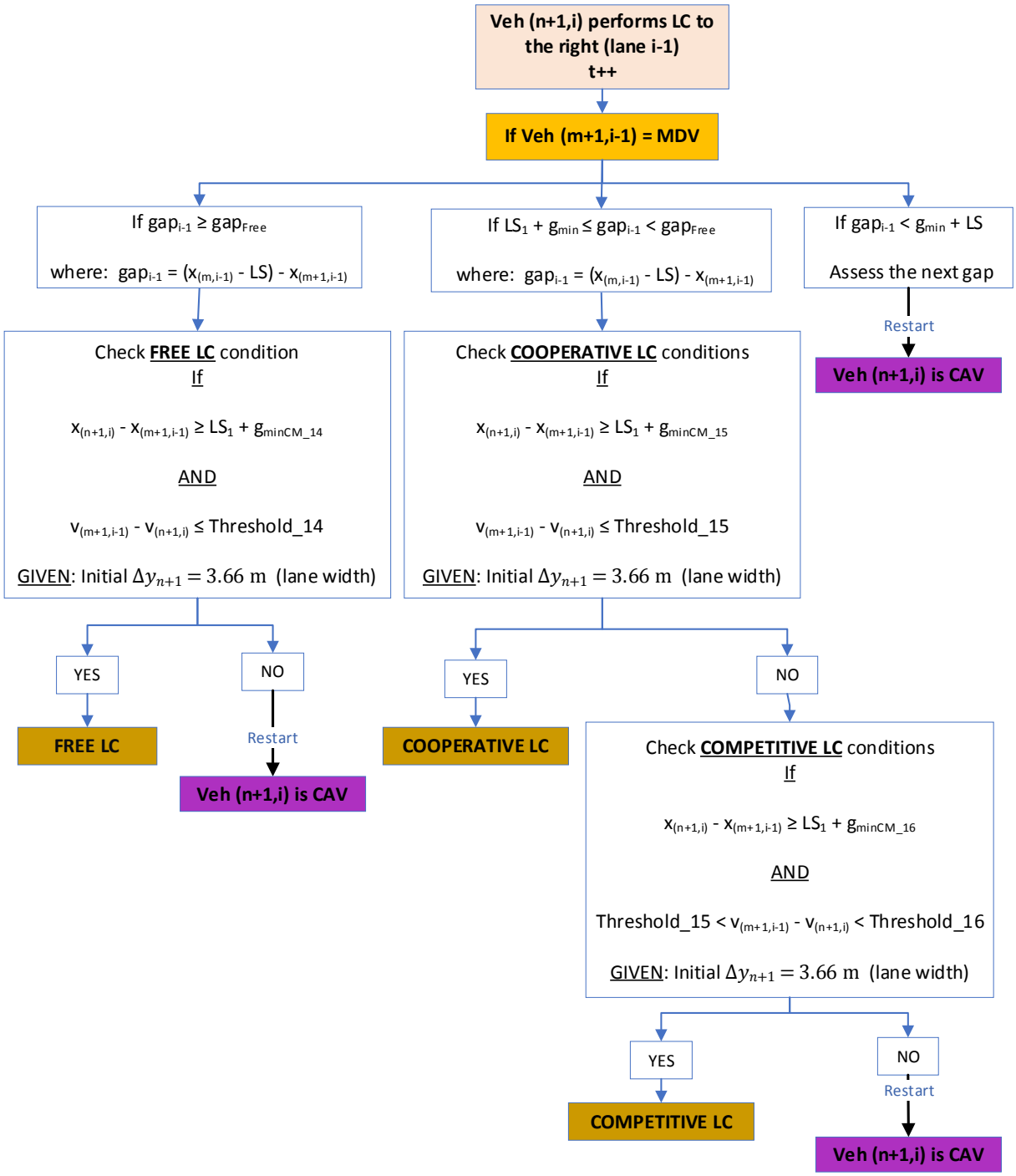

Figure 3-18 Flowchart of the CAV-MDV right-lane-changing model

If the current gap in the target lane is available for a free lane change ($gap_{i-1} \geq gap_{Free}$), firstly, the algorithm will assess if the lag gap is greater than or equal to $LS + g_{min}$, as shown in Equation (3-4a). The corresponding value of g_{min} in this case is assigned as g_{min_CM14} in the simulation models.

Secondly, the velocity difference between the subject vehicle and the potential follower in the target lane is assessed, as presented in Equation (3-23).

$$v_{(m+1,\ i-1)} - v_{(n+1,\ i)} \leq Threshold\_14 \qquad (3\text{-}23)$$

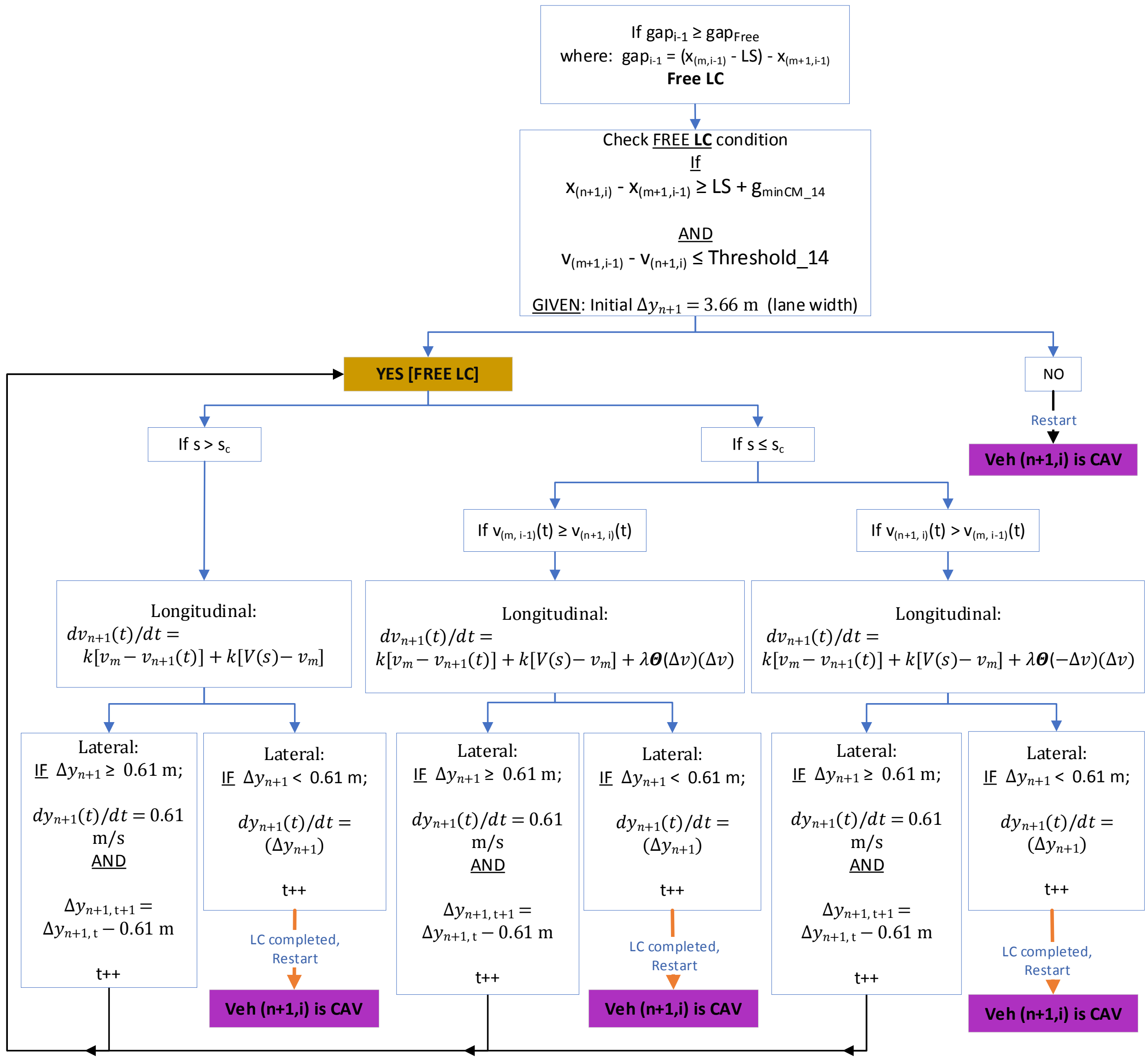

Figure 3-19 CAV-MDV free right-lane-changing model

If both of the conditions simultaneously turn to be true, the free lane-changing maneuver to the right lane (lane *i-1*) will be initiated by the subject vehicle in the next step. Otherwise, the subject vehicle will assess the next gap and the process will restart back to the beginning of the algorithm to recheck the type of the leading vehicle, as presented in Figure 3-19.

Similarly, if the current gap in the target lane is detected to be available for a cooperative lane change ($LS + g_{min} \leq gap_{i-1} < gap_{Free}$), firstly, the lag gap will be assessed using Equation (3-4a). The corresponding value of g_{min} in this case is assigned as g_{min_CM15} in the simulation models. Secondly, the velocity difference between the subject vehicle and the potential follower is assessed, as displayed in Equation (3-24).

$$v_{(m+1,\,i-1)} - v_{(n+1,\,i)} \leq Threshold\_15 \qquad (3\text{-}24)$$

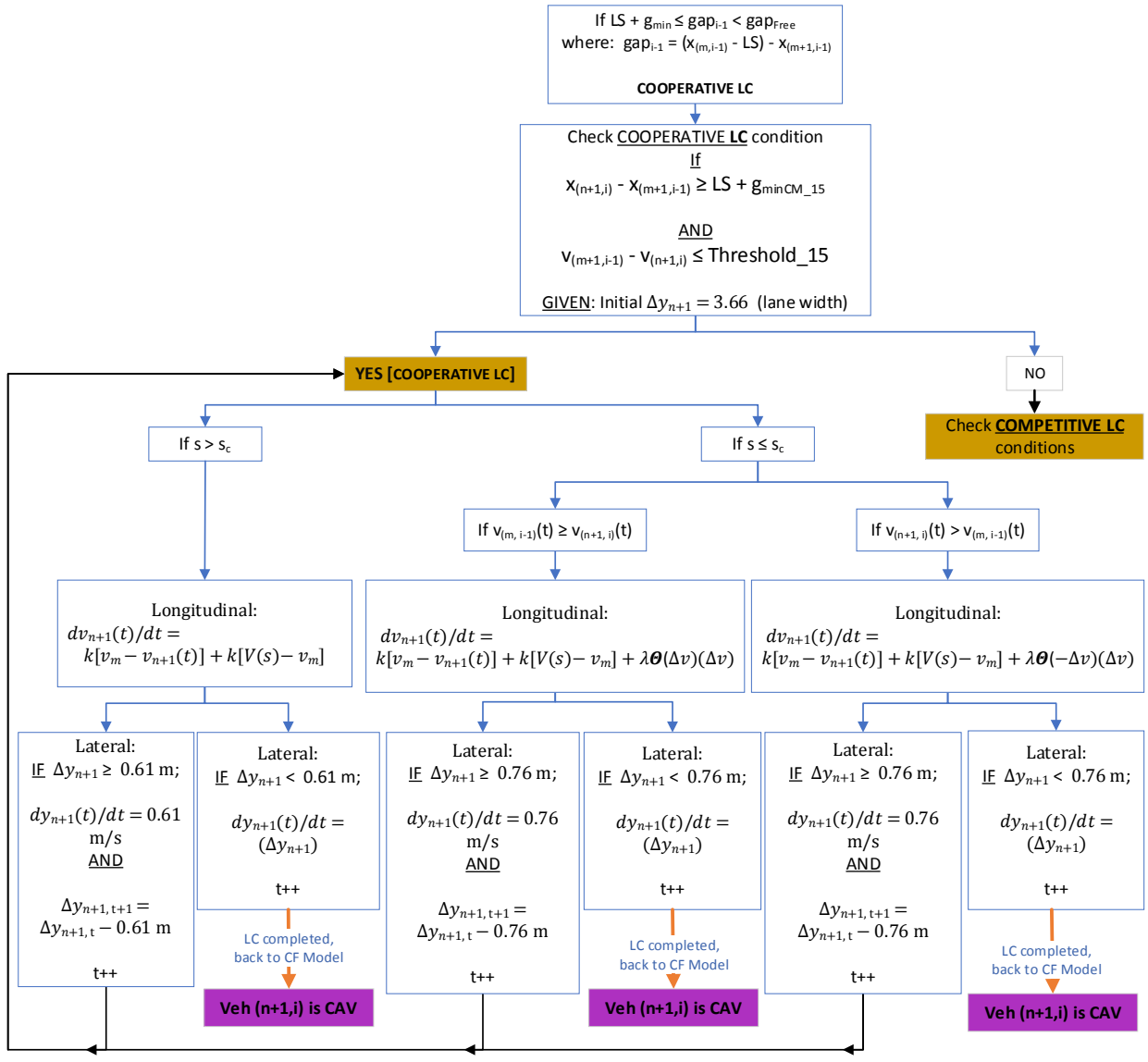

Figure 3-20 CAV-MDV cooperative right-lane-changing model

If both of these conditions simultaneously turn to be true, the cooperative lane-changing maneuver to the right lane (lane *i*-1) will be initiated by the subject vehicle in the next step. Otherwise, the competitive lane change conditions will be checked, as presented in Figure 3-20.

The competitive lane change conditions are assessed in case the cooperative lane change conditions are false. Similarly, there are two conditions of longitudinal distance and velocity differences between the subject vehicle and the potential follower in the target lane. However, the form of the velocity difference condition is different from those in the free and cooperative lane change conditions, as illustrated in Figure 3-21.

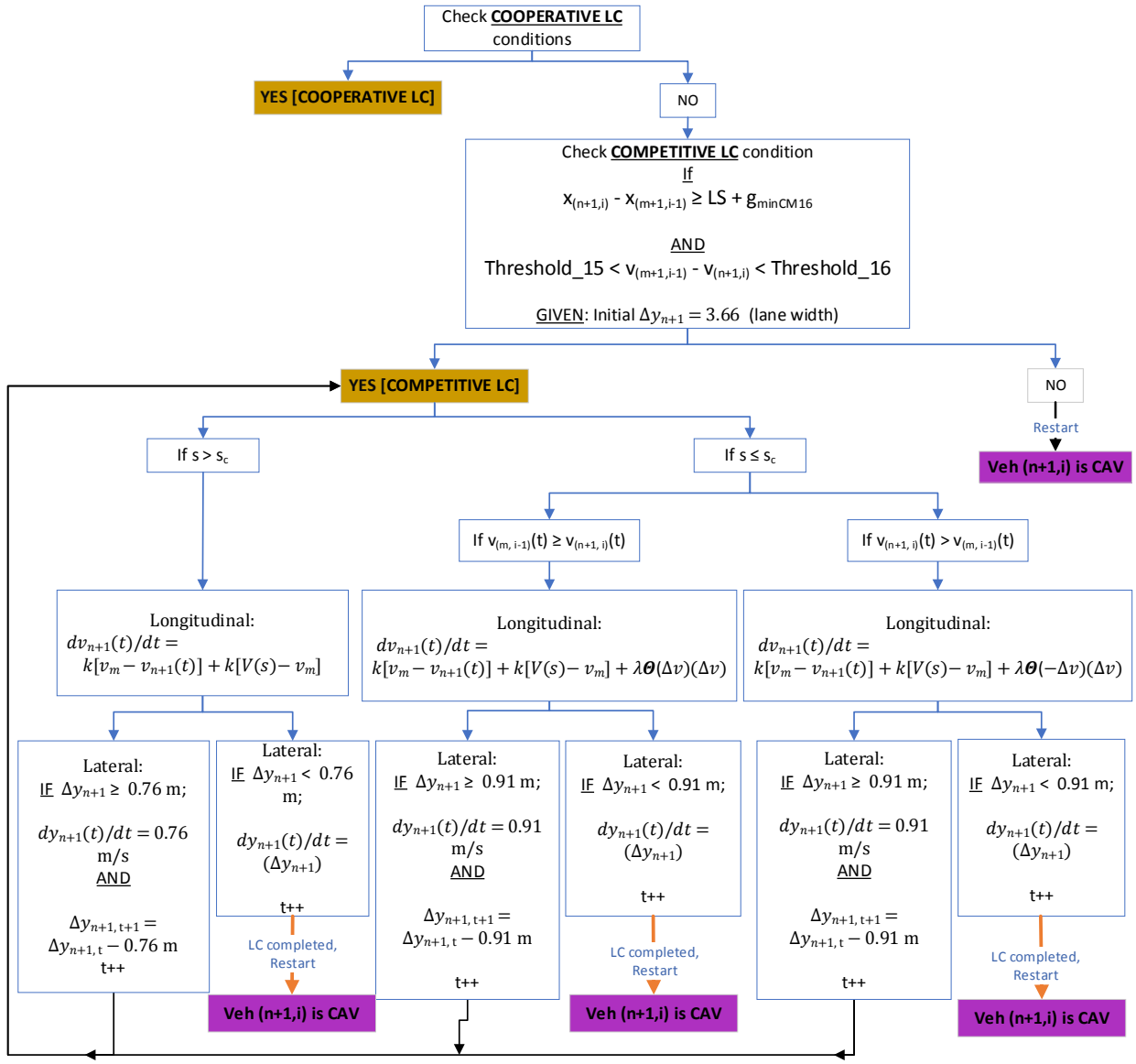

Figure 3-21 CAV-MDV competitive right-lane-changing model

Firstly, the lag gap is assessed based on Equation (3-4a). The corresponding value of g_{min} in this case is assigned as g_{min_CM16} in the simulation models. Secondly, the algorithm then inspects the velocity difference between the subject vehicle and the potential follower, as presented in Equation (3-25).

$$Threshold\_15 < v_{(m+1,\, i+1)} - v_{(n+1,\, i)} < Threshold\_16 \quad (3\text{-}25)$$

If both of these conditions simultaneously turn out to be true, the competitive lane-changing maneuver to the right lane (lane *i-1*) will be initiated by the subject vehicle in the next step. Otherwise, the next gap will be assessed and the algorithm will restart back to the beginning to recheck the type of the leading vehicle.

All the CAV-MDV right-lane-changing models also begin with the car-following part. The acceleration rate of the subject vehicle in each time step is also determined based on the FVD car-following model by adopting Equations (3-1), (3-2), or (3-3); depending on the car-following conditions in that time step. Once the longitudinal acceleration of the subject vehicle is calculated, the model then determines the lateral velocity of the vehicle based on Equation (3-19). The default lateral velocity of the subject vehicle is 0.61 m/s (α = 0.61 m/s) for all cases in the CAV-MDV free right-lane-changing model, as seen in Figure 3-19. In the CAV-MDV cooperative right-lane-changing model, the default lateral velocity of the subject vehicle is 0.61 m/s (α = 0.61 m/s) when the current space headway between the subject vehicle and its leader is greater than the critical space headway ($s > s_c$); whereas the default lateral velocity of the subject vehicle is 0.76 m/s (α = 0.76 m/s) when the current space headway is smaller than or equal to the critical space headway ($s \leq s_c$), as seen in Figure 3-20. However, in the CAV-MDV competitive right-lane-changing model, the default lateral velocity of the subject vehicle is 0.76 m/s (α = 0.76 m/s) when the current space headway is greater than the critical space headway ($s > s_c$); while the default lateral velocity of the subject vehicle is 0.91 m/s (α = 0.91 m/s) when the current space headway is smaller than or equal to the critical space headway ($s \leq s_c$), as seen in Figure 3-21.

3.1.1.7 The CAV-CAV Right-Lane-Changing Models

On the other hand, if the anticipated lane change is in the situation that the potential follower is CAV, the CAV-CAV right-lane-changing model will be activated. The structure of this model is similar to the CAV-MDV right-lane-changing model; however, the competitive lane-changing interaction between CAVs was not programmed to occur. Again, the reason is that the

CAV-CAV lane-changing maneuvers are expected to occur only in cooperative characteristics by utilizing the benefits of connected environment to maximize traffic safety.

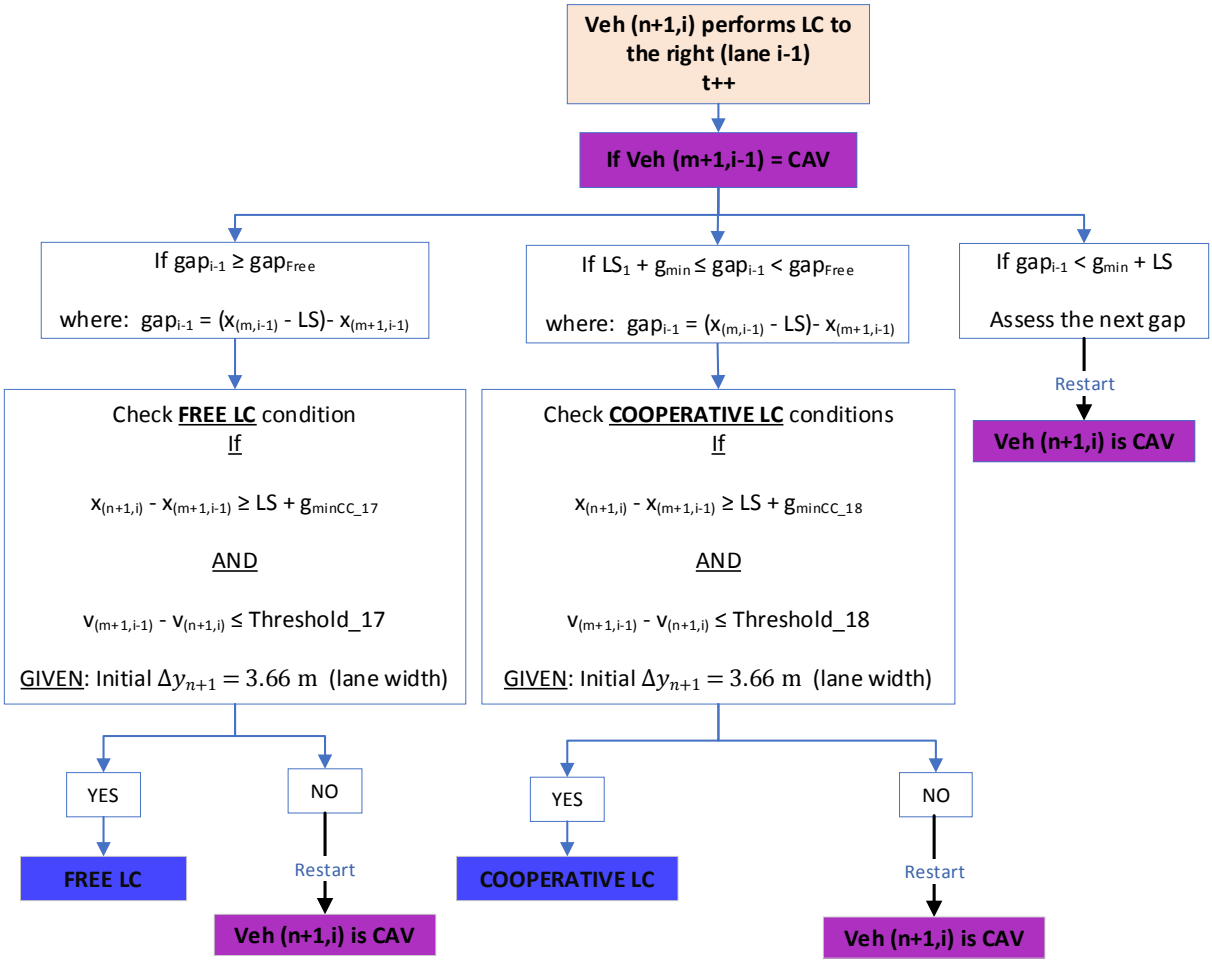

Figure 3-22 Flowchart of the CAV-CAV right-lane-changing model

First of all, the current gap in the target lane on the left (gap_{i-1}) is assessed by the algorithm; as determined by Equation (3-14b). The current gap is then used to identify the potential type of the lane change, as shown in Figure 3-22.

Next, if the algorithm detects that the current gap in the target lane is available for a free lane change ($gap_{i-1} \geq gap_{Free}$), firstly, the lag gap is assessed based on Equation (3-4a). The corresponding value of g_{min} in this case is assigned as g_{min_CC17} in the simulation models. Secondly, the velocity difference between the subject vehicle and the potential follower is assessed, as displayed in Equation (3-26).

$$v_{(m+1,\,i-1)} - v_{(n+1,\,i)} \leq Threshold\_17 \quad (3\text{-}26)$$

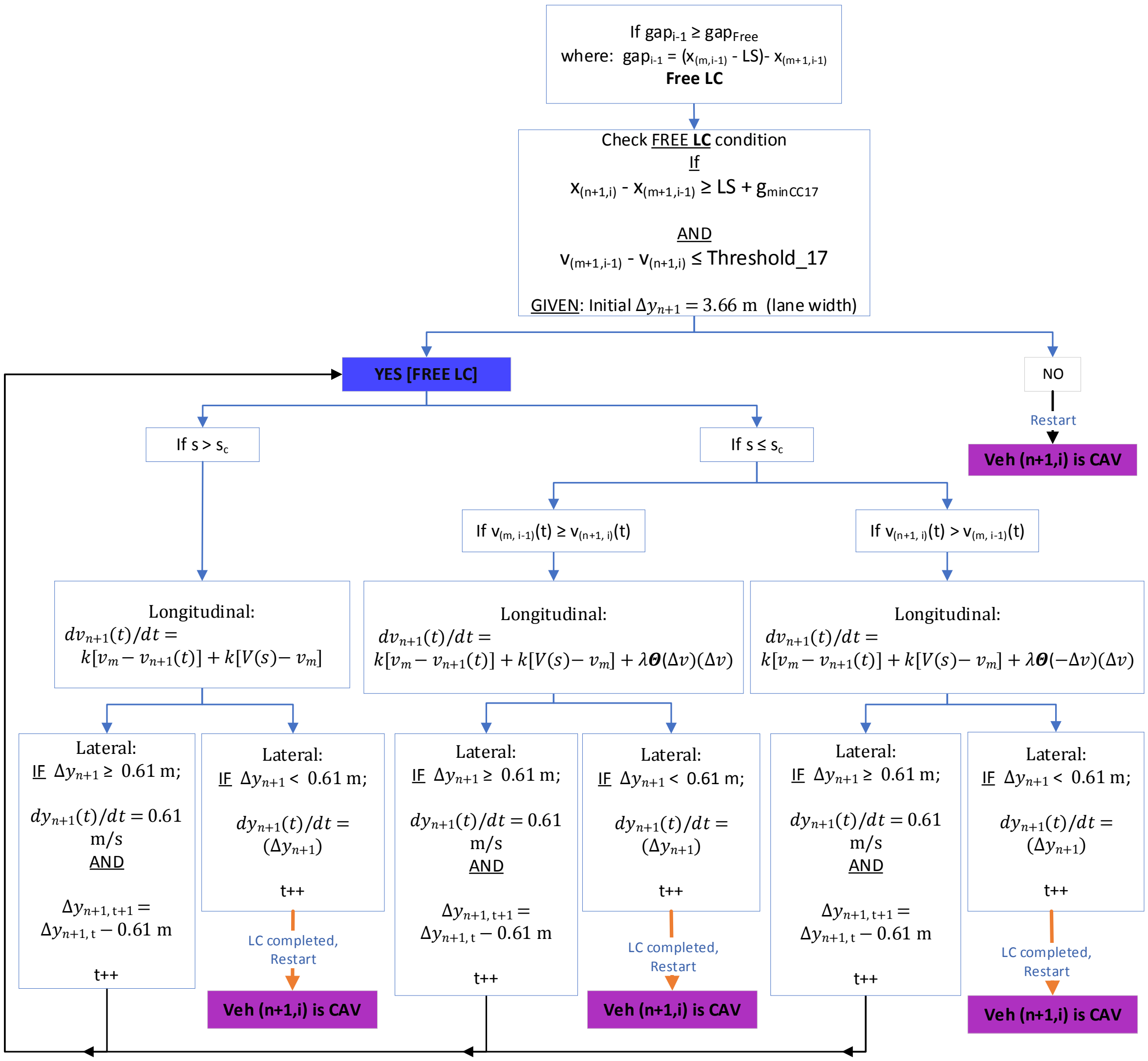

Figure 3-23 CAV-CAV free right-lane-changing model

If both of these conditions are true, the free lane-changing maneuver to the right lane (lane *i-1*) will be initiated. Otherwise, the subject vehicle will be made to assess the next gap, as presented in Figure 3-23.

Similarly, if the current gap in the target lane is detected to be available for a cooperative lane change ($LS + g_{min} \leq gap_{i-1} < gap_{Free}$), the lag gap in the target lane will be assessed using Equation (3-4a). The corresponding value of g_{min} in this case is assigned as g_{min_CC18} in the simulation models. The velocity difference between the subject vehicle and the potential follower is assessed, as presented in Equation (3-27).

$$v_{(m+1,\, i-1)} - v_{(n+1,\, i)} \leq Threshold\_18 \quad (3\text{-}27)$$

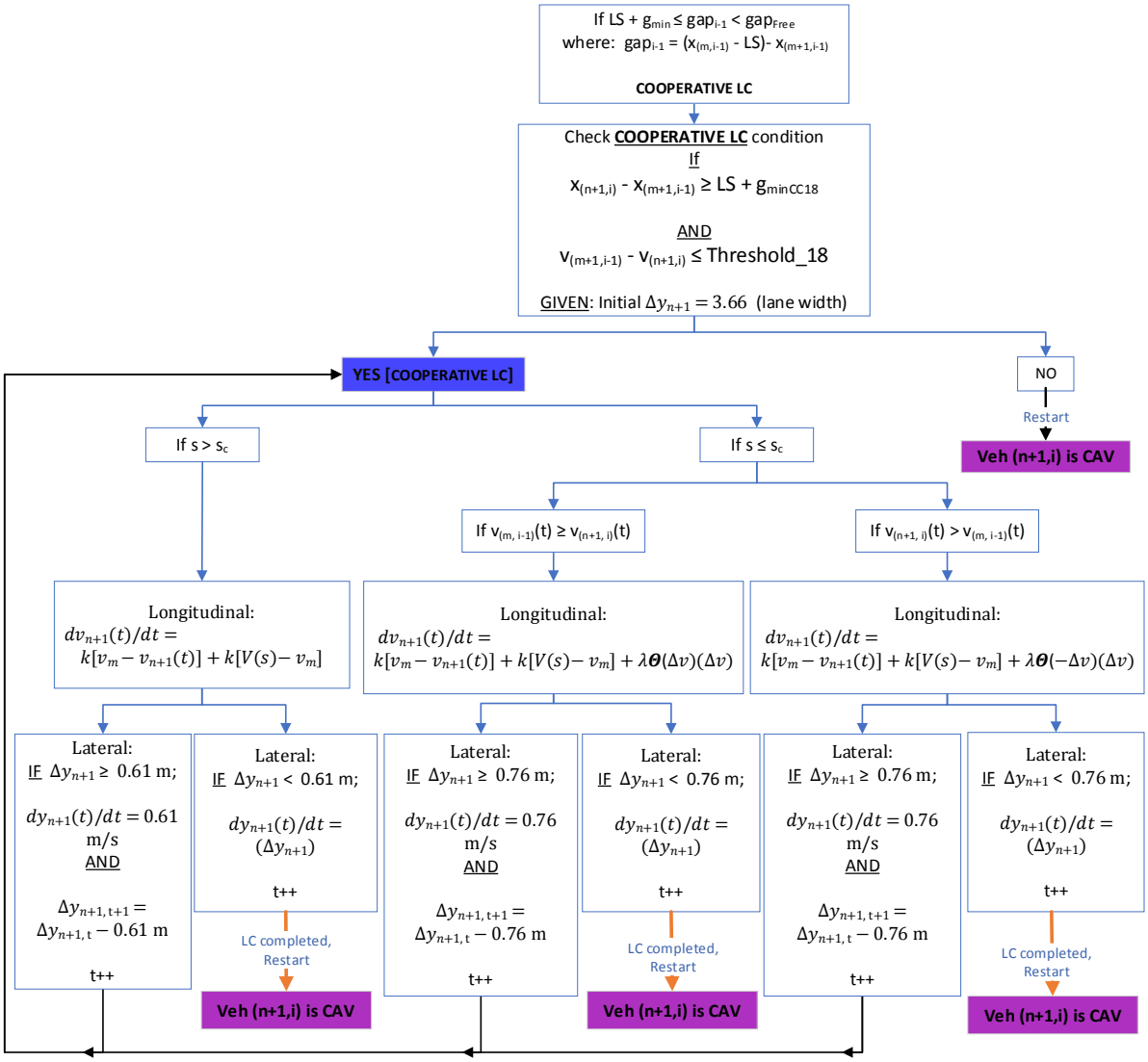

Figure 3-24 CAV-CAV cooperative right-lane-changing model

If both conditions are true, the cooperative lane-changing maneuver to the right lane (lane *i-1*) will be initiated. Otherwise, the subject vehicle will assess the next gap, as illustrated in Figure 3-24.

All the CAV-CAV right-lane-changing models also begin with the car-following part, followed by examining the lane-changing conditions. The acceleration rate of the subject vehicle in each time step is also determined based on the FVD car-following model by adopting Equations (3-1), (3-2), or (3-3); depending on the car-following conditions in that time step.

When the longitudinal acceleration of the subject vehicle is calculated, the model then determines the lateral velocity of the vehicle based on Equation (3-19). The default lateral velocity

of the subject vehicle is 0.61 m/s (α = 0.61 m/s) for all cases in the CAV-CAV free right-lane-changing model, as seen in Figure 3-23. However, in the CAV-CAV cooperative right-lane-changing model, the default lateral velocity of the subject vehicle is 0.61 m/s (α = 0.61 m/s) when the current space headway between the subject vehicle and its leader is greater than the critical space headway ($s > s_c$); whereas the default lateral velocity of the subject vehicle is 0.76 m/s (α = 0.76 m/s) when the current space headway is smaller than or equal to the critical space headway ($s \leq s_c$), as seen in Figure 3-24.

If any time the status of the subject vehicle is examined and it turns out that the vehicle is the first vehicle traversing the lane or the space headway between the subject vehicle and its predecessor is greater than or equal to the free-flow space headway ($s \geq s_{free\ flow}$), the vehicle will be automatically switched from the Automated Car-Following/Lane-Changing Algorithm to the Automated Platoon-Leading/Lane-Changing Algorithm.

3.1.2 Automated Platoon-Leading/Lane-Changing Algorithm

The Automated Platoon-Leading/Lane-Changing Algorithm is the sub-algorithm that controls the longitudinal and lateral movements of a CAV when the vehicle is the platoon leader, without any leading vehicle ahead or with a leading vehicle maintaining the space headway of greater than or equal to the free-flow headway ($s_{free\ flow}$). Subsequently, the status of the subject vehicle is denoted by *veh(1, i*), indicating that the vehicle is the platoon leader in lane i.

The algorithm starts by recognizing that the subject vehicle itself occupying lane i, denoted by *veh(1, i*) is a CAV. Next, the algorithm proceeds to check if there is a vehicle traveling ahead in the lane it is occupying. If the vehicle perceives that there is a vehicle ahead, the current space headway (s) between the vehicle and its leading vehicle will be checked whether it exceeds the free-flow space headway ($s_{free\ flow}$). If there is no leading vehicle in the occupying lane (*lane i*) or the current space headway between the vehicles is greater than or equal to the defined free-flow headway ($s \geq s_{free\ flow}$), the subject vehicle will accelerate to free flow speed, as shown in the diagram below. The acceleration rate of the subject vehicle (*veh(1, i)*) at this stage is determined based on the difference between the maximum allowable velocity in the traffic stream (or the speed limit) and the longitudinal velocity of the subject vehicle, multiplied by the constant value k, as seen in Equation (3-28).

$$dv_1(t)/dt = \kappa[v_m - v_1(t)] \quad (3\text{-}28)$$

However, if the space headway between the subject vehicle and its leading vehicle is found to be smaller than the free-flow space headway, the algorithm will promptly be alternated to the Automated Car-Following/Lane-Changing Algorithm, as shown in Figure 3-25.

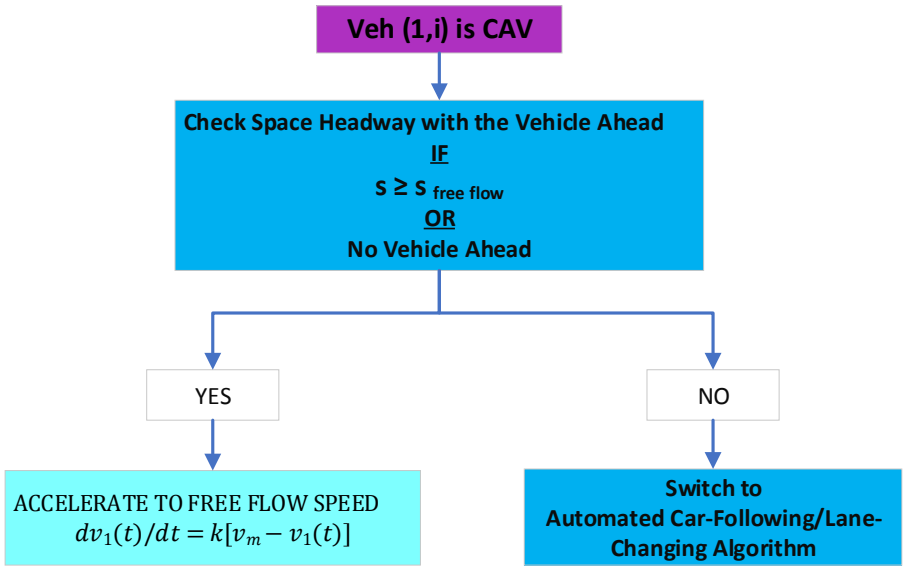

Figure 3-25 Mechanism for switching between the automated platoon-leading/lane-changing algorithm and the automated car-following/lane-changing algorithm

In case the subject vehicle is indicated as the platoon leader and the acceleration rate is determined as explained, the algorithm then proceeds to check if there is a lane drop within 0.8-km ahead of the vehicle. If there is currently no lane drop ahead within the distance defined, the subject vehicle will be programmed to continue on the current lane. In addition, the time step will proceed by one second to mark the end of the lane-drop checking process and the algorithm will return to check the space headway with its leading vehicle as a loop. However, if there is a lane drop ahead of the vehicle within the 0.8-km distance, the algorithm will automatically proceed to perform the mandatory lane change to the left (*lane i+1*) to continue on the freeway without stopping. Likewise, the time step will be counted forward by one second and the algorithm will proceed to check the lane-changing conditions in the next phase, as presented in Figure 3-26.

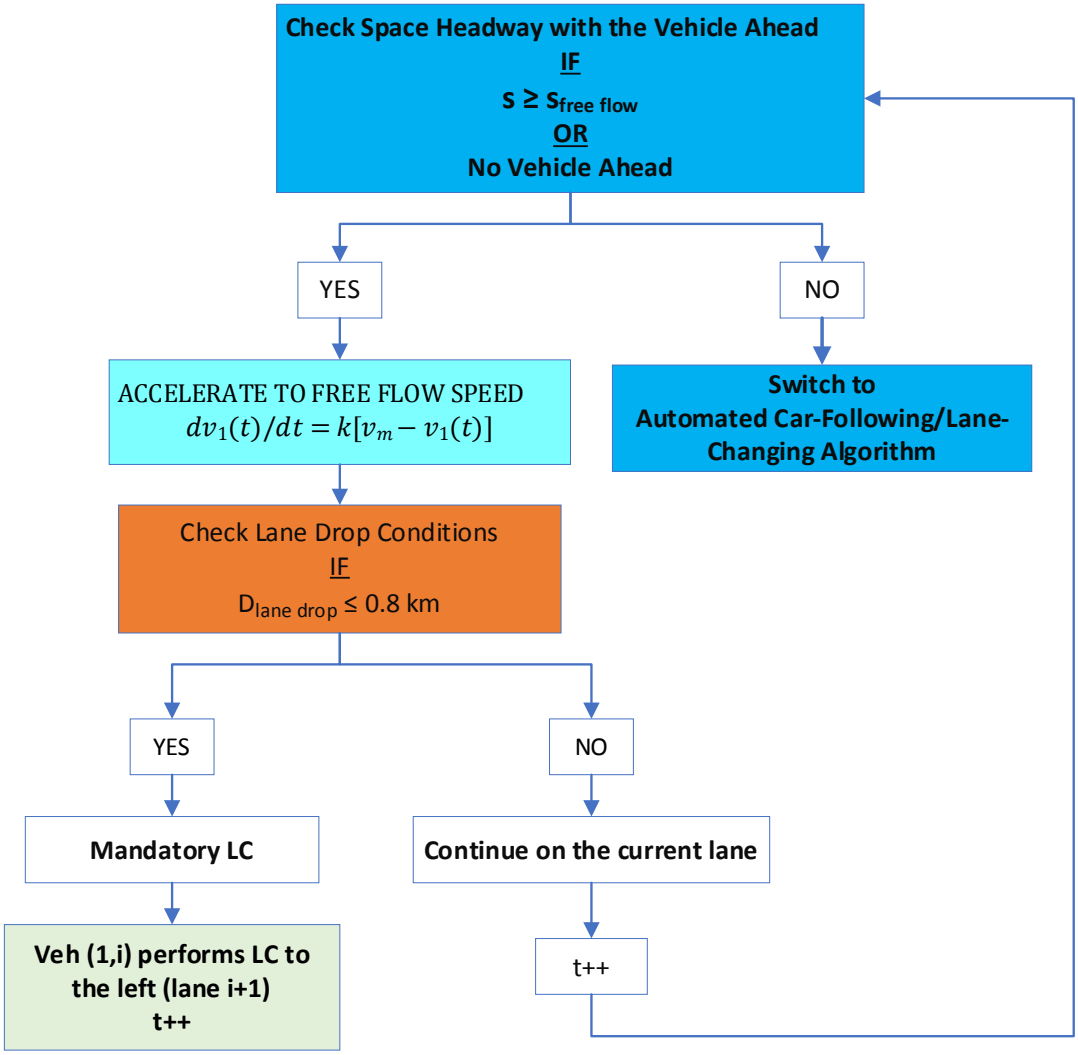

Figure 3-26 Flowchart of the automated platoon-leading/lane-changing algorithm

In case the subject vehicle is forced by the lane drop condition to perform a lane change to the left (*lane i+1*), there are two possible cases that can occur under this circumstance: 1) the potential follower in the target lane ($veh_{(m+1,\, i+1)}$) is MVD and 2) the potential follower in the target lane is CAV, as shown in Figure 3-27.

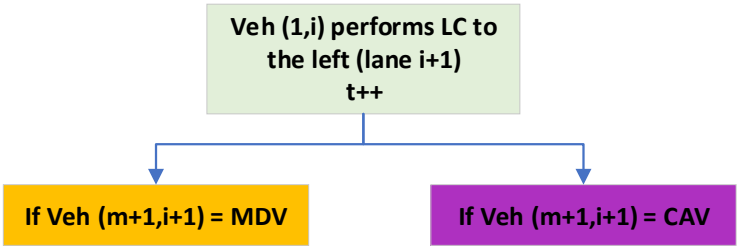

Figure 3- 27 Possible lane-changing scenarios for platoon-leading vehicles

3.1.2.1 The CAV-MDV Left-Lane-Changing Models for Platoon-Leading Vehicles

In case the anticipated lane change is occurring when the potential follower is a MDV, the current gap in the target lane on the left (gap_{i+1}) is assessed by the algorithm in the first place. The current gap in the target lane on the left is defined as the difference in the longitudinal displacements between the rear-end of the potential leading vehicle ($x_{(m,i+1)} - LS$) and the front-end of the potential follower ($x_{(m+1,i+1)}$), where $x_{(m+1,\,i+1)} \leq x_{(1,\,i)} \leq x_{(m,\,i+1)}$, as displayed in Equation (3-14a).

There are three possible lane-changing cases that can occur while the gap in the target lane is being assessed: 1) free lane change ($gap_{i+1} \geq gap_{Free}$), 2) cooperative or competitive lane changes ($LS + g_{min} \leq gap_{i+1} < gap_{Free}$), and 3) the next gap needs to be assessed ($gap_{i+1} < g_{min} + LS$).

In case the subject vehicle is programmed by the algorithm to assess the next gap, the vehicle proceeds to adjust its acceleration rate towards the average speed of the target lane (*lane i +1*) prior to returning to check the lane drop condition whether the distance between the vehicle and the lane drop ahead is less than or equal to 0.8 km, as a loop as illustrated in Figure 3-28. The adjusted acceleration rate towards the average speed of the target lane for the subject vehicle is determined by the difference between the longitudinal velocity subject vehicle ($v_1(t)$) and the average longitudinal velocity of the target lane ($v_{AVG\ lane\_i+1}$) multiplied by the constant value k, as displayed in Equation (3-29).

$$dv_1(t)/dt = k\,[v_{AVG\ lane\_i+1} - v_1(t)] \tag{3-29}$$

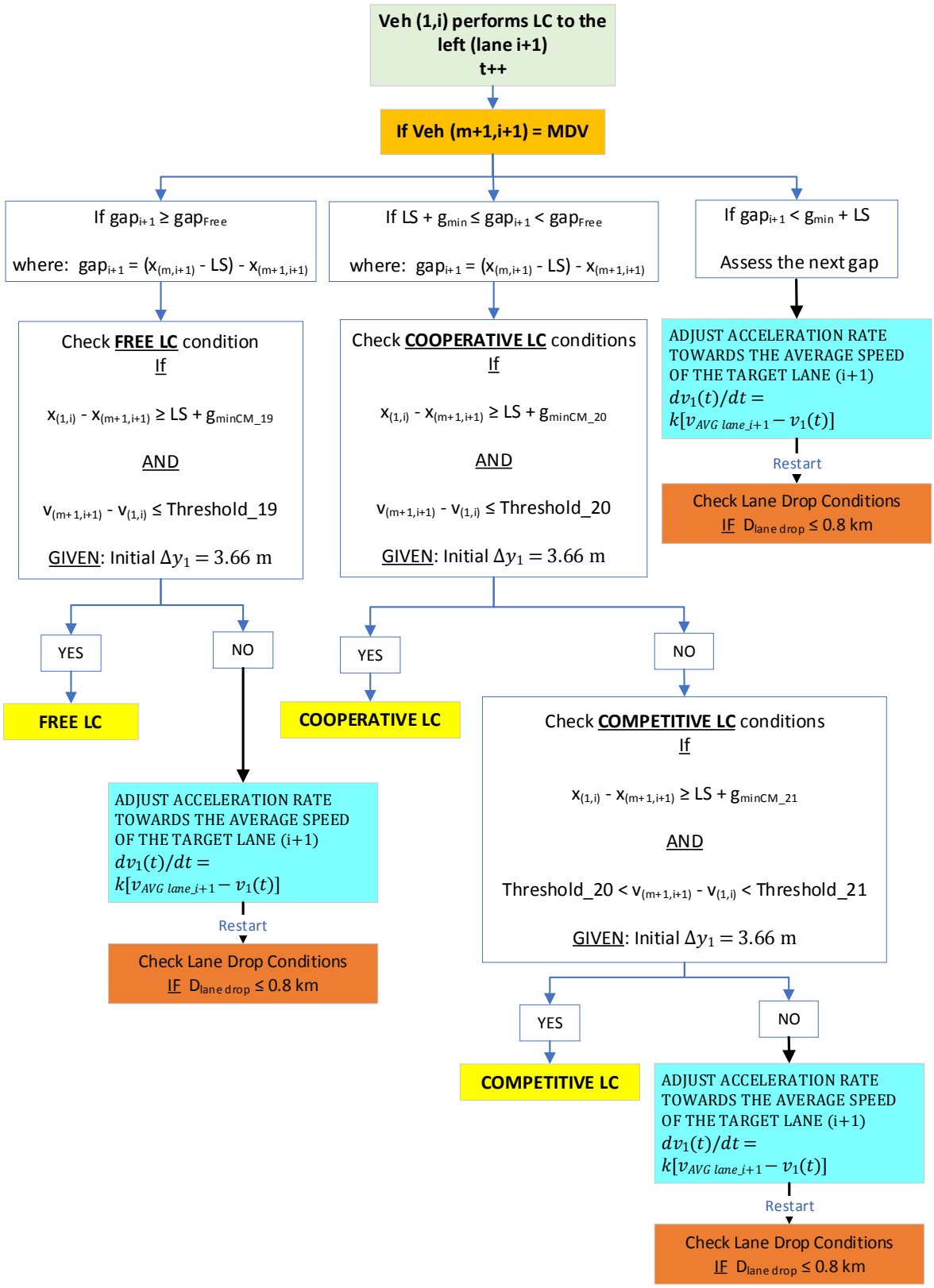

Figure 3-28 Flowchart of the CAV-MDV left-lane-changing model for platoon-leading vehicles

If the algorithm detects that the current gap in the target lane is available for a free lane change ($gap_{i+1} \geq gap_{Free}$), two conditions of longitudinal distance and velocity differences between the subject vehicle and the potential follower in the target lane will be inspected prior to the initiation of lane change to ensure a safe lane-changing maneuver. These two conditions are elaborated as follows:

Firstly, for the longitudinal distance difference, the algorithm assesses if the lag gap is greater than or equal to $LS + g_{min}$, as shown in Equation (3-30). The corresponding value of g_{min} in this case is assigned as g_{min_CM19} in the simulation models.

$$x_{(1,\,i)} - x_{(m+1,\,i+1)} \geq LS + g_{min} \tag{3-30}$$

Secondly, the velocity difference between the subject vehicle and the potential follower is assessed, as presented in Equation (3-31).

$$v_{(m+1,\,i+1)} - v_{(1,\,i)} \leq Threshold\_19 \tag{3-31}$$

If both of these conditions simultaneously turn out to be true, the free lane-changing maneuver to the left lane (*lane i+1*) will be initiated by the subject vehicle in the next step. In addition, the anticipated lateral displacement for lane change (Δy_{n+1}) will be initiated as 3.66 m (12 ft), which is the lane width used in the model. Otherwise, the subject vehicle will proceed to adjust its acceleration rate towards the average speed of the target lane prior to returning to check the lane drop condition whether the distance between the vehicle and the lane drop ahead is less than or equal to 0.8 km, as a loop, as presented in Figure 3-29. The adjusted acceleration rate towards the average speed of the target lane for the subject vehicle is determined by Equation (3-29).

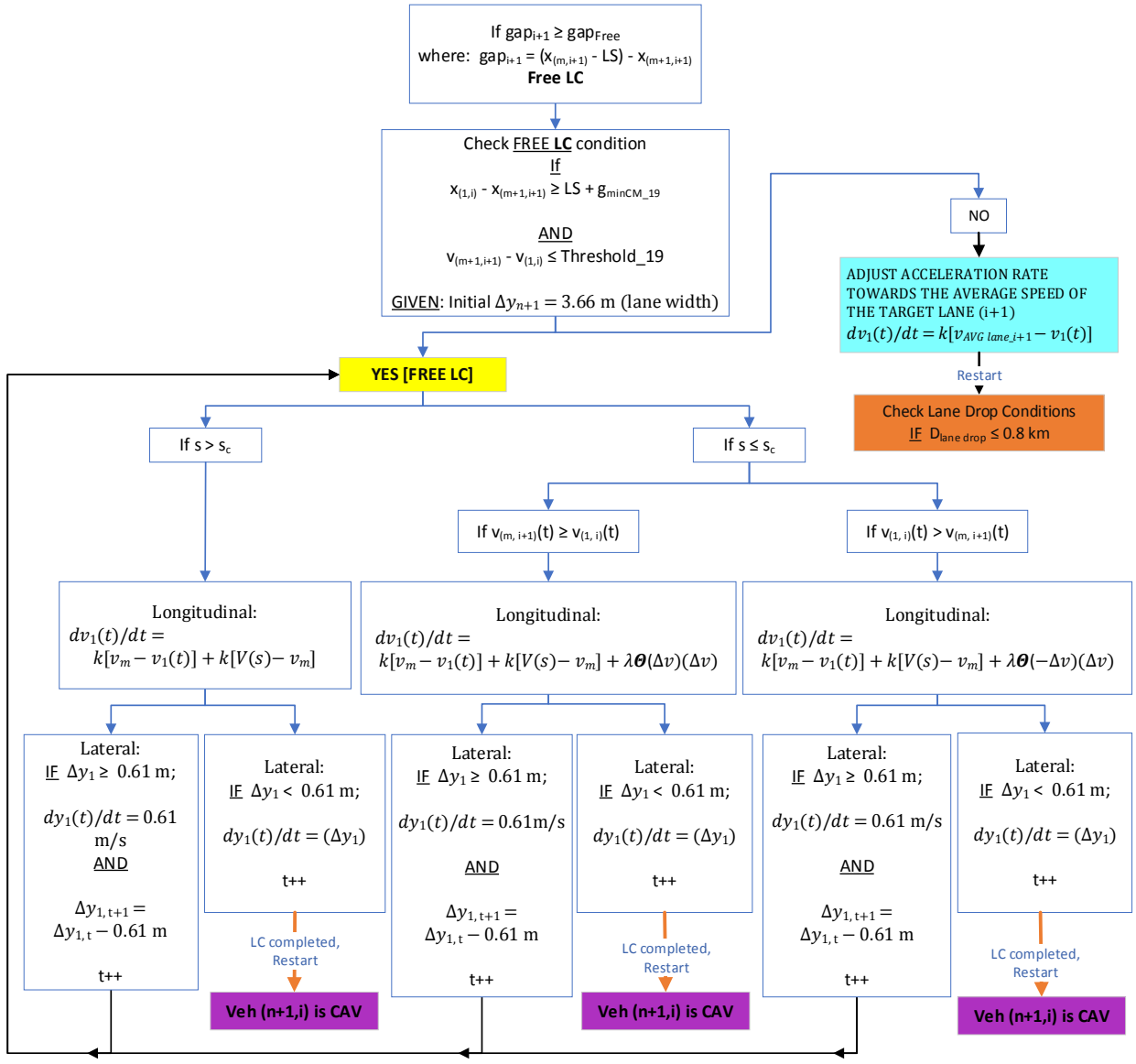

Figure 3-29 CAV- MDV free left-lane-changing model for platoon-leading vehicles

Similarly, if the current gap in the target lane is detected to be available for a cooperative lane change ($LS + g_{min} \leq gap_{i+1} < gap_{Free}$), firstly, the algorithm will assess if the lag gap is greater than or equal to $LS + g_{min}$, as displayed by Equation (3-30). The corresponding value of g_{min} in this case is assigned as g_{min_CM20} in the simulation models. Secondly, the velocity difference between the subject vehicle and the potential follower is examined, as presented in Equation (3-32).

$$v_{(m+1,\,i+1)} - v_{(1,\,i)} \leq Threshold\_20 \qquad (3\text{-}32)$$

If both of these conditions simultaneously turn to be true, the cooperative lane-changing maneuver to the left lane (*lane i+1*) will be initiated by the subject vehicle in the next step. Otherwise, the competitive lane change conditions will be assessed, as presented in Figure 3-30.

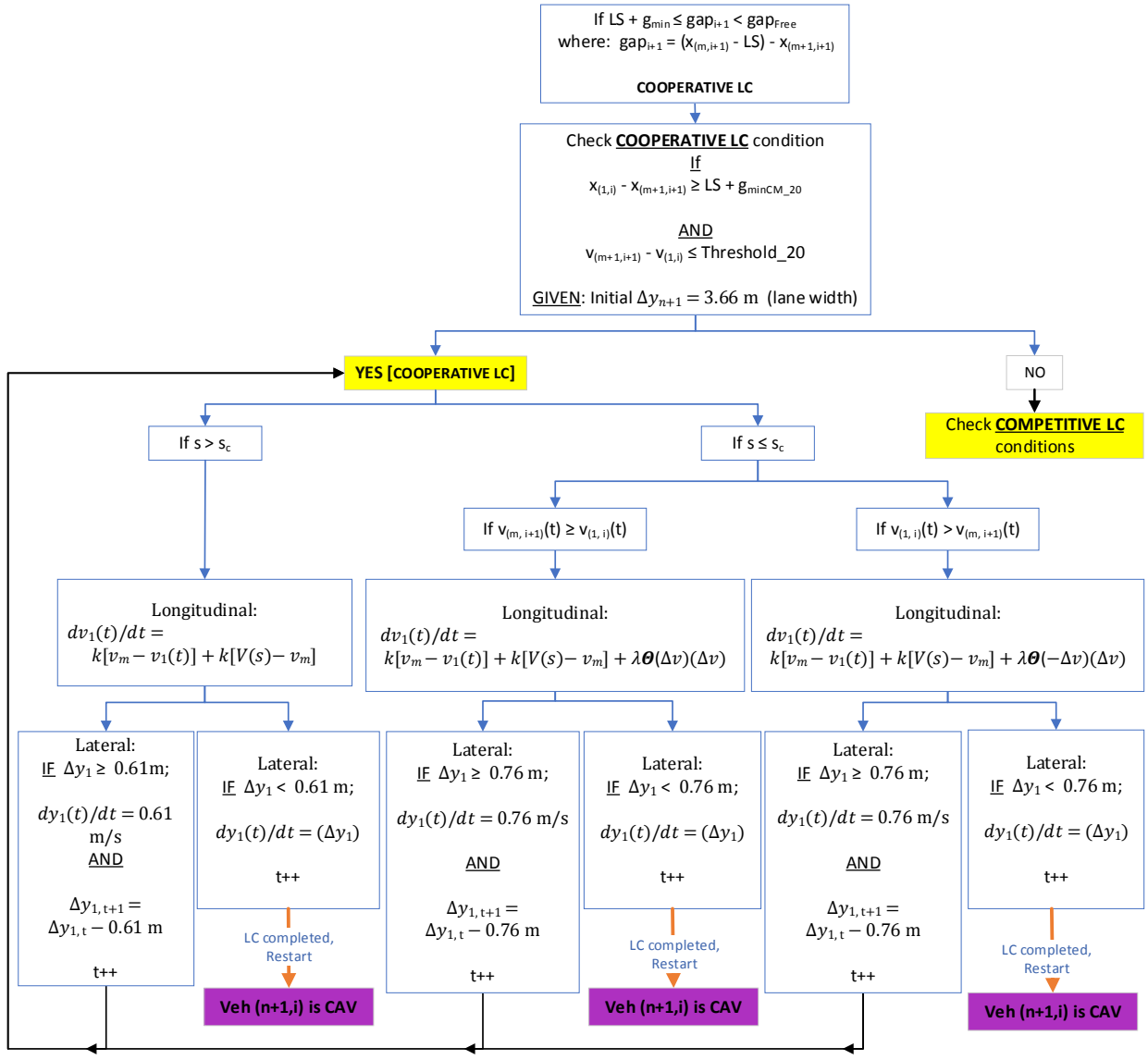

Figure 3-30 CAV- MDV cooperative left-lane-changing model for platoon-leading vehicles

The competitive lane change conditions are assessed in case the cooperative lane change conditions are false. There are two conditions of longitudinal distance and velocity differences between the subject vehicle and the potential follower in the target lane. The longitudinal distance difference condition is identical among the models; however, the form of the velocity difference condition is different from those in the free and cooperative lane change conditions.

Firstly, the longitudinal distance difference between the subject vehicle ($x_{(1,\ i)}$) and the potential follower in the target lane ($x_{(m+1,\ i+1)}$) is assessed based on Equation (3-30). The corresponding value of g_{min} in this case is assigned as g_{min_CM21} in the simulation models. Secondly, for the velocity difference, the algorithm then inspects if the difference between the current velocity of the subject vehicle ($v_{(1,\ i)}$) and the current velocity of the potential follower in the target lane ($v_{(m+1,\ i+1)}$) falls between these thresholds, as presented in Equation (3-33).

$$Threshold\_20 < v_{(m+1,\ i+1)} - v_{(1,\ i)} < Threshold\_21 \quad (3\text{-}33)$$

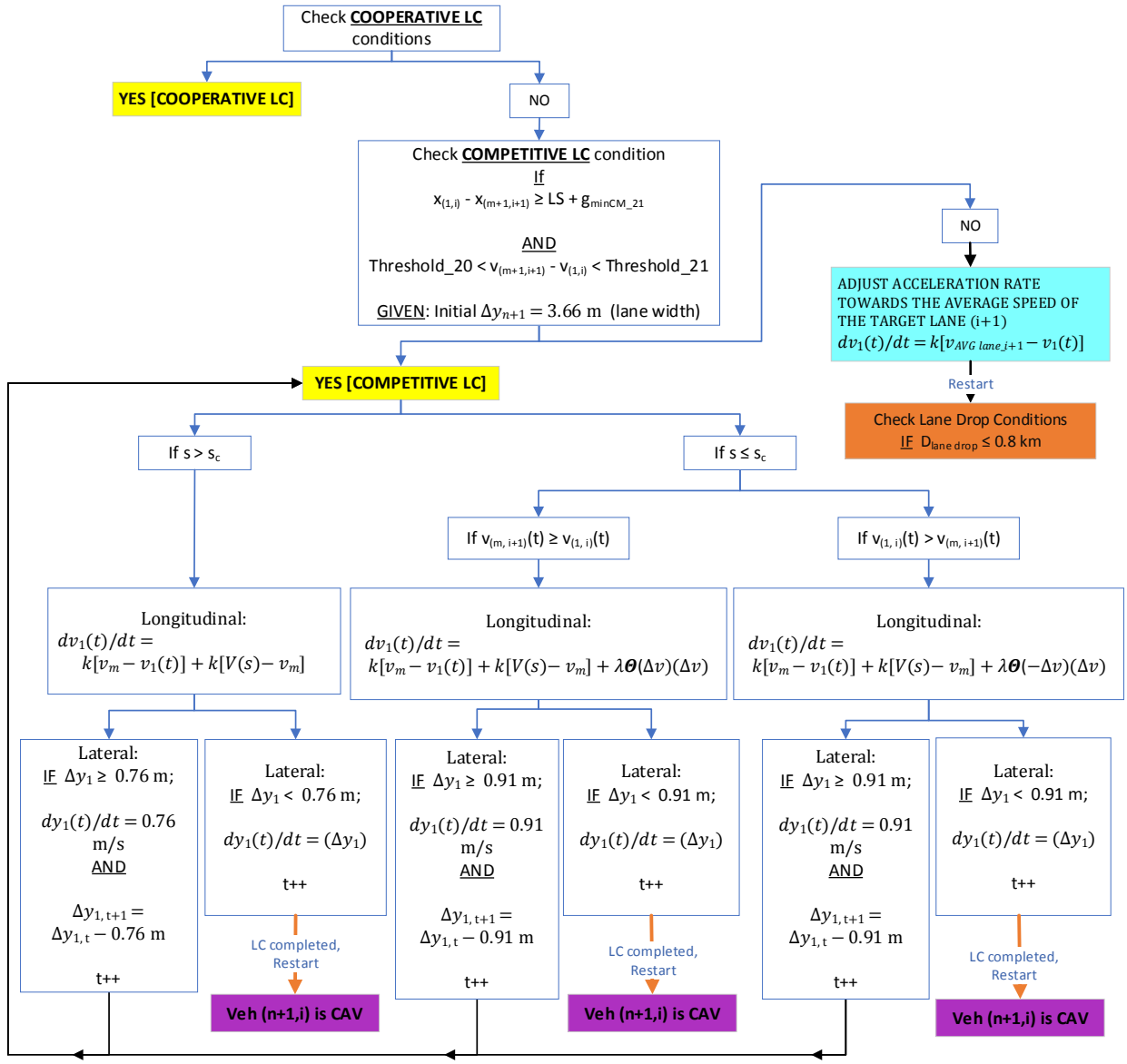

Figure 3-31 CAV- MDV competitive left-lane-changing model for platoon-leading vehicles

If both of these conditions simultaneously turn out to be true, the competitive lane-changing maneuver to the left lane (*lane i+1*) will be initiated by the subject vehicle in the next step. Otherwise, the subject vehicle will proceed to adjust its acceleration rate towards the average speed of the target lane prior to returning to check the lane drop condition whether the distance between the vehicle and the lane drop ahead is less than or equal to 0.8 km, as a loop, as shown in Figure 3-31. The adjusted acceleration rate towards the average speed of the target lane for the subject vehicle is determined by Equation (3-29).

All the CAV-MDV left-lane-changing models for platoon-leading vehicles begin with the car-following part, followed by determining the lateral movement conditions. The acceleration rate of the subject vehicle in each time step is also determined based on the FVD car-following model by adopting Equations (3-1), (3-2), or (3-3); depending on the car-following conditions in that time step.

After the longitudinal acceleration of the subject vehicle is determined, the model then determines the lateral velocity of the vehicle based on the remaining anticipated lateral displacement for a lane change (Δy_1). When the remaining anticipated lateral displacement for lane change in the time step is greater than or equal to β m ($\Delta y_{n+1} \geq \beta$ m), where β is the default lateral displacement in the current case in which the space headway and velocity difference conditions fall into, the lateral velocity of the subject vehicle in that time step will be β m/s, as displayed by Equation (3-34).

$$dy_1(t)/dt = \beta \text{ m/s} \tag{3-34}$$

It means that the vehicle will displace in the lateral direction by β m by the end of the time step. Therefore, the remaining anticipated lateral displacement for lane change for the next time step ($\Delta y_{1,\ t+1}$) will be the previous anticipated lateral displacement for lane change ($\Delta y_{1,\ t}$) subtracted by the distance of β m, as displayed by Equation (3-35).

$$\Delta y_{1,\ t+1} = \Delta y_{1,\ t} - \beta \text{ m} \tag{3-35}$$

The default lateral velocity of the subject vehicle is 0.61 m/s (β = 0.61 m/s) for all cases in the CAV-MDV free left-lane-changing model for platoon-leading vehicles, as seen in Figure 3-29. In the CAV-MDV cooperative left-lane-changing model for platoon-leading vehicles, the default lateral velocity of the subject vehicle is 0.61 m/s (β = 0.61 m/s) when the current space headway

between the subject vehicle and its leader is greater than the critical space headway ($s > s_c$); whereas the default lateral velocity of the subject vehicle is 0.76 m/s (β = 0.76 m/s) when the current space headway is smaller than or equal to the critical space headway ($s \leq s_c$), as seen in Figure 3-30. However, in the CAV-MDV competitive left-lane-changing model for platoon-leading vehicles, the default lateral velocity of the subject vehicle is 0.76 m/s (β = 0.76 m/s) when the current space headway is greater than the critical space headway ($s > s_c$); while the default lateral velocity of the subject vehicle is 0.91 m/s (β = 0.91 m/s) when the current space headway is smaller than or equal to the critical space headway ($s \leq s_c$), as seen in Figure 3-31.

Next, the process then starts over to check the current space headway (s) between the subject vehicle and the potential leader in the target lane, as a loop. This loop runs until the remaining anticipated lateral displacement for a lane change (Δy_1) in that time step is smaller than the default lateral displacement in the current case where the space headway and velocity difference conditions fall into ($\Delta y_1 < \beta$ m). In this phase, the calculated lateral velocity of the subject vehicle in that time step is Δy_1 m/s, as displayed by Equation (3-36), so that the vehicle can complete its lane-changing maneuver by positioning in the middle of the target lane at the end of this time step.

$$dy_1(t)/dt = (\Delta y_1) \text{ m/s} \tag{3-36}$$

Further, the time step is then proceeded by one at the end of this step to indicate the completion of the CAV-MDV left lane-changing model for platoon-leading vehicles. Subsequently, the algorithm then restarts back to the beginning of the algorithm by recognizing its type of the vehicle and rechecking the type of the new leader in this newly changed lane in the next phase.

However, if either of the conditions of longitudinal distance or velocity differences between the subject vehicle and the potential follower in the target lane, or both, are not met at the beginning of this model; the subject vehicle will proceed to adjust its acceleration rate towards the average speed of the target lane based on Equation (3-29). Finally, the algorithm will proceed to recheck the lane drop condition whether the distance between the vehicle and the lane drop ahead is less than or equal to 0.8 km, as a loop.

3.1.2.2 The CAV-CAV Left-Lane-Changing Models for Platoon-Leading Vehicles

On the other hand, if the potential follower of the lane-changing platoon leader in the target lane is a CAV, the CAV-CAV left-lane-changing model for platoon-leading vehicles will be triggered to activate. Fundamentally, the structure of this model is similar to the CAV-MDV left-lane-changing model; however, the competitive lane-changing interaction between CAVs was not programmed to occur. The reason is that the CAV-CAV lane-changing maneuvers are expected to occur only in cooperative characteristics by utilizing the benefits of connected environment to maximize traffic safety on freeways.

In this model, first of all, the current gap in the target lane on the left (gap_{i+1}) is assessed by the algorithm, as determined by Equation (3-14a). The current gap is then adopted to justify whether the anticipated lane-changing maneuver is a free lane change ($gap_{i+1} \geq gap_{Free}$), a cooperative lane change ($LS + g_{min} \leq gap_{i+1} < gap_{Free}$), or the next gap needs to be assessed prior to the emergence of the lane-changing maneuver ($gap_{i+1} < g_{min} + LS$).

If the subject vehicle is programmed by the algorithm to assess the next gap, the vehicle will adjust its acceleration rate towards the average speed of the target lane (*lane i +1*) prior to returning to check the lane drop condition whether the distance between the vehicle and the lane drop ahead is less than or equal to 0.8 km, as a loop, as seen in Figure 3-32. The adjusted acceleration rate towards the average speed of the target lane for the subject vehicle is determined by Equation (3-29).

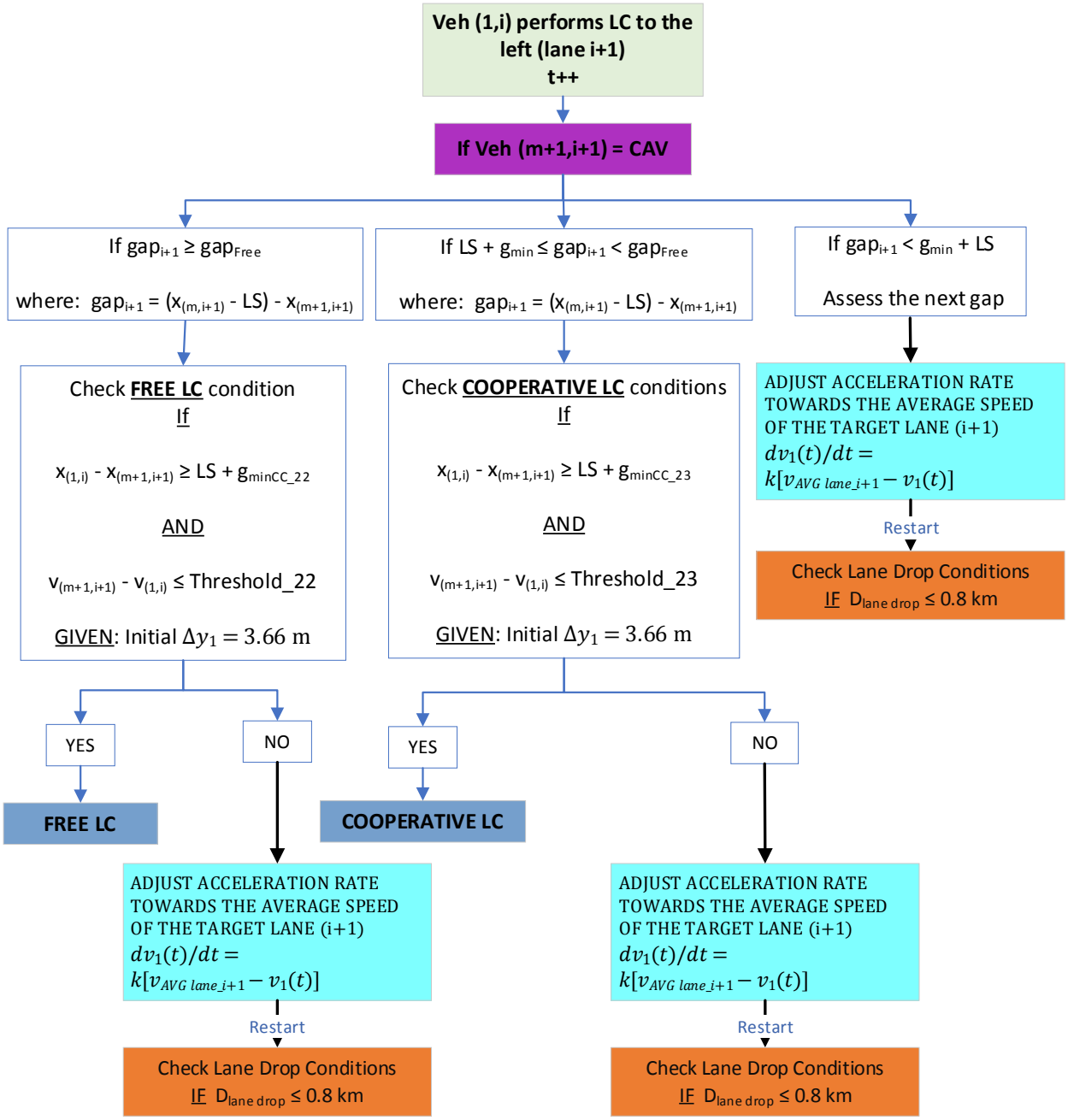

Figure 3-32 Flowchart of the CAV-CAV left-lane-changing model for platoon-leading vehicles

However, if the algorithm detects that the current gap in the target lane is available for a free lane change ($gap_{i+1} \geq gap_{Free}$), firstly, the lag gap will be assessed based on Equation (3-30), where $x_{(m+1,\ i+1)} \leq x_{(1,\ i)} \leq x_{(m,\ i+1)}$. Secondly, the algorithm then assesses the velocity difference between the subject vehicle and the potential follower, as presented in Equation (3-37).

$$v_{(m+1,\ i+1)} - v_{(1,\ i)} \leq Threshold\_22 \quad (3\text{-}37)$$

If both of these conditions simultaneously turn out to be true, the free lane-changing maneuver to the left lane (*lane i+1*) will be initiated in the next step. Otherwise, the subject vehicle will proceed to adjust its acceleration rate towards the average speed of the target lane, via Equation (3-29), prior to returning to check the lane drop condition whether the distance between the vehicle and the lane drop ahead is less than or equal to 0.8 km, as a loop, as illustrated in Figure 3-33.

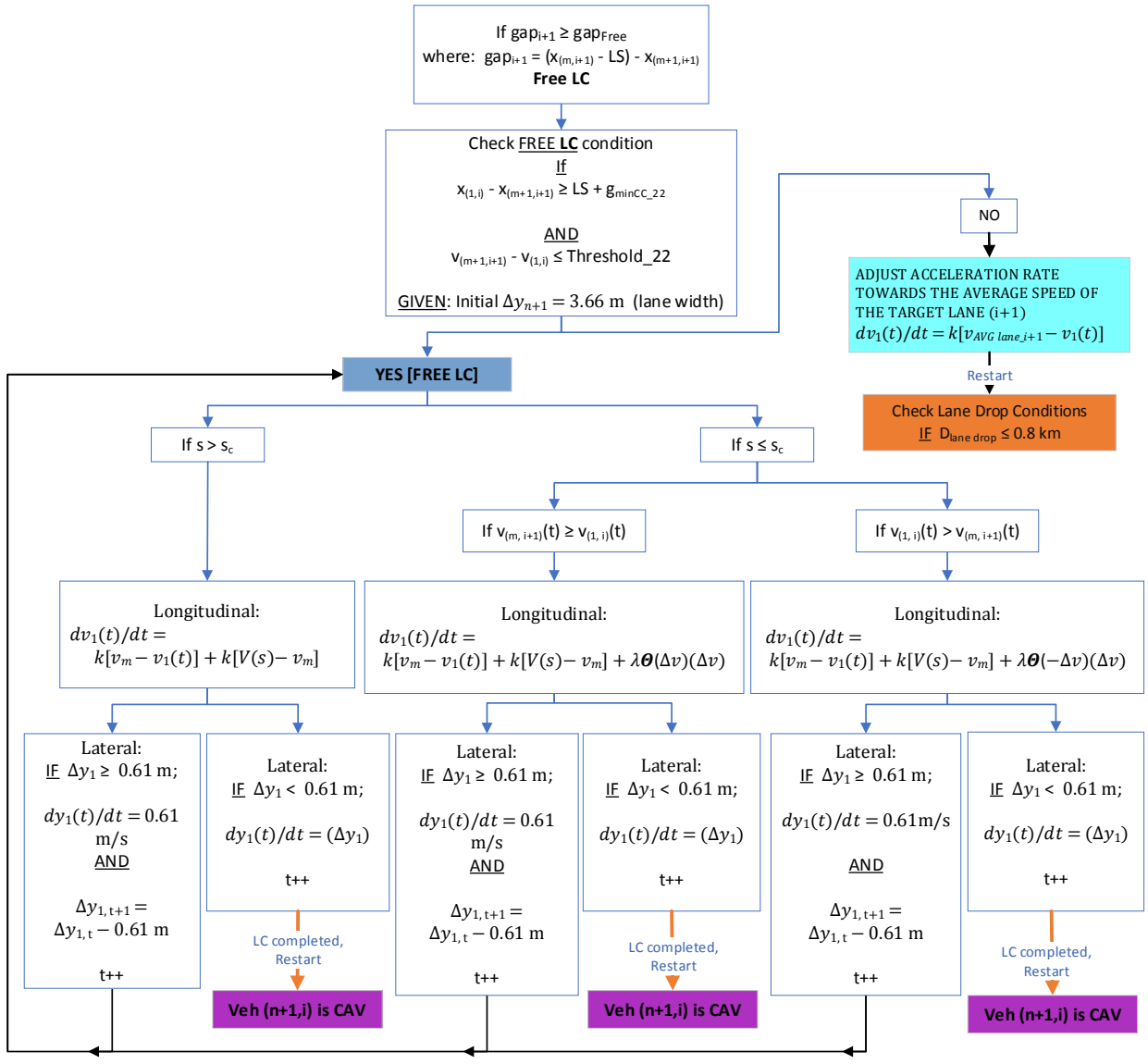

Figure 3-33 The CAV-CAV free left-lane-changing model for platoon-leading vehicles

Finally, if the current gap in the target lane is detected to be available for a cooperative lane change ($LS + g_{min} \leq gap_{i+1} < gap_{Free}$), firstly, the lag gap between the subject vehicle and the potential follower in the target lane will be assessed based on Equation (3-30). Secondly, the velocity difference between the subject vehicle and the potential follower in the target lane is assessed, as displayed in Equation (3-38).

$$v_{(m+1,\, i+1)} - v_{(1,\, i)} \leq Threshold\_23 \tag{3-38}$$

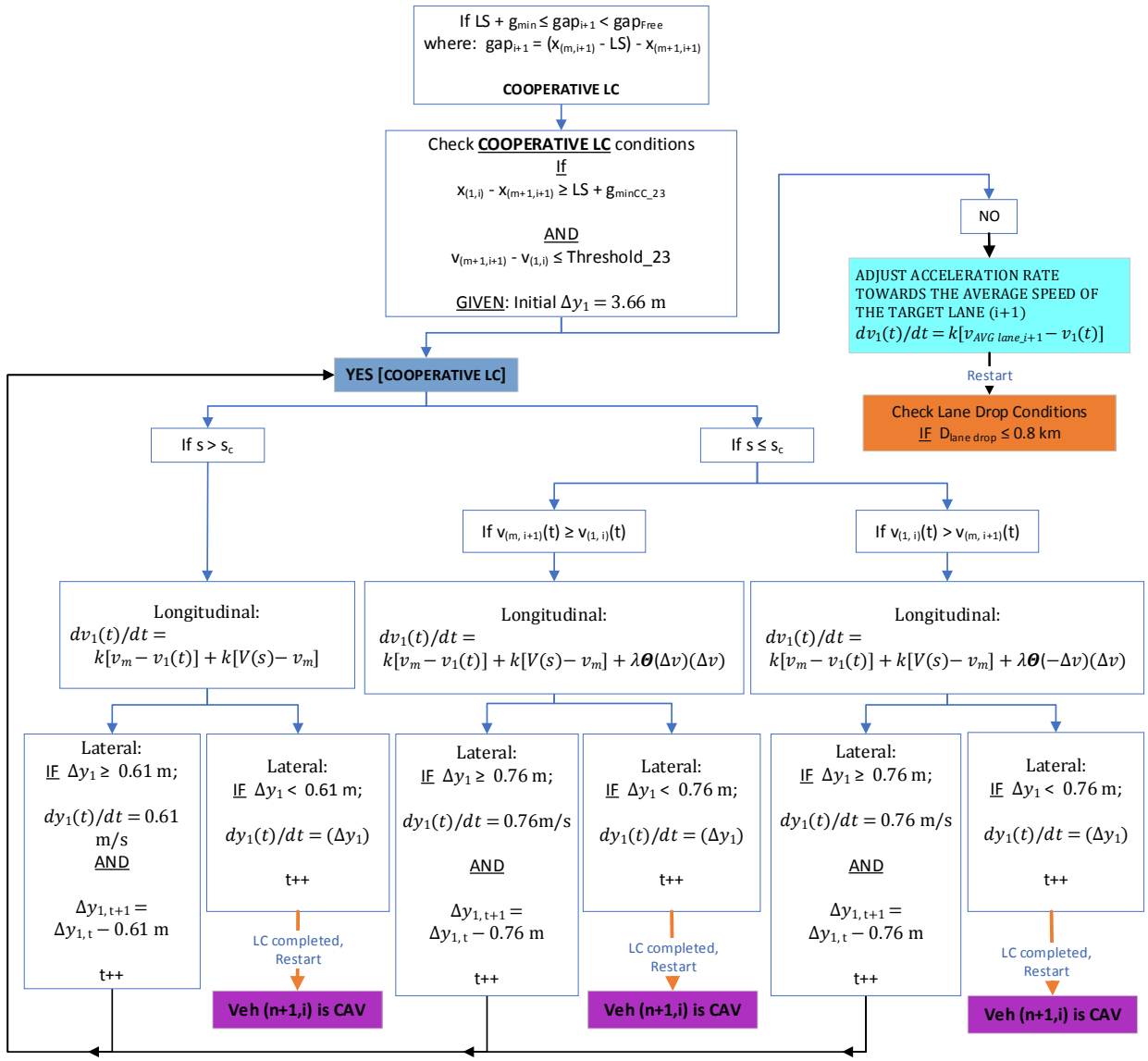

Figure 3-34 CAV- CAV cooperative left-lane-changing model for platoon-leading vehicles

If both of these conditions simultaneously turn to be true, the cooperative lane-changing maneuver to the left lane (*lane i+1*) will be initiated. Otherwise, the subject vehicle will proceed to adjust its acceleration rate towards the average speed of the target lane, based on Equation (3-29), prior to returning to check the lane drop condition whether the distance between the vehicle and the lane drop ahead is less than or equal to 0.8 km, as a loop, as presented in Figure 3-34.

All the CAV- CAV left-lane-changing models for platoon-leading vehicles also begin with the car-following process, followed by assessing the lane-changing conditions. The acceleration rate of the subject vehicle in each time step is determined based on the FVD car-following model by adopting Equations (3-1), (3-2), or (3-3); depending on the car-following conditions in that time step.

Since the longitudinal acceleration of the subject vehicle is calculated, the model then determines the lateral velocity of the vehicle based on Equation (3-34). The default lateral velocity of the subject vehicle is 0.61 m/s (β = 0.61 m/s) for all cases in the CAV- CAV free left-lane-changing model for platoon-leading vehicles, as seen in Figure 3-33. However, in the CAV-CAV cooperative left-lane-changing model for platoon-leading vehicles, the default lateral velocity of the subject vehicle is 0.61 m/s (β = 0.61 m/s) when the current space headway between the subject vehicle and its leader is greater than the critical space headway ($s > s_c$); whereas the default lateral velocity of the subject vehicle is 0.76 m/s (β = 0.76 m/s) when the current space headway is smaller than or equal to the critical space headway ($s \leq s_c$), as seen in Figure 3-34.

This process then starts over to check the current space headway (s) between the subject vehicle and the potential leader in the target lane as a loop. This loop runs until the remaining anticipated lateral displacement for lane change (Δy_1) in that time step is smaller than the default lateral displacement in the current case where the space headway and velocity difference conditions fall into ($\Delta y_1 < \beta$ m). In this phase, the calculated lateral velocity of the subject vehicle in that time step is Δy_1 m/s, as displayed by Equation (3-36).

Further, the time step is then proceeded by one at the end of this step to indicate the completion of the CAV-CAV left lane-changing model for platoon-leading vehicles. Consequently, the algorithm then restarts back to the beginning of the algorithm by rechecking the type of the new leader in this newly changed lane in the next phase.

However, if either of the conditions of longitudinal distance or velocity differences between the subject vehicle and the potential follower in the target lane, or both, are not met at the beginning of this model; the subject vehicle will proceed to adjust its acceleration rate towards the average speed of the target lane based on Equation (3-29). In the end, the algorithm will proceed to recheck the lane drop condition whether the distance between the vehicle and the lane drop ahead is less than or equal to 0.8 km, as a loop.

3.2 The MDV Algorithm

The MDV algorithm is a set of logic for replicating the driving behavior of MDVs in both the longitudinal and lateral directions in a traffic stream. The algorithm is composed of the car-following/cruising and lane-changing models, with the conditional linkage between these models, for governing the decision-making of MDV when interacting with the surrounding vehicles and the geometry of a freeway segment.

Basically, the structure of the MDV algorithm and the logic behind it are comparable to those of the CAV algorithm. However, the decisive thresholds in most of the decision-making equations and the stochasticity of the parameters in the MDV algorithm differentiate this algorithm from the CAV algorithm, in which the parameters were designed to be more deterministic as the driving behavior of this type of vehicle are speculated to be.

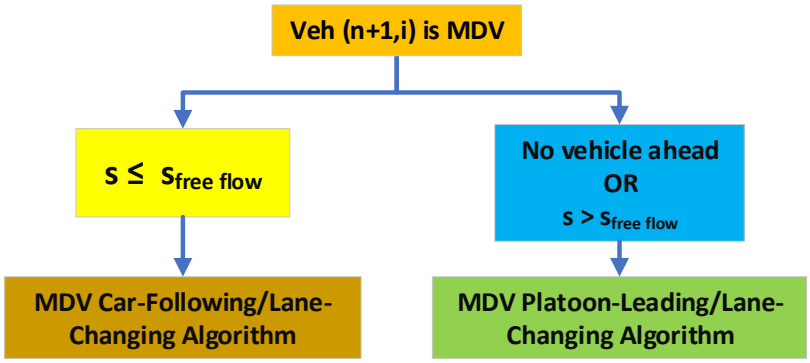

Figure 3-35 Flowchart of the MDV algorithm

The MDV algorithm is also composed of two sub-algorithms: 1) MDV Car-Following/Lane-Changing Algorithm and 2) MDV Platoon-Leading/Lane-Changing Algorithm. The subject vehicle is programmed to switch between these sub-algorithms based on the current space headway (s) between the vehicle and its leader. The MDV Car-Following/Lane-Changing

Algorithm is activated when the space headway between the vehicle and its leader is smaller than the free-flow space headway ($s_{free\ flow}$). Otherwise, the vehicle is assigned to follow the MDV Platoon-Leading/Lane-Changing Algorithm when there is no leading vehicle ahead or when the space headway between the vehicle and its leader is greater than $s_{free\ flow}$, as seen in Figure 3-35.

3.2.1 MDV Car-Following/Lane-Changing Algorithm

Although the MDV algorithm shares the same structure with the CAV algorithm, the major differences between these algorithms are the values of the decisive thresholds in most of the decision-making equations and the level of stochasticity of the parameters in the MDV algorithm. Another major difference between these two algorithms is that the ability of the subject vehicle to identify the types of the interacting vehicles, whether they are MDV or CAV, is diminished in the MDV algorithm. This assumption is established to replicate the typical driving behavior of the conventional vehicles due to the lack of connection and communication capabilities that the CAVs are assumed to possess. Consequently, the subject vehicle, *veh(n+1, i)* in the MDV Car-Following/Lane-Changing Algorithm follows the mechanism of the Automated Car-Following/Lane-Changing Algorithm without considering the difference between the type of its leader occupying the same lane, *veh(n, i)*, as shown in Figure 3-36.

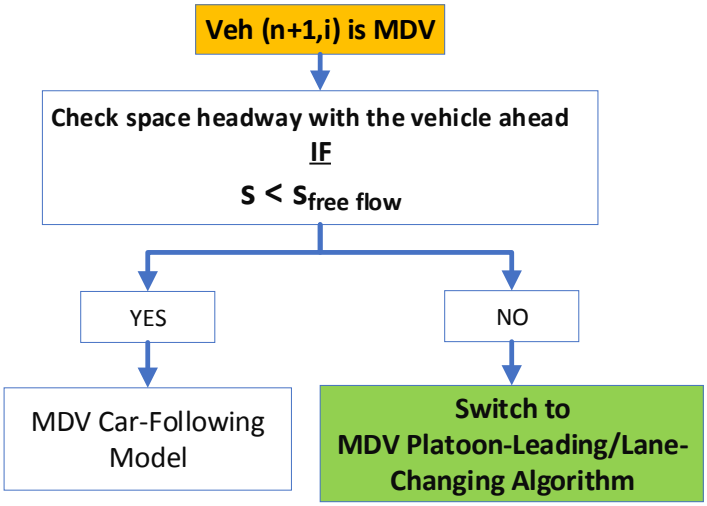

Figure 3-36 Flowchart of the MDV Car-Following/Lane-Changing Algorithm

3.2.1.1 The MDV Car-Following Model

The structure of the MDV Car-Following Model is basically the same as Automated Car-Following Model, with the elimination of the cooperative gap creation model between CAVs and the capability to identify the types of the interacting vehicles.

The MDV Car-Following Model used in this study was adopted from the Full Velocity Difference (FVD) car-following model and confined Full Velocity Difference model (c-FVD) with an adjustment in the sensitivity value (λ), as described in Equation (2-7) with the application of all the default parameters to replicate the driving behavior of MDVs. The value of the sensitivity parameter (λ) of 0.13 is applied in this algorithm instead of 0.5 suggested in the original FVD model, based on the results from the calibrated model. The critical space headway (s_c) of 30 meters and the vehicle length of 4.5 meters were applied. The sensitivity constant (κ) and the empirical value of $V(s)$ are adopted from the c-FVD model in section 2.2.1 (Yu et al., 2019; Qu et al., 2019); however, the values of the calibrated parameters V_1 is modified as 23.610. The acceleration rate of the subject vehicle is generated based on the current space headway (s) and the velocity difference between vehicles (Δv), as presented in Figure 3-3.

Once the acceleration rate of the subject vehicle is determined for a time step based on the conditions in FVD model, the algorithm proceeds to check whether its current leader still exists in the current lane (*lane i*). This process follows the same logic of the CAV car-following model described in section 3.1.1.1, as illustrated in Figure 3-4.

If the leading vehicle is still occupying the current lane, the model will check if there is a lane change performing ahead by a vehicle from the adjacent lane (*lane i+1* or *lane i-1*). Although following the same logic, this process in the MDV car-following model is different from the CAV car-following model due to the assumption that types of the lane-changing vehicle ahead cannot be detected by the MDV. As a result, if the lane changing maneuver is being performed ahead of the MDV by any types of vehicle, the subject vehicle will only recognize the lane-changing vehicle as a new leader and the order of the subject vehicle and all the vehicles behind in the platoon will be moved down by one position, while the time step is forwarded by one second. However, if there is no lane change occurring ahead of the subject vehicle, the algorithm will proceed to assess the distance to the lane drop whether it is smaller than 0.8 km, which is the same as in the CAV car-following model, as seen in Figure 3-37.

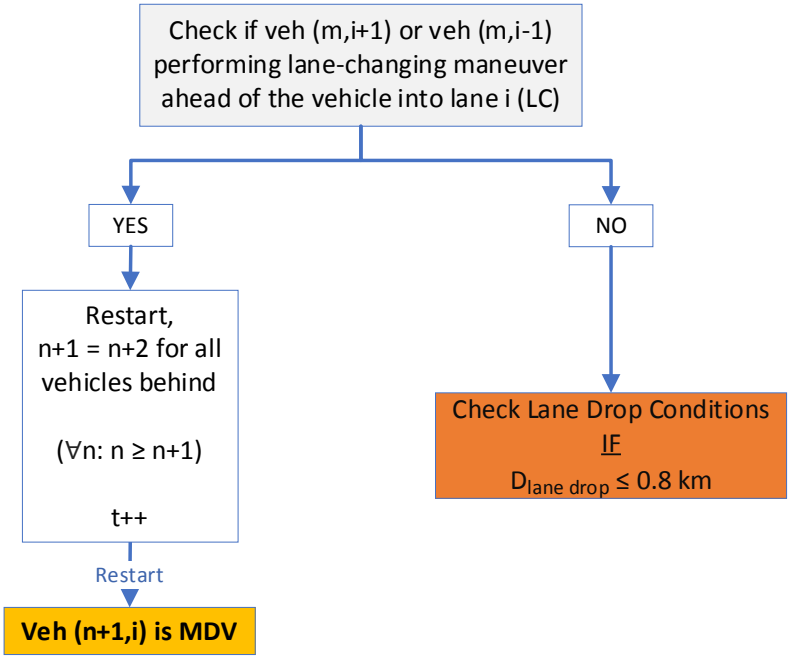

Figure 3-37 Process for checking the occurrence of lane-changing maneuver ahead of MDV

3.2.1.2 Linkage between the Car-Following and the Lane-Changing Models for MDVs

The linkage between the car-following and the lane-changing models for MDVs is quite similar to the linkage between these models for CAVs, except that a speed difference condition for the right lane change is eliminated and the desired speed (v_d) of an MDV is used instead of the current speed in some speed difference conditions. In addition, the desired speed is assigned for each MDV as a permanent attribute of that vehicle in this algorithm. Based on the study performed by Hill et al., the mean desired speed sampled from 46 drivers on freeways was found to be 111.89±7.83 km/h. Therefore, this value will be assigned to the MDVs in this model in a stochastic manner. Besides, the average number of discretionary lane changes of 0.74±0.60 times per kilometers was also found from the field experiment in that study (Hill et al., 2015).

The algorithm initially proceeds to check whether there is a lane drop within 0.8 km ahead of the vehicle. If there is currently no lane drop ahead within the distance, the discretionary lane-changing conditions will be assessed in the next step. However, if there is a lane drop ahead of the vehicle within the specific distance, the algorithm will automatically proceed to perform the mandatory lane change to the left.

In case there is no lane drop within 0.8 km ahead of the subject vehicle, the conditions for performing lane-changing maneuver to the right (slower lane) is assessed. The decision for

performing a lane change to the right will occur only if the following conditions simultaneously are true.

Firstly, the velocity difference is checked whether the average velocity of the current lane ($v_{AVG\ lane\_i}$) is actually greater than the average velocity of the target lane on the right ($v_{AVG\ lane\_i\text{-}1}$) by the threshold, as shown in Equation (3-39).

$$v_{AVG\ lane\_i} - v_{AVG\ lane\_i\text{-}1} > Threshold\_4M \tag{3-39}$$

Secondly, the velocity difference is checked if the current velocity of the leading vehicle in the current lane ($v_n(t)$) exceeds the desired speed of the subject vehicle ($v_{d\ n+1}(t)$) by Threshold_5M, as shown in Equation (3-40).

$$v_n(t) - v_{d\ n+1}(t) > Threshold\_5M \tag{3-40}$$

Otherwise, the algorithm will proceed to check the conditions for performing a lane-changing maneuver to the left (faster lane). The decision for performing a lane change to the left will occur only if three of these conditions simultaneously turn out to be true.

Firstly, the velocity difference between the permitted maximum longitudinal velocity or the speed limit (v_m) and the current velocity of the subject vehicle ($v_{n+1}(t)$) is assessed if the margin is greater than the threshold, as seen in Equation (3-41). If the permitted maximum longitudinal velocity (v_m) is greater than the current velocity of the subject vehicle ($v_{n+1}(t)$) by Threshold_6M, the output of this condition will be returned as true.

$$v_m - v_{n+1}(t) > Threshold\_6M \tag{3-41}$$

Secondly, the velocity difference is assessed if the average velocity of the target lane on the left ($v_{AVG\ lane\_i+1}$) is actually greater than the average velocity of the current lane ($v_{AVG\ lane\_i}$) by Threshold_7M, as shown in the Equation (3-42).

$$v_{AVG\ lane\_i+1} - v_{AVG\ lane\_i} > Threshold\_7M \tag{3-42}$$

Finally, the velocity difference is checked if the current velocity of the leading vehicle in the current lane ($v_n(t)$) is smaller than the desired speed of the subject vehicle ($v_{d\ n+1}(t)$) by Threshold_8M, as shown in Equation (3-43).

$$v_{d\ n+1}(t) - v_n(t) > Threshold\_8M \tag{3-43}$$

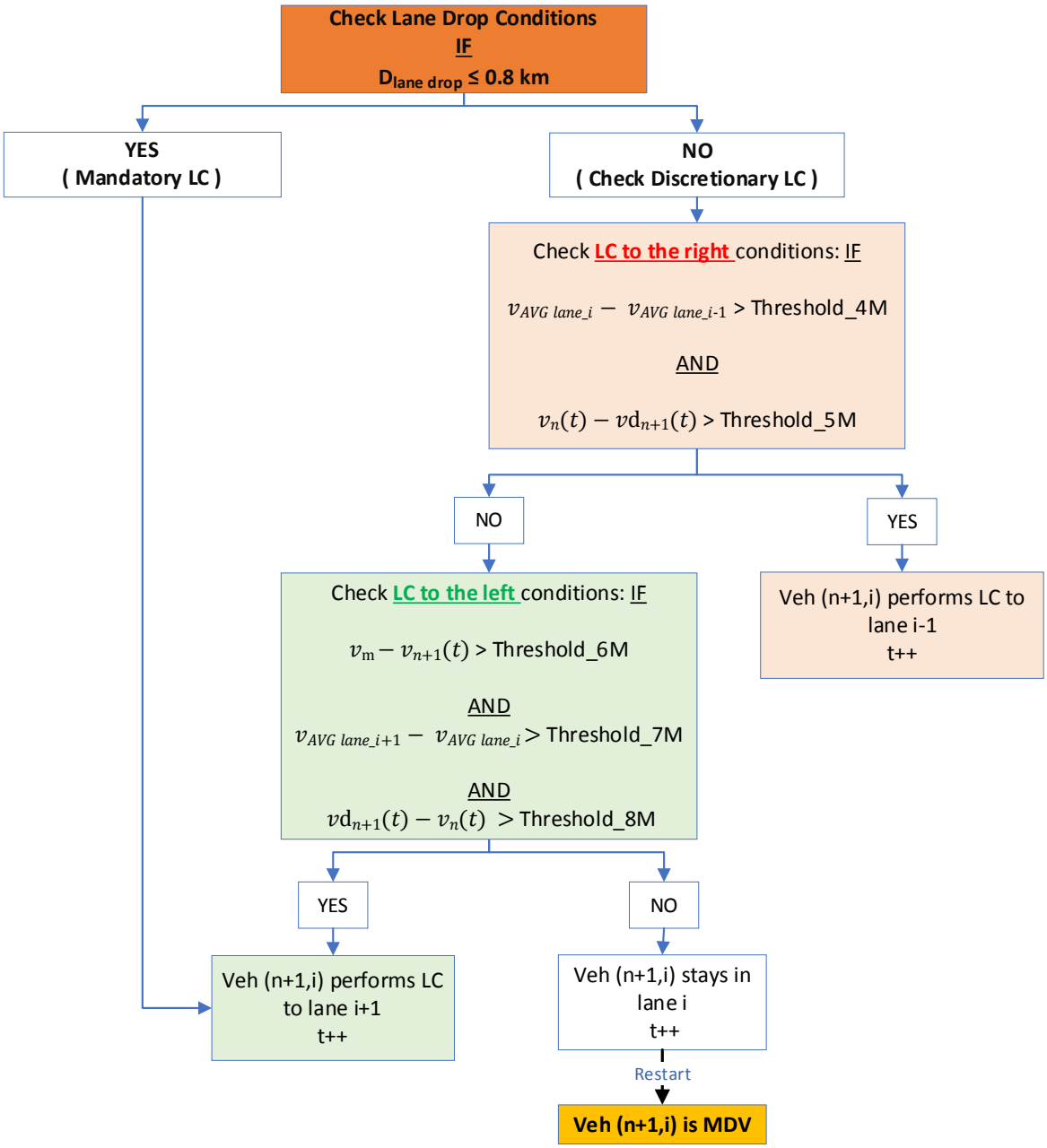

Figure 3-38 Linkage between the car-following and the lane-changing models for MDVs

Otherwise, the subject vehicle will be assigned to maintain in the current lane (*lane i*) and the algorithm will be restarted back to the beginning to recheck the type of the leading vehicle, as presented in Figure 3-38. These parameters will eventually be adjusted in the simulation run to make the calibrating parameter, which is capacity in this study, of the model and the field data fit each other in the calibration process.

3.2.1.3 The MDV Left-Lane-Changing Model

Besides the values of the parameters used, the difference between the left-lane-changing models for MDVs and CAVs is that the capability to recognize the types of the surrounding vehicles is eliminated in the MDV left-lane-changing model. Furthermore, the stochasticity of the parameters used in the MDV left-lane-changing model is another difference. However, the fundamental structure of the MDV left-lane-changing model still follows the similar structure used in the CAV left-lane-changing models.

The model starts by assessing the current gap in the target lane on the left (gap_{i+1}), as determined by Equation (3-14a). Three cases of the current gap are also used to identify whether the anticipated lane-changing maneuver is a free lane change ($gap_{i+1} \geq gap_{Free}$), a cooperative and competitive lane changes ($LS + g_{min} \leq gap_{i+1} < gap_{Free}$), or the next gap needs to be assessed prior to the occurrence of the lane-changing maneuver ($gap_{i+1} < g_{min} + LS$), as shown in Figure 3-39.

If the algorithm detects that the current gap in the target lane is available for a free lane change ($gap_{i+1} \geq gap_{Free}$), two conditions of the longitudinal distance and velocity differences between the subject vehicle and the potential follower in the target lane will be assessed prior to the initiation of lane changing maneuver. The free lane changing maneuver will occur only if these two conditions simultaneously turn to be true. The longitudinal distance difference condition in the MDV free left-lane-changing model is determined by Equation (3-4b); however, the minimum gap accepted for MDVs in this model is programmed to be a stochastic parameter, instead of the deterministic ones applied for CAVs. The corresponding value of g_{min} in this case is assigned as g_{min_M24} in the simulation models.

Based on the study conducted by Hill et al., the mean lag gap accepted under uncongested and congested conditions were found to be 26.60±13.76 meters and 13.92±9.44 meters, respectively, with gamma distribution (Hill et al., 2015). Therefore, one of these values of g_{min} will be assigned for MDVs in this model in a stochastic manner, based on the immediate density in the vicinity of the vehicle. To be specific, if the density in the vicinity of 200 meters surrounding the vehicle (100-meter distance ahead and behind the vehicle) is greater than 25 veh/km/lane (40 veh/mi/lane), the lag gap of 13.92±9.44 meters will be accepted under congested conditions; otherwise, the lag gap of 26.60±13.76 meters will be accepted under uncongested conditions.

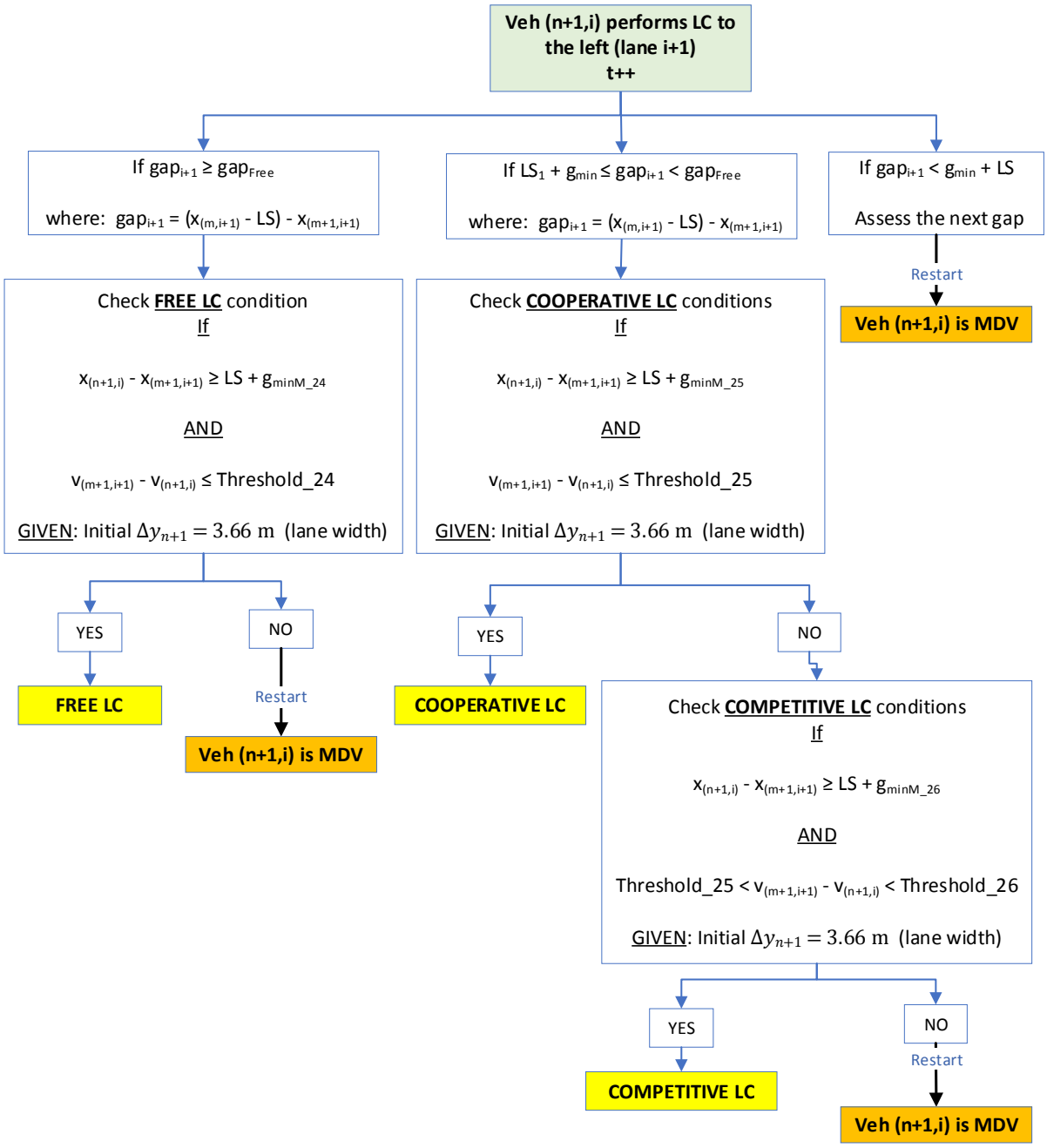

Figure 3-39 Flowchart of the MDV left-lane-changing model

In addition, the velocity difference conditions in the MDV free left-lane-changing model is displayed by Equation (3-44).

$$v_{(m+1,\,i+1)} - v_{(n+1,\,i)} \leq Threshold\_24 \tag{3-44}$$

Once the current gap in the target lane is detected to be available for a cooperative lane change ($LS + g_{min} \leq gap_{i+1} < gap_{Free}$), the cooperative lane changing maneuver will occur only if

the following two conditions simultaneously turn out to be true. Firstly, the lag gap is assessed, as shown in Equation (3-4b). A lag gap of 26.60±13.76 meters or 13.92±9.44 meters will be assigned for g_{min} of MDVs in a stochastic manner, depending on whether the traffic is under uncongested or congested conditions. The corresponding value of g_{min} in this case is assigned as g_{min_M25} in the simulation models. Secondly, the velocity difference conditions in the MDV cooperative left-lane-changing model is assessed, as displayed by Equation (3-45).

$$v_{(m+1,\, i+1)} - v_{(n+1,\, i)} \leq Threshold\_25 \tag{3-45}$$

The competitive lane change conditions are assessed in case the cooperative lane change conditions are false for the same range of gap in the target lane. The competitive lane changing maneuver will occur only if the following two conditions simultaneously turn out to be true. Firstly, the lag gap is examined, as shown in Equation (3-4b). Similar to the cooperative lane change, a lag gap of 26.60±13.76 meters or 13.92±9.44 meters will be assumed for g_{min} of MDVs in a stochastic manner, depending on whether the traffic is under uncongested or congested conditions. Secondly, the velocity difference conditions in the MDV competitive left-lane-changing model is assessed, as displayed by Equation (3-46).

$$Threshold\_25 < v_{(m+1,\, i+1)} - v_{(n+1,\, i)} < Threshold\_26 \tag{3-46}$$

When the longitudinal acceleration of the subject vehicle is calculated, the model then proceeds to determine the lateral velocity of the vehicle based on the remaining anticipated lateral displacement for lane change (Δy_{n+1}), which is initially set as 3.66 m (12 ft) by the beginning of the lane-changing process. This process for the MDV left-lane-changing models was designed to be consistent with the comparable process in the CAV left-lane-changing models, as described in section 3.1.1.3.

3.2.1.4 The MDV Right-Lane-Changing Model

Similar to the MDV left-lane-changing model; the stochasticity of the parameters also exists in the MDV right-lane-changing model, as well as the elimination of the capability of the subject vehicle to recognize the types of the surrounding vehicles.

The model begins with the assessment of the current gap in the target lane on the right (gap_{i-1}), as determined by Equation (3-14b). Again, three cases of the current gap are also used to identify whether the anticipated lane-changing maneuver is a free lane change ($gap_{i-1} \geq gap_{Free}$), a

cooperative and competitive lane changes ($LS + g_{min} \leq gap_{i-1} < gap_{Free}$), or the next gap needs to be assessed prior to the occurrence of the lane-changing maneuver ($gap_{i-1} < g_{min} + LS$), as shown in Figure 3-40.

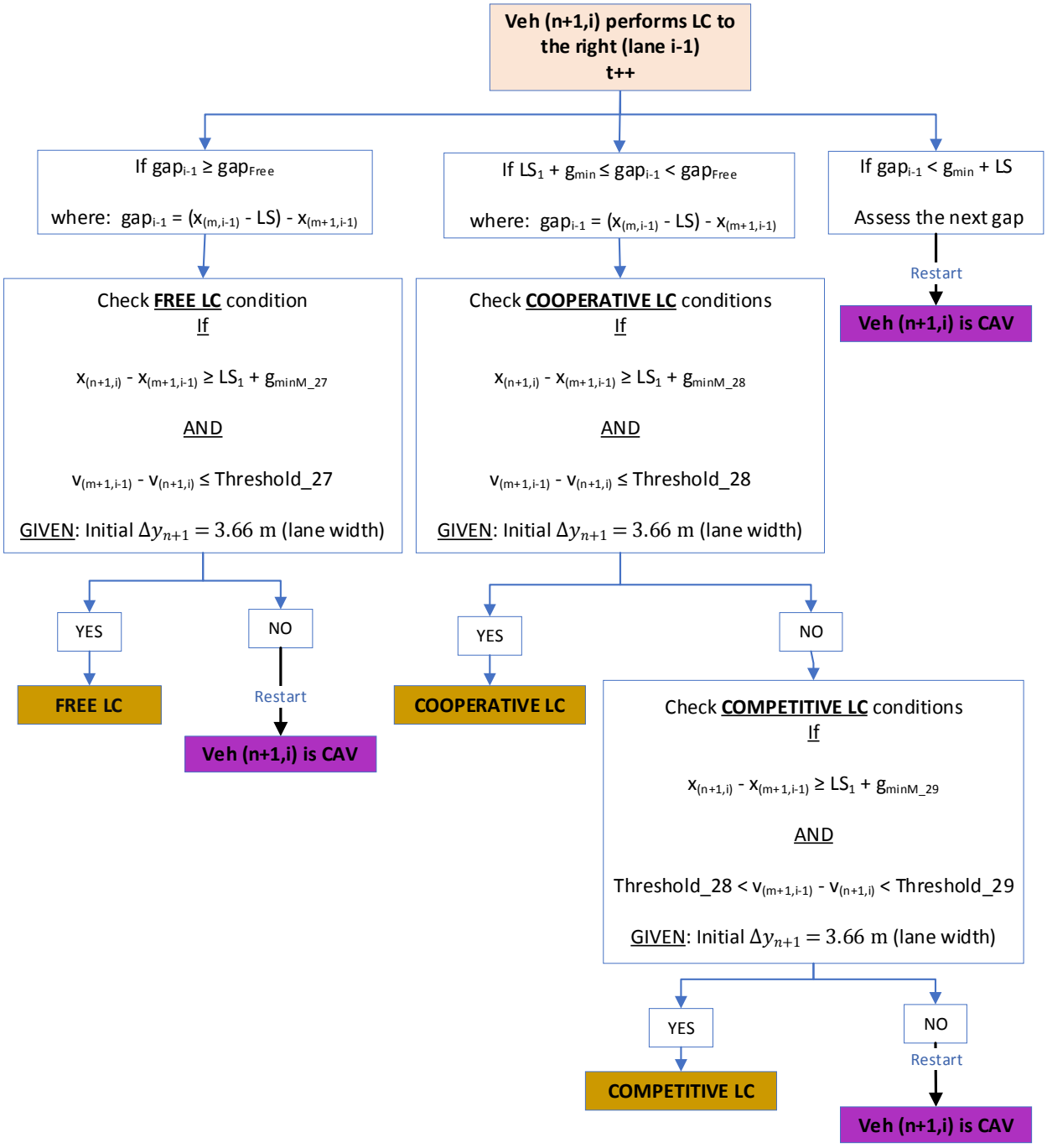

Figure 3-40 Flowchart of the MDV right-lane-changing model

If the algorithm detects that the current gap in the target lane is available for a free lane change ($gap_{i-1} \geq gap_{Free}$), two conditions of the longitudinal distance and velocity differences between the subject vehicle and the potential follower in the target lane will be assessed prior to the initiation of the lane changing maneuver. The free lane changing maneuver will occur only if these two conditions simultaneously are true. The longitudinal distance difference condition in the MDV free right-lane-changing model is determined by Equation (3-4a); however, the minimum gap accepted for MDVs in this model is programmed to be a stochastic parameter. A lag gap of 26.60±13.76 meters or 13.92±9.44 meters will be assigned for g_{min} of MDVs in a stochastic manner, based on the density in the 200-meter vicinity of the MDV. The corresponding value of g_{min} in this case is assigned as g_{min_M27} in the simulation models. Secondly, the velocity difference conditions in the MDV free left-lane-changing model is displayed by Equation (3-47).

$$v_{(m+1,\, i+1)} - v_{(n+1,\, i)} \leq Threshold\_27 \tag{3-47}$$

Once the current gap in the target lane is detected to be available for a cooperative lane change ($LS + g_{min} \leq gap_{i-1} < gap_{Free}$), the cooperative lane changing maneuver will occur only if the following two conditions simultaneously turn out to be true. Firstly, the longitudinal distance difference between the subject vehicle and the potential follower in the target lane is assessed, as shown in Equation (3-4a). A lag gap of 26.60±13.76 meters or 13.92±9.44 meters will be assigned for g_{min} of MDVs in a stochastic manner, depending on whether the traffic is under uncongested or congested conditions. The corresponding value of g_{min} in this case is assigned as g_{min_M28} in the simulation models. Secondly, the velocity difference conditions in the MDV cooperative right-lane-changing model is assessed, as displayed by Equation (3-48).

$$v_{(m+1,\, i+1)} - v_{(n+1,\, i)} \leq Threshold\_28 \tag{3-48}$$

The competitive lane change conditions are assessed in case the cooperative lane change conditions are false for the same range of gap in the target lane. The competitive lane changing maneuver will occur only if the following two conditions simultaneously are true. Firstly, the longitudinal distance difference between the subject vehicle and the potential follower in the target lane is assessed, as shown in Equation (3-4a). Similar to the cooperative lane change, a lag gap of 26.60±13.76 meters or 13.92±9.44 meters will be assumed for g_{min} of MDVs in a stochastic manner, depending on whether the traffic is under uncongested or congested conditions. Secondly,

the velocity difference conditions in the MDV competitive right-lane-changing model is assessed, as displayed by Equation (3-49).

$$Threshold\_28 < v_{(m+1,\, i+1)} - v_{(n+1,\, i)} < Threshold\_29 \quad (3\text{-}49)$$

The model then proceeds to determine the lateral velocity of the vehicle based on the remaining anticipated lateral displacement for a lane change (Δy_{n+1}). This process for the MDV right-lane-changing models was designed to be consistent with the comparable process in the CAV right-lane-changing models, as described in section 3.1.1.6.

3.2.2 MDV Platoon-Leading/Lane-Changing Algorithm

The MDV Platoon-Leading/Lane-Changing Algorithm is the sub-algorithm that controls the longitudinal and lateral movements of an MDV when the vehicle is the platoon leader, without any leading vehicle ahead or with a leading vehicle maintaining the space headway of greater than or equal to the free-flow headway ($s_{free\ flow}$). Similar to the Automated Platoon-Leading/Lane-Changing Algorithm, MDVs in this case are programmed to accelerate to their free-flow speeds.

However, unlike the Automated Platoon-Leading/Lane-Changing Algorithm where the CAV is programmed to accelerate to the speed limit (v_m); the acceleration rate of the platoon-leading MDV in this algorithm is set to accelerate to the desired speed (v_d), which is a specific attribute that varies from vehicle to vehicle. The acceleration rate of the subject vehicle at this stage is determined by Equation (3-50).

$$dv_1(t)/dt = k[v_d - v_1(t)] \quad (3\text{-}50)$$

Nevertheless, if the space headway between the subject vehicle and its leading vehicle is found to be smaller than the free-flow space headway, the algorithm will automatically be switched to the MDV Car-Following/Lane-Changing Algorithm, as shown in Figure 3-41.

Similar to the case in which a CAV is a platoon leader, the algorithm always assesses if there is a lane drop within 0.8 km ahead of the vehicle. If there is currently no lane drop ahead within the distance defined, the subject vehicle will be programmed to continue on the current lane. However, if there is a lane drop within the 0.8-km distance, the vehicle will find opportunities to perform the mandatory lane change to the left (*lane i+1*). Likewise, the time step will be

proceeded by one second and the vehicle will assess the lane-changing conditions in the next phase, as presented in Figure 3-42.

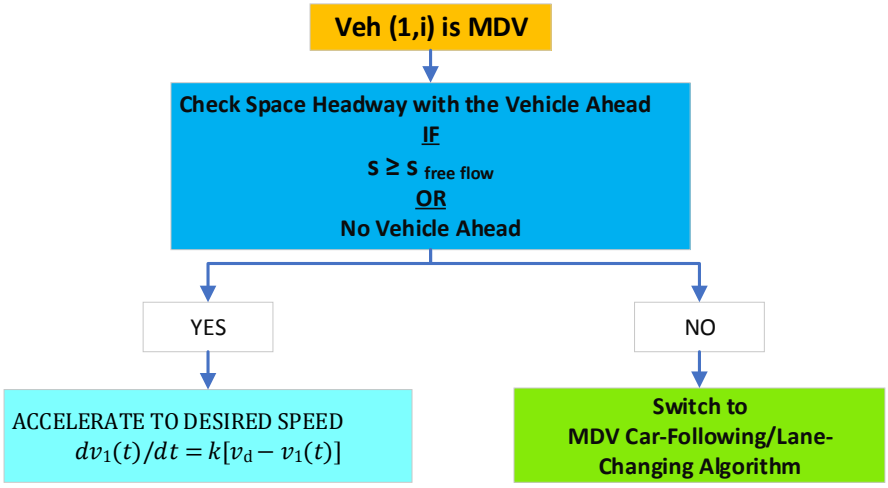

Figure 3-41 Mechanism for switching between the MDV Platoon-Leading/Lane-Changing Algorithm and the MDV Car-Following/Lane-Changing Algorithm

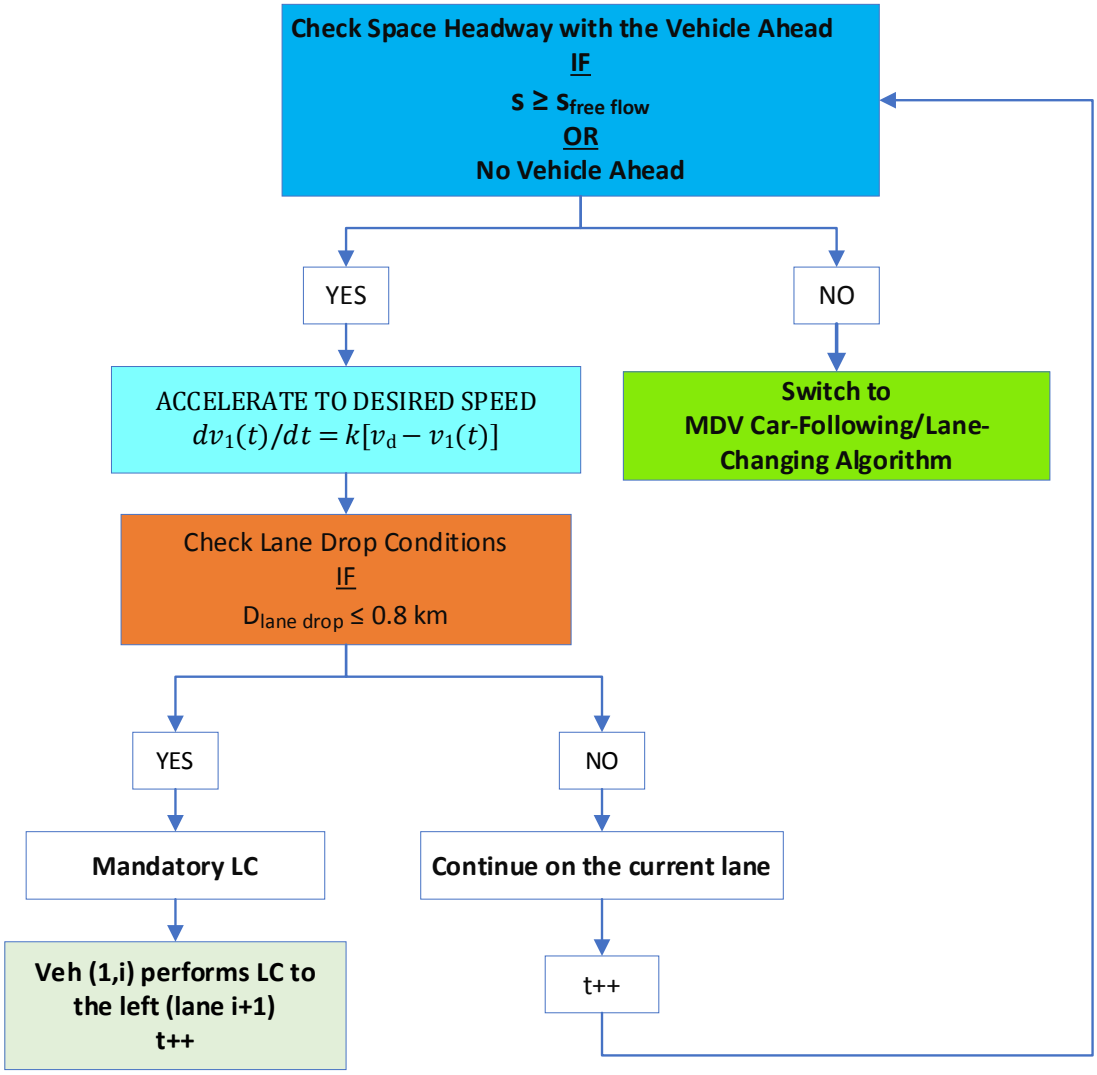

Figure 3-42 Flowchart of the MDV Platoon-Leading/Lane-Changing Algorithm

3.2.2.1 The MDV Left-Lane-Changing Models for Platoon-Leading Vehicles

Since the lane drop is always designed to be at the rightmost lane, the platoon leaders only need to change lane to the left to avoid the lane drop. The model starts by assessing the current gap in the target lane on the left (gap_{i+1}), as was determined by Equation (3-14a). Like the case when the vehicle is in a car-following/cruising mode, there are three possible cases for a lane-changing maneuver based on the available gap: a free lane change ($gap_{i+1} \geq gap_{Free}$), cooperative and competitive lane changes ($LS + g_{min} \leq gap_{i+1} < gap_{Free}$), or the next gap needs to be assessed prior to the occurrence of the lane-changing maneuver ($gap_{i+1} < g_{min} + LS$), as shown in Figure 3-43.

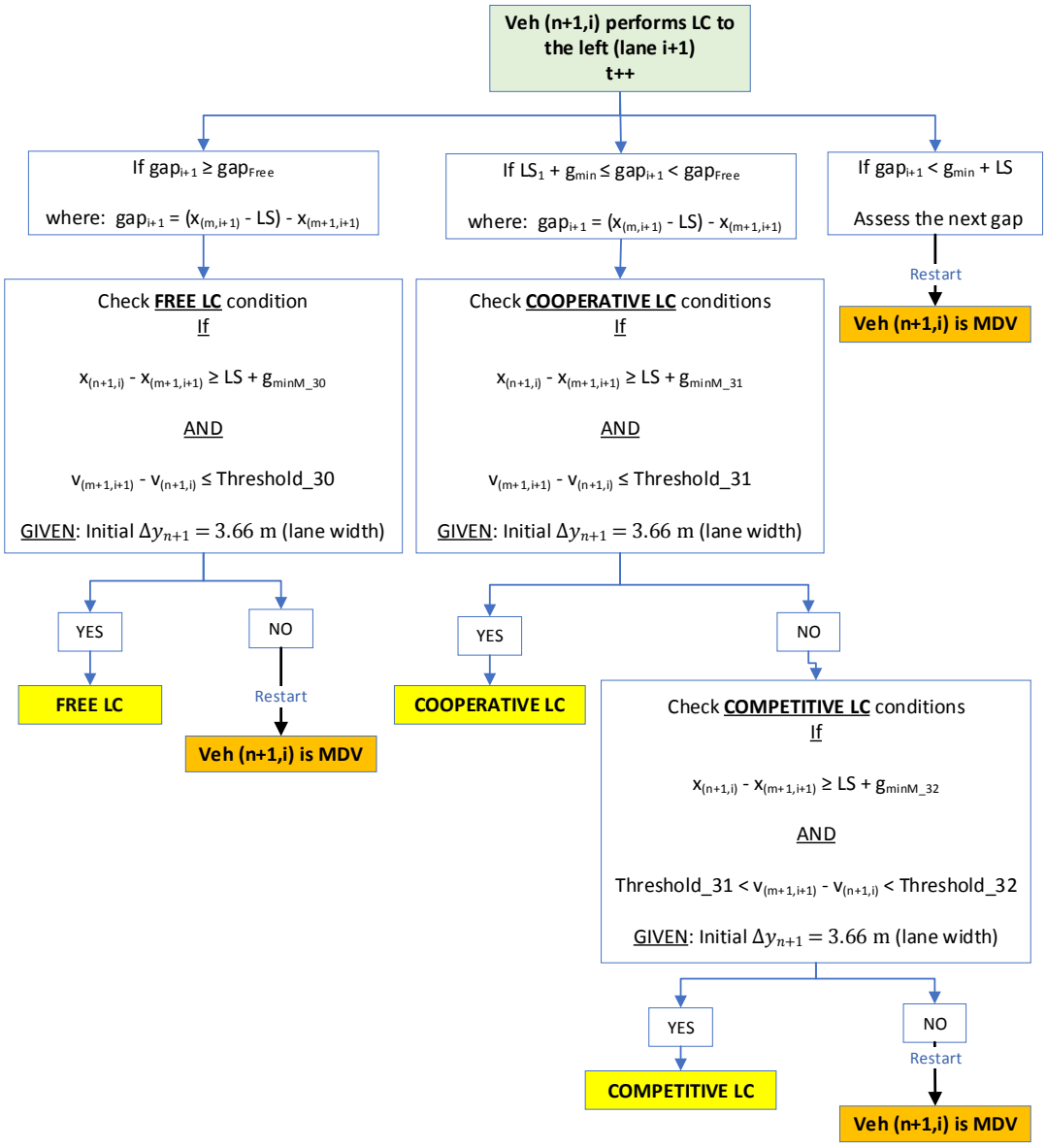

Figure 3-43 Flowchart of the MDV left-lane-changing model

If the algorithm detects that the current gap in the target lane is available for a free lane change ($gap_{i+1} \geq gap_{Free}$), two conditions of the longitudinal distance and velocity differences between the subject vehicle and the potential follower in the target lane will be assessed prior to the initiation of the lane changing maneuver. The free lane changing maneuver will occur only if these two conditions simultaneously are true. The longitudinal distance difference condition in the MDV free left-lane-changing model for platoon-leaders is determined by Equation (3-30); however, the minimum gap accepted for MDVs in this model is programmed to be a stochastic parameter instead of the deterministic ones applied for CAVs. A lag gap of 26.60±13.76 meters or

13.92±9.44 meters will be assigned for g_{min} of MDVs in a stochastic manner, depending on whether the traffic is under uncongested or congested conditions. The corresponding value of g_{min} in this case is assigned as g_{min_M30} in the simulation models. Secondly, the velocity difference conditions in the MDV free left-lane-changing model for platoon-leaders is displayed by Equation (3-51).

$$v_{(m+1,\, i+1)} - v_{(n+1,\, i)} \leq Threshold\_30 \tag{3-51}$$

When the current gap in the target lane is detected to be available for a cooperative lane change ($LS + g_{min} \leq gap_{i+1} < gap_{Free}$), the cooperative lane changing maneuver will occur only if the following two conditions simultaneously turn out to be true. Firstly, the longitudinal distance difference between the subject vehicle and the potential follower in the target lane is assessed, as shown in Equation (3-30). The value of g_{min} of 26.60±13.76 or 13.92±9.44 meters will be assigned for MDVs in this model in a stochastic manner. The corresponding value of g_{min} in this case is assigned as g_{min_M31} in the simulation models. Secondly, the velocity difference conditions in the MDV cooperative left-lane-changing model for platoon-leaders is assessed, as displayed by Equation (3-52).

$$v_{(m+1,\, i+1)} - v_{(n+1,\, i)} \leq Threshold\_31 \tag{3-52}$$

The competitive lane change conditions are assessed in case the cooperative lane change conditions are false for the same range of gap in the target lane. The competitive lane changing maneuver will occur only if the following two conditions simultaneously turn out to be true. Firstly, the longitudinal distance difference between the subject vehicle and the potential follower in the target lane is assessed, as shown in Equation (3-30). Similar to the cooperative lane change, the value of g_{min} of 26.60±13.76 or 13.92±9.44 meters will be assigned for MDVs in this model in a stochastic manner. Secondly, the velocity difference conditions in the MDV competitive left-lane-changing model for platoon-leaders is assessed, as displayed by Equation (3-53).

$$Threshold\_31 < v_{(m+1,\, i+1)} - v_{(n+1,\, i)} < Threshold\_32 \tag{3-53}$$

When the longitudinal acceleration of the subject vehicle is calculated, the model then proceeds to determine the lateral velocity of the vehicle based on the remaining anticipated lateral displacement for lane change (Δy_{n+1}), which is initially set as 3.66 m (12 ft) by the beginning of the lane-changing process. This process for the MDV left-lane-changing models for platoon-

leaders was designed to be consistent with the comparable process in the automated left-lane-changing models for platoon-leaders, as explained in section 3.1.2.1.

3.3 Summary of the Parameters in CAV and MDV Algorithms

The calibrated parameters used in the car-following and lane-changing models of the proposed algorithms are shown in Tables 3-1 and 3-2, respectively.

Table 3-1 Car-following parameters applied in the CAV and MDV algorithms

Car-Following Parameter	Value
Speed Limit (m/s)	33.5
Constant k (CAV)	0.30
Constant k (MDV)	0.41
Critical Space Headway (m)	30
Free Flow Space Headway (m)	200
CAV sensitivity constant	0
MDV sensitivity constant	0.13
Max Deceleration rate (m/s^2)	-9.8
Max Acceleration rate (m/s^2)	9.8
Desired Speed (m/s)	31.08±2.175
Gap_{free}	30
V_1 (MDV)	23.610
V_2 (MDV)	15.997
C_1 (MDV)	0.066
C_2 (MDV)	1.508
V_1 (CAV)	31.500
V_2 (CAV)	1.997
C_1 (CAV)	0.066
C_2 (CAV)	1.508

Table 3-2 Lane-changing parameters applied in the CAV and MDV algorithms

No.	Threshold (CAV)	Threshold_M (MDV)	g_{minC} (CAV lag gap)	Uncongested g_{minM} (MDV lag gap)	Congested g_{minM} (MDV lag gap)
1	3.00	-	18.00	-	-
2	3.75	-	20.00	-	-
3	5.00	-	-	-	-
4	2.50	10.00	-	-	-
5	2.00	10.00	-	-	-
6	10.00	6.00	-	-	-
7	0	10.00	-	-	-
8	0	10.00	-	-	-
9	3.00	-	18.00	-	-
10	3.75	-	20.00	-	-
11	5.00	-	25.00	-	-
12	3.00	-	18.00	-	-
13	3.75	-	20.00	-	-
14	3.00	-	18.00	-	-
15	3.75	-	20.00	-	-
16	5.00	-	25.00	-	-
17	3.00	-	18.00	-	-
18	3.75	-	20.00	-	-
19	3.00	-	18.00	-	-
20	3.75	-	20.00	-	-
21	5.00	-	25.00	-	-
22	3.00	-	18.00	-	-
23	3.75	-	20.00	-	-
24	2.50	-	-	24.70±13.76	13.92±9.44
25	3.75	-	-	24.70±13.76	13.92±9.44
26	5.36	-	-	24.70±13.76	13.92±9.44
27	2.50	-	-	24.70±13.76	13.92±9.44
28	3.75	-	-	24.70±13.76	13.92±9.44
29	5.36	-	-	24.70±13.76	13.92±9.44
30	2.50	-	-	24.70±13.76	13.92±9.44
31	3.75	-	-	24.70±13.76	13.92±9.44
32	5.36	-	-	24.70±13.76	13.92±9.44

CHAPTER 4 METHODOLOGY

This chapter presents the details on the experimental studies to evaluate the proposed algorithms via simulation. The simulation model development phase was started by coding and implementing the proposed CAV and MDV algorithms via JAVA programming language, followed by designing the roadway network for testing the traffic simulation. In addition, the parallel experiment of mixed traffic simulation in VISSIM was also conducted to provide a comparison and investigate the realism of the proposed model. Next, the scenario of the 100% MDV traffic was calibrated with field data on a comparable roadway network to validate the realism of the designed MDV characteristics prior to testing the mixed traffic scenarios. Finally, the mixed traffic scenarios of various CAV penetration rates were simulated in JAVA and VISSIM to measure the changes in roadway capacity and travel times produced by the simulation runs.

4.1 Simulation Model Development

4.1.1 Model Implementation in JAVA

The proposed CAV and MDV algorithms were coded via JAVA programming language in Eclipse, which is a JAVA programming platform, to replicate the driving behavior of the MDVs and the assumed characteristics of the CAVs on freeways. Fundamentally, the vehicle in the simulation is viewed as an object, in which its attributes are influenced by the interacting vehicles in real time. Therefore, JAVA was selected as a programming medium due to its capability to develop the object-oriented applications. As a result, each vehicle in the simulation was coded as an object which possesses specific attributes; such as the type of the vehicle, longitudinal displacement, velocity, acceleration rate, occupying lane, lane-changing status, and elapsed time of the vehicle in the simulation run.

A virtual one directional three-lane freeway segment with a lane drop was developed in JAVA to replicate the longitudinal dimension of the roadway. The length of the roadway segment and the location of the lane drop on the segment were programmed to be adjustable to provide flexibility when simulating various traffic scenarios. Furthermore, the vehicles in the simulation were programmed to be stochastically generated based on the user-defined traffic volume and the

negative exponentially-distributed interarrival time, which is the characteristic of arrivals in nature, according to the queuing theory (Winston and Goldberg, 2004).

The proportion between the CAVs and MDVs in a scenario, along with the volume per lane, were also programmed to be adjustable to evaluate the corresponding performance measures of the mixed traffic. In addition, the simulation time of each run was coded to be modifiable. Furthermore, the parameters in the CAV and MDV algorithms were coded to be adjustable to support the user-defined inputs and provide flexibility in the model calibration process. The logs of the longitudinal displacement and occupying lane of all the vehicles in the simulation runs were programmed to be exportable in the form of a spreadsheet for the purpose of data analysis.

To do so, JAVA packages, which work jointly and simultaneously, were created in Eclipse to categorize simulation entities and collect relevant classes for each entity (Table 4.1). The classes in these packages were assigned to run in conjunction with each other to simulate the traffic scenarios and produce the results.

Table 4-1 The JAVA packages and their descriptions

JAVA package name	Description
CarType.java	Classifies vehicles as MDV or CAV
Car.java	Represents the classes and attributes of a vehicle
Roadway.java	Contains attributes of the virtual roadway segment
Lane.java	Represents lanes in the roadway network
Simulator.java	Contains codes for the car-following and lane-changing models of MDVs and CAVs to emulate the interactions between vehicles in traffic
LaneChangeType.java	Classifies types of lane changing maneuver
ReleaseSchedule.java	Controls the arrivals of vehicles in traffic
IntervalOutput.java	Creates the intervals for fitting-in the resultant performance measures
SimulationResults.java	Displays the collected performance measures

All equations and conditions associated with each entity were then coded to the related package. The codes were compiled and run to figure out and resolve the error messages until the syntaxes of the whole program are logical.

4.1.2 Traffic Simulation Models in VISSIM

VISSIM 11 was used to simulate the mixed traffic scenarios since this software has the ability to simulate the characteristics of various types of AVs. The characteristics of the default car, based on Wiedemann 99 car-following model and the existing lane-changing parameters, were adopted for the MDVs in VISSIM. In addition, the CAVs were modeled based on the default characteristic of the all-knowing AVs in VISSIM, which is based on the Wiedemann 99 car-following model. The desired speed of the MDVs was assumed to be 111.89±7.83 km/h to match with the desired speed used for MDVs in the JAVA simulation. This was done by adjusting the probability distribution of the desired speed function based on normal distribution. The desired speed of CAVs in VISSIM was adjusted to 120 km/h to pair with the same desired speed applied for CAVs in the JAVA platform.

4.2 Test Network Design

Since this study aims to evaluate the effect of the CAV algorithm on freeway capacity, a roadway network with a bottleneck was created. A three-lane tangent freeway segment of 4-kilometers length with a lane drop (3-to-2 configuration) at the 3rd kilometer measured from the beginning of the segment was applied in both simulation platforms. The lane width was 3.66 m (12 ft), which is the base condition for lane width of a freeway, was adopted (Roess et al., 2011). In addition, the speed limit of 120 km/h was adopted for the freeway segment to bound the maximum longitudinal velocity available for the vehicles. Virtual speed detectors and vehicle counters were placed 40 meters upstream and downstream of the lane drop location to collect data in the simulation runs. The freeway segment was designed as a single extended section with 0% grade; therefore, the effects of grade was not tested. In addition, the effects of the lateral clearance and the curvature of the freeway segment were neglected in this study due to the limitation of the models used. The schematic of the proposed freeway segment is illustrated in Figure 4-1.

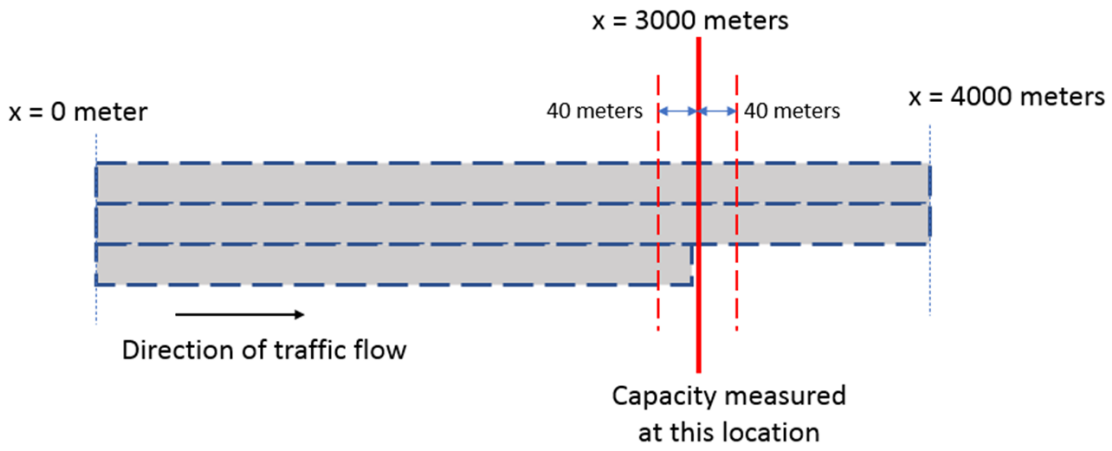

Figure 4-1 The proposed 3-lane freeway segment with a lane drop for testing the scenarios

4.3 Model Calibration

Next, the traffic scenario of 100% MDVs was calibrated in both JAVA and VISSIM using speed and flow field data until the acceptable statistical parameter was achieved. Speed and throughput were two main performance measures used to calibrate the models. The speed-flow data (shown in Figure 4-2) were adopted from a lane drop bottleneck on a German freeway, with comparable configuration (Brilon et al., 2005). Traffic data were collected based on 5-minute intervals during a period of one year and the lane drop capacity was found to be 4,284 veh/h, or 2,142 veh/h/ln (Brilon et al., 2005). The Brilon's speed-flow data were extracted using WebPlotDigitizer 4.2, which is a tool to extract the underlying numerical data of graphs (Rohatgi, 2019), to obtain the raw data of the scatterplot.

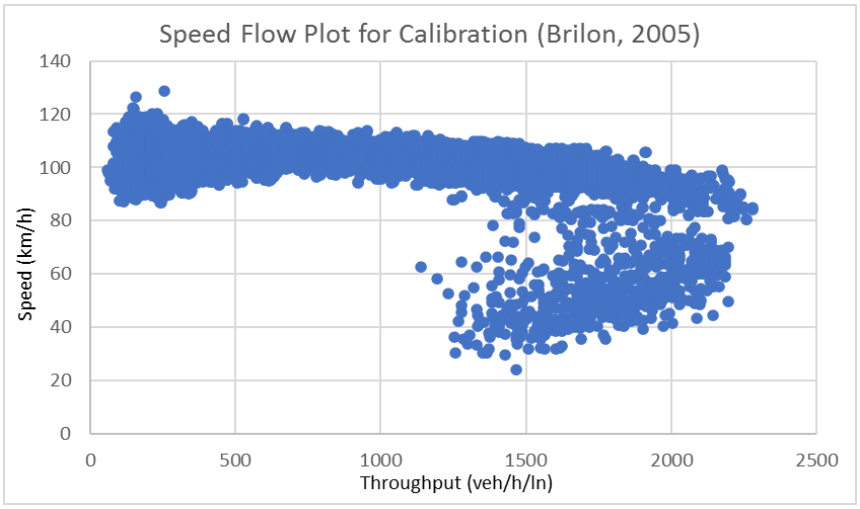

Figure 4-2 Speed-flow diagram used for calibrating the base models (Brilon, 2005)

Root Mean Square Error (RMSE) was used as a main statistical indicator to evaluate the model calibrations. Since fluctuations around the mean is in the nature of traffic phenomena, penalizing small errors might lead to an over-specified model. Therefore, penalizing large values of RMSE is practical in the context of stochastic traffic modeling (Hollander and Liu, 2008). For the RMSE calculation the raw data were divided into intervals based on the throughput range of 20 veh/h/ln. Next, the average speed of the datapoints within each interval was determined to represent the corresponding speed of the throughput interval. Ultimately, the datapoints of the calculated average speed of the raw data in each interval and the mid-value of the throughput interval were applied to represent the field data in the model calibration process.

4.3.1 Calibration Method for JAVA Simulation Model

The field-measured speed-flow data from Brilon et al., (2005) were used to calibrate the 100% MDV traffic scenario. Speed and throughput data were collected at 5-minute intervals and measured slightly downstream of the lane drop location. The simulation time of each run was set as one hour, with a time step of one second, to obtain datapoints for a specific demand volume. The datapoint obtained during the first 5-minute interval of every simulation run was discarded to avoid including the datapoints produced during the time that the steady state of traffic has not yet been reached. Therefore, 11 datapoints were obtained from each simulation run. The values of the throughput in vehicles per hour per lane and its corresponding space-mean speed were extracted for each time interval from each run.

Each parameter in the model was then adjusted and run to test for the sensitivity and impacts of the parameter on the resultant speed and throughput of the 100% MDV scenario. Once the positive and negative impacts of each parameter on speed and throughput were perceived, the viable range of the parameter was scoped for running the simulation model in the further steps. Initially, the models were run for the purpose of reaching the capacity in the region of around 2,100 – 2,200 veh/h/ln; in order to closely match with the field capacity of 2,142 veh/h/ln. Other speed-related parameters were then readjusted to calibrate the speed-flow diagram. The parameters which were found to considerably affect the speed and throughput were: sensitivity function (λ), sensitivity constant (κ), acceleration rates, optimal velocity parameters (C_1, C_2, V_1, and V_2), critical space headway (s_c), and desired speed (v_d). Consequently, these parameters were mainly adjusted in the model to fit the generated speed-flow diagram with the field data.

Next, each complete simulation with a specific set of parameters was run 65 times with the same set of various demand volumes ranging from 100 veh/h/ln to 2,000 veh/h/ln to acquire a speed-flow plot. Therefore, each resultant speed-flow diagram contains 715 datapoints (N = 715). The speed-flow datapoints were then plotted to produce a speed-flow diagram and the RMSE and the R-square of the simulation were calculated.

Eventually, the best-fit model was found to produce an RMSE of 4.78 km/h; along with the capacity of 2,131 veh/h/ln; which was 0.5 percent, or 11 veh/h/ln, smaller than the capacity of the field data. In addition, the calibrated model yielded the R^2 of 0.90 with the corresponding p-value of < 0.001, as shown in Figure 4-3.

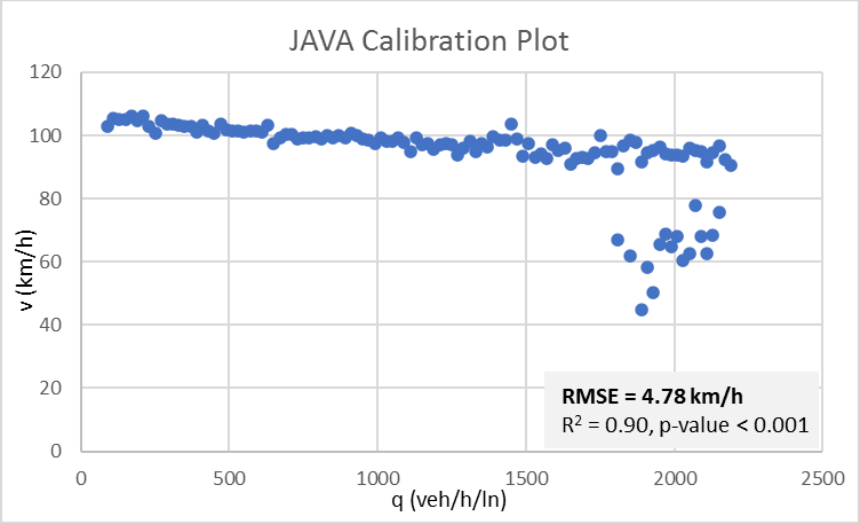

Figure 4-3 The calibrated speed-flow diagram of JAVA simulation model

4.3.2 Calibration Method for VISSIM Simulation Model

The calibration method for the 100% MDV traffic scenario in VISSIM followed a similar process with the calibration in JAVA. Initially, the designed freeway network with a 4-kilometer length with a bottleneck at the third kilometer (3-to-2 lane configuration) was created in VISSIM, using connectors to connect the 3-lane and 2-lane freeway links together. Next, a group of data collectors were placed at the bottleneck and 40-meter downstream of the bottleneck to collect average speed, vehicle count, and delays in each interval for further analyses. Travel time measurements were also placed on the links to collect the average travel time of vehicles in each interval, as seen in Figure 4-4.

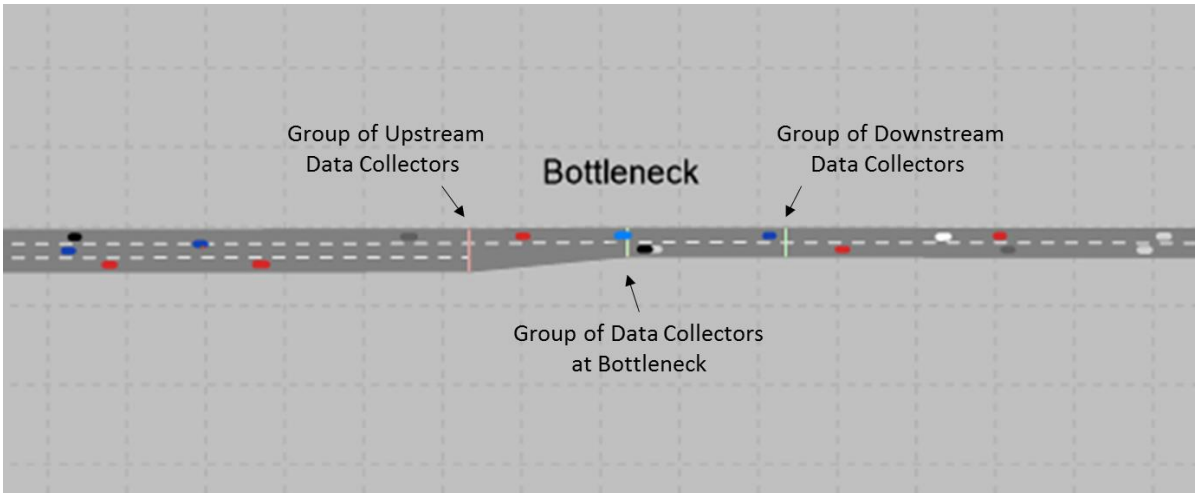

Figure 4-4 The freeway segment with data collectors created in VISSIM

Next, vehicle inputs were added at the entry lanes of the network to generate vehicles in the traffic stream. A 5-minute interval was also established to collect the space-mean speed and throughput data in each simulation run. In addition, the desired speed profile of the MDVs was established to follow the normal distribution of 111.89±7.83 km/h, which is the desired speed assumed for MDVs in the JAVA simulation. Once the network, detectors, and the desired speed profile were setup; the vehicle composition was modified to contain only the default car type, which was adopted to replicate the characteristics of MDV in VISSIM. The created desired speed profile was assigned to the selected vehicle type, together with the relative flow of 1.0. Furthermore, the edited vehicle composition profile was assigned to the vehicle inputs to generate vehicles with the modified characteristics in the network. The simulation time of each run was also set to one hour and the datapoint gained during the first 5-minute interval of every simulation run was discarded to avoid including datapoints produced before the network reaches steady state.

Next, each complete simulation with a specific set of parameters ran multiple times with the same set of various demand volumes ranged from 100 veh/h/ln to 2,000 veh/h/ln to acquire a speed-flow plot. Each resultant speed-flow diagram contains 1,397 datapoints (N = 1,397). In the calibration process, the freeway network was broken down into three parts: 3-lane upstream, 2-lane downstream segments, and the merge area, for the purpose of fitting the speed-flow diagram with the field data. Three parameters in Wiedemann 99 car-following model used for the MDVs were then readjusted to calibrate the model: standstill distance between vehicles (CC0), time headway (CC1), and following variation between vehicles (CC2). Finally, the best-fit model was

achieved by assigning CC0 and CC1 in the upstream segment and merge area to be 2 meters and 1.5 seconds, respectively; whereas the CC0 and CC1 in the downstream segment were respectively set at 1.2 meters and 0.5 seconds. In addition, the CC2 in the upstream and downstream segments were both set at 4 meters, while the CC2 in the merge area was assigned to be 7 meters.

The best-fit model created was found to produce an RMSE of 6.48 km/h, with the capacity of 2,072 veh/h/ln; which was 3.3 percent, or 70 veh/h/ln, less than the capacity of the field data. The R^2 value of the model was 0.95, with the corresponding p-value of < 0.001, as illustrated in Figure 4-5.

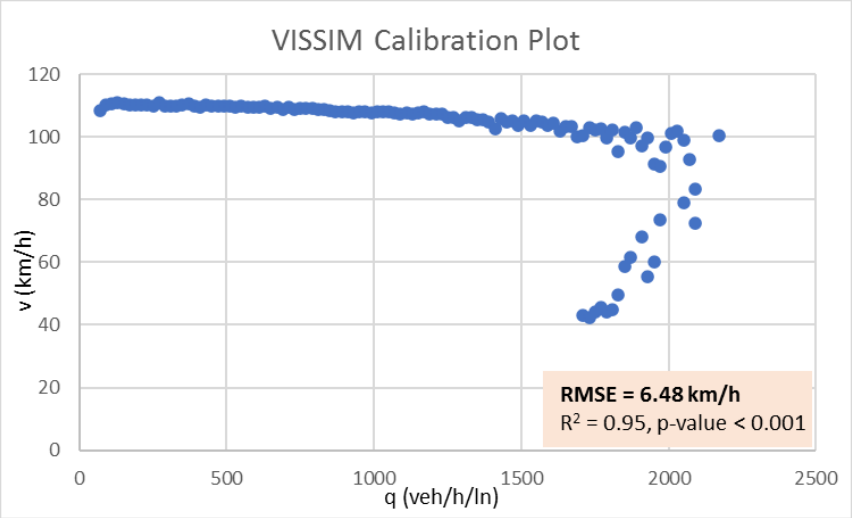

Figure 4-5 The calibrated speed-flow diagram of VISSIM model

4.4 Mixed Traffic Simulation based on CAV Penetration Rates

Once both models were calibrated for 100 MDVs, the mixed traffic scenarios of various proportions of CAV and MDV on the designed freeway segment were simulated to evaluate the performance measures of interest. The mixed traffic scenarios of partial CAVs and MDVs were generated based on the 10-percent increment of the CAV penetration rate, varying from 10 percent to 100 percent of CAVs in the traffic stream. As a result, the total 10 scenarios of various proportions of CAVs in the traffic stream (scenario 2 – scenario 11) were simulated in JAVA and VISSIM, in addition to the scenario of 100% MDV (scenario 1), as shown in Figure 4-6. In addition, each traffic scenario was simulated for a number of runs until a full curve is obtained, and the aggregated results were used to represent the outcome of the scenario. Ultimately, the

resultant speed-flow diagrams were plotted and compared to evaluate the impacts of CAVs in traffic operations.

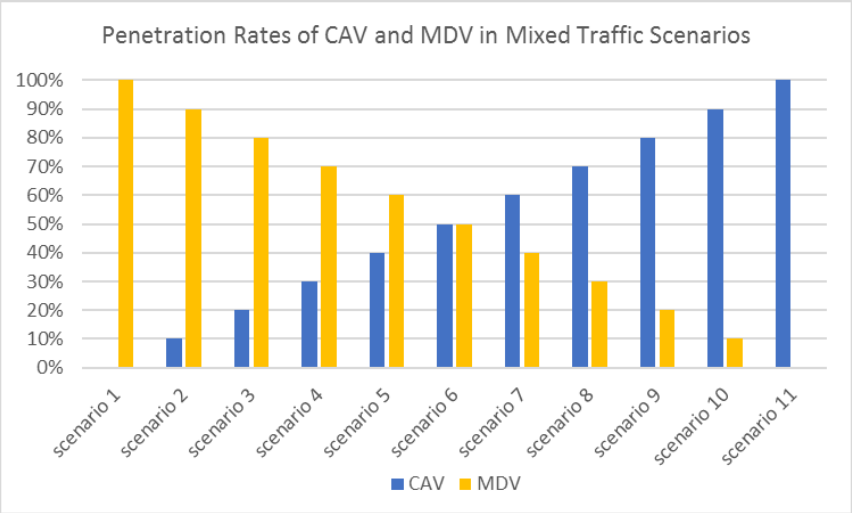

Figure 4-6 Mixed traffic scenarios based on CAV and MDV penetration rates in this study

For this part of the analysis, the calibrated parameters in the JAVA and the VISSIM models were used. Similar to the calibration process, data were obtained in 5-minute intervals and the same lane drop network was used. Each datapoint generated in both the JAVA and VISSIM simulation represents the average throughput per hour per lane and its corresponding average space-mean speed of all the vehicles counted during an interval. The speed-flow diagrams for traffic flows downstream of the lane drop were then constructed from the collected data in each scenario.

To simulate the mixed traffic scenarios in JAVA, first of all, the case of 90% MDV and 10% CAV mixed traffic was simulated to generate the speed-flow diagrams of the upstream and downstream traffic. To simulate the mixed traffic scenarios in VISSIM, the vehicle composition was modified to contain two vehicle types: MDV and CAV. In addition, the desired speed of all CAVs in VISSIM was modified to be 120 km/h, as applied for the characteristic of CAVs in JAVA. Once these steps were accomplished, the next scenario was simulated by increasing the penetration rate of CAVs by 10 percent and dropping the penetration rate of MDVs by 10 percent. The simulation process ran in this fashion until the speed-flow diagrams of all the 10 scenarios with CAV penetration rates were obtained. Each scenario ran multiple times using various demand

volume inputs which ranged from 100 veh/h/ln to 2,000 veh/h/ln to achieve the speed-flow plots that contains the datapoints in the speed-drop region.

This study adopted an assumption that the length of vehicle was identical among all the vehicles in the JAVA simulation and equal to 4.5 meters, whereas the average length of vehicles in VISSIM turned to be 4.4 meters. However, the length of each vehicle in VISSIM was randomized based on the stochasticity of the software package. In addition, the critical space headway for a vehicle to switch from car-following mode to cruising mode was calibrated to be 30 meters in the JAVA model. However, the effects of the lateral clearance, grade, and curvature of the freeway segment were neglected in this study due to the limitation of the fundamental models adopted.

4.5 Performance Measures

In this study, two performance measures were evaluated: capacity and travel time. Capacity was measured by identifying the point of the traffic breakdown event. To do so, the average speed of the freeway segment measured at the capacity point was carried out for each traffic volume simulated to justify the speed-drop cut-off from the speed-flow graph for determining the capacity. In addition, the travel times produced in the traffic scenarios were measured and compared to the travel times of the default scenario, where the traffic was composed of 100% MDV, to ascertain the changes in travel time with regard to the increments in the CAV penetration rates.

4.6 Summary of Methodology

This chapter presents the methodology used in the dissertation. The proposed algorithms, along with a 3-to-2 virtual freeway segment, were coded in JAVA to create a simulation platform, prior to calibrating the default model with the field data. The traffic scenario of 100-percent MDVs was calibrated in both JAVA and VISSIM using speed and flow field data until the acceptable statistical parameter was achieved. RMSE and R-Square were used as statistical indicators to evaluate the model calibrations. Eleven mixed traffic scenarios were simulated in the developed platform, along with the parallel simulation in VISSIM, to generate the resultant speed-flow diagrams. The comprehensive analyses on the simulation results are discussed in the next chapter.

CHAPTER 5 RESULTS

This chapter presents the results of the simulation obtained from JAVA and VISSIM, along with the analyses of the performance measures. The speed-flow diagrams of the downstream traffic at the bottleneck on the 3-to-2 freeway segment in each mixed traffic scenario are presented. Furthermore, the performance measures of traffic in each scenario are analyzed to highlight the changes in roadway capacity and travel times as the penetration rate of CAV increases. A comparison of the results between the JAVA and VISSIM simulation models is discussed. The effect of the proposed algorithm on the vehicle trajectories and their gap acceptance decisions is also presented.

5.1 Simulation Results

The results of 11 traffic scenarios simulated in JAVA and VISSIM based on the 10-percent increments in penetration rates of CAV are presented in the following sections.

5.1.1 Scenario 1: 100% MDV Traffic Scenario

The speed-flow diagrams measured downstream of the lane closure in scenario 1 simulated in JAVA and VISSIM appear to have similar shape, with comparable level of maximum throughput obtained. Also, the slopes of the curves simulated in both platforms appear to be similar. However, the speed during uncongested conditions in the VISSIM model seems to be slightly higher than the speed during uncongested conditions in the JAVA model. The capacity of this scenario obtained from the JAVA model was estimated to be 2,131 veh/h/ln; while the capacity obtained from the VISSIM model was estimated to be 2,072 veh/h/ln, which is 2.8 percent less than the JAVA capacity. The speed-flow diagrams in scenario 1 simulated in JAVA and VISSIM are presented in Figure 5-1.

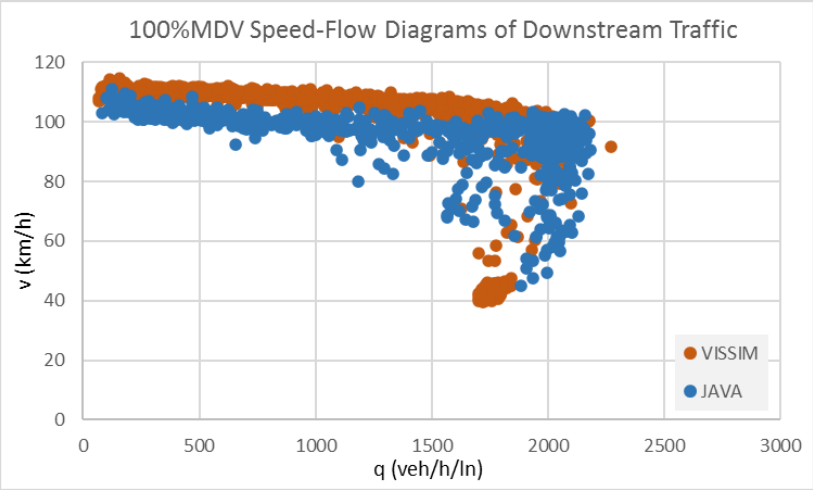

Figure 5-1 Speed-flow diagrams of the downstream traffic in scenario 1

5.1.2 Scenario 2: 90% MDV and 10% CAV Mixed Traffic Scenario

The speed-flow diagram of the scenario 2 obtained from JAVA simulation shows that the breakdowns started to occur for the throughputs that fell in the region of 2,000 – 2,300 veh/h/ln. According to the analysis, the capacity of the mixed traffic in scenario 2 simulated in JAVA was estimated to be 2,166 veh/h/ln; which is 1.6 percent greater than the capacity in the scenario of 100% MDV, or increased by 35 veh/h/ln. The speed-flow diagrams in scenario 2 generated by the JAVA model is illustrated in Figure 5-2.

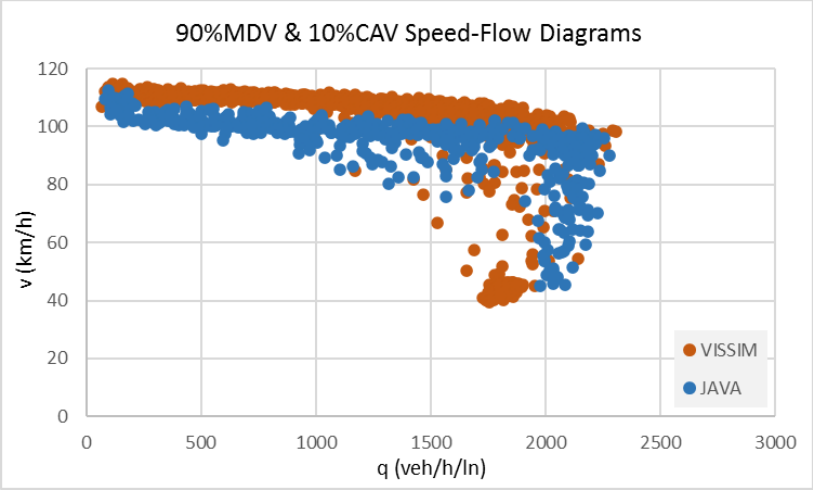

Figure 5-2 Speed-flow diagrams of the downstream traffic in scenario 2

Figure 5-2 also illustrates the speed-flow diagram in scenario 2 generated by the VISSIM model. The estimated capacity in scenario 2 was 2,126 veh/h/ln, or increased by 2.6 percent from scenario 1.

It was found that both JAVA and VISSIM models yielded similar results in terms of capacity and shape of the curve. The capacity of scenario 2 obtained from the algorithms simulated in JAVA was found to be greater than the capacity obtained from the VISSIM model by 40 veh/h/ln, or 1.9 percent. However, the speed-flow curves produced by VISSIM model are slightly sharper than the curves obtained from JAVA for the 90% MDV and 10% CAV mixed traffic scenario. In addition, there are greater number of datapoints scattering in the high-flow region in the JAVA model's diagrams than in the VISSIM's diagrams. In other words, the speed-flow data generated by the JAVA model seem to move slightly towards more sustained flow than the data obtained in VISSIM.

5.1.3 Scenario 3: 80% MDV and 20% CAV Mixed Traffic Scenario

The JAVA model's speed-flow diagram of the traffic in scenario 3 displays somewhat similar characteristics of the diagram in scenario 2; however, the diagram appears to move towards higher throughputs. In addition, there are fewer datapoints at high flows and low speeds in this scenario, compared to scenario 2. The capacity of the mixed traffic in scenario 3 simulated in JAVA was estimated to be 2,224 veh/h/ln; which is 2.7 percent greater than the capacity in scenario 2, or increased by 58 veh/h/ln. The capacity of scenario 3 yielded by the VISSIM model was estimated to be 2,143 veh/h/ln; which was found to improve from the capacity in scenario 2 by 17 veh/h/ln, or an increase of 0.8 percent. Furthermore, the overall speed in the uncongested flow region in this scenario slightly increased from the speed of the same region in the previous scenario. The speed-flow diagrams in scenario 3 generated by JAVA and VISSIM models are displayed in Figure 5-3.

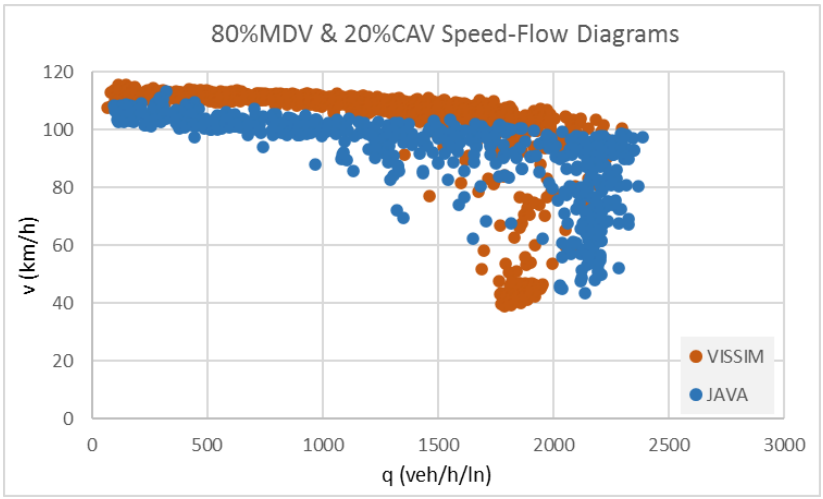

Figure 5-3 Speed-flow diagrams of the downstream traffic in scenario 3

Both JAVA and VISSIM models produced similar results in terms of capacity and shape of the curve in this scenario. The capacity of scenario 3 simulated in JAVA was found to be greater than the capacity obtained from the VISSIM model by 81 veh/h/ln, or 3.8 percent. Obviously, the speed-flow curve obtained from the VISSIM model is slightly sharper than the curve generated by the JAVA model.

5.1.4 Scenario 4: 70% MDV and 30% CAV Mixed Traffic Scenario

The shape of the JAVA model's speed-flow diagram of the traffic flow in scenario 4 seems to be similar to the diagram in scenario 3; however, the curve extends to higher throughputs. Obviously, the slope of the speed-flow curve appears to be slightly steeper than the downstream speed-flow curve in scenario 3. The capacity of the mixed traffic in scenario 4 in JAVA was estimated to be 2,329 veh/h/ln; which is 4.7 percent greater than the capacity in scenario 3, or increased by 105 veh/h/ln. The capacity of the scenario 4 produced by VISSIM was estimated to be 2,260 veh/h/ln; which is an increase from the capacity in scenario 3 of 117 veh/h/ln, or an increase of 5.5 percent. The overall speed in the uncongested flow region in this scenario seems to be slightly higher than the overall speed in the previous scenario. The speed-flow diagrams of this scenario generated by JAVA and VISSIM are displayed in Figure 5-4.

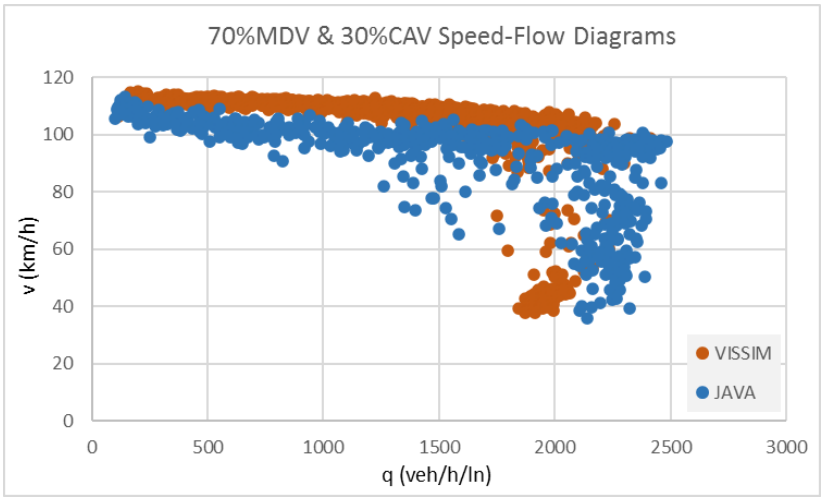

Figure 5-4 Speed-flow diagrams of the downstream traffic in scenario 4

The capacity and shape of the curves produced by VISSIM and JAVA models are similar in this scenario. The estimated capacity of scenario 4 obtained in JAVA turned to be greater than the capacity obtained from the VISSIM model by 3.1 percent, or 69 veh/h/ln. Although, the speed-flow curve obtained from the JAVA model is slightly sharper than the curve generated by the VISSIM model, the difference is smaller in this scenario than in the previous scenarios.

5.1.5 Scenario 5: 60% MDV and 40% CAV Mixed Traffic Scenario

The shape of the JAVA model's speed-flow diagram of scenario 5 appears to be similar to the diagram in scenario 4. However, the range of the curve slightly expanded to the higher throughputs, while the overall speed of the datapoints in the uncongested flow region increased from the overall speed of the same region in the previous scenarios. The angle of the speed-flow curve seems to be sharper than the angle of the curve in scenario 4. The capacity of the mixed traffic in scenario 5 simulated in JAVA was estimated to be 2,416 veh/h/ln; an increase of 87 veh/h/ln, or 3.7 percent from scenario 4. The speed-flow diagram of the JAVA model in scenario 5 is presented in Figure 5-5.

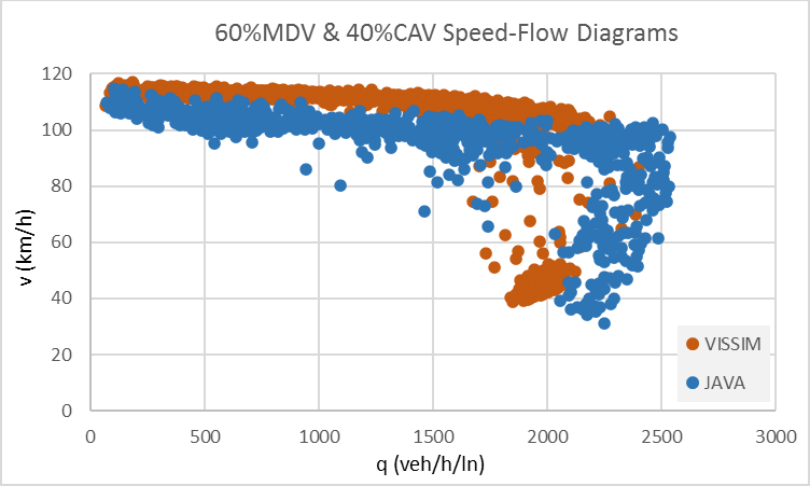

Figure 5-5 Speed-flow diagrams of the downstream traffic in scenario 5

Figure 5-5 also shows the speed-flow diagram obtained from the VISSIM model. The capacity of scenario 5 in VISSIM was 2,292 veh/h/ln; which is slightly higher than scenario 4 by 32 veh/h/ln, or 1.4 percent. Furthermore, the overall speed of the traffic in the uncongested flow region in this scenario seems to be slightly higher than the overall speed in the previous scenario.

The shape of the curves produced by VISSIM and JAVA models are slightly different in this scenario; however, the capacities yielded by both models are still comparable. The estimated capacity of scenario 5 obtained from the algorithms simulated in JAVA were greater than the capacity obtained from the VISSIM model by 124 veh/h/ln, or 5.4 percent. In addition, most of the datapoints in the congested flow of the speed-flow diagram obtained from the VISSIM model fall into the speed range of 40 – 55 km/h, with the corresponding throughput of 1,900 -2100 veh/h/ln, while there is still a considerable amount of datapoints scattered around the peak of the JAVA model's curve.

5.1.6 Scenario 6: 50% MDV and 50% CAV Mixed Traffic Scenario

The speed-flow diagrams of the downstream traffic in scenario 6 and scenario 5 simulated in JAVA appear to have similar shape. However, the range of the curve in scenario 6 slightly extends to higher throughputs compared to the previous scenario, while the overall speed of the datapoints in the uncongested flow region are slightly higher than the speed in the previous scenarios. The capacity of the mixed traffic in scenario 6 simulated in JAVA was estimated to be

2,445 veh/h/ln; which increased from the capacity in scenario 5 by 29 veh/h/ln, or 1.2 percent. The JAVA model's speed-flow diagrams in scenario 6 is presented in Figure 5-6.

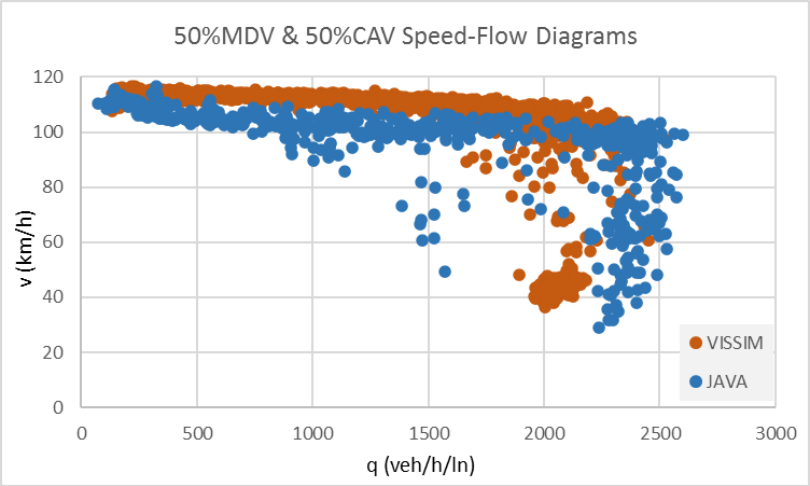

Figure 5-6 Speed-flow diagrams of the downstream traffic in scenario 6

The capacity of the scenario 6 simulated in VISSIM was estimated to be 2,362 veh/h/ln; which increased from the capacity in scenario 5 by 70 veh/h/ln, or 3.1 percent. Also, the overall speed in the uncongested flow region seems to be substantially higher than the overall speed of the same region in the previous scenario. The speed-flow diagram of the downstream traffic in scenario 6 generated by VISSIM is also presented in Figure 5-6.

The capacity in the JAVA model is greater than the capacity in the VISSIM model by 83 veh/h/ln, or 3.5 percent. In addition, the shape of the speed-flow curves obtained from both models appear to be similar in this scenario.

5.1.7 Scenario 7: 40% MDV and 60% CAV Mixed Traffic Scenario

Compared to scenario 6, the range of the downstream speed-flow curve obtained from JAVA simulation slightly extends to the higher throughputs. The angle of the JAVA model's speed-flow curve appears to be sharper than the speed-flow curve in scenario 6. The capacity of scenario 7 simulated in JAVA was estimated to be 2,461 veh/h/ln; which escalated from the capacity in scenario 6 by 16 veh/h/ln, or 0.7 percent. The JAVA model's speed-flow diagram in scenario 7 is illustrated in Figure 5-7.

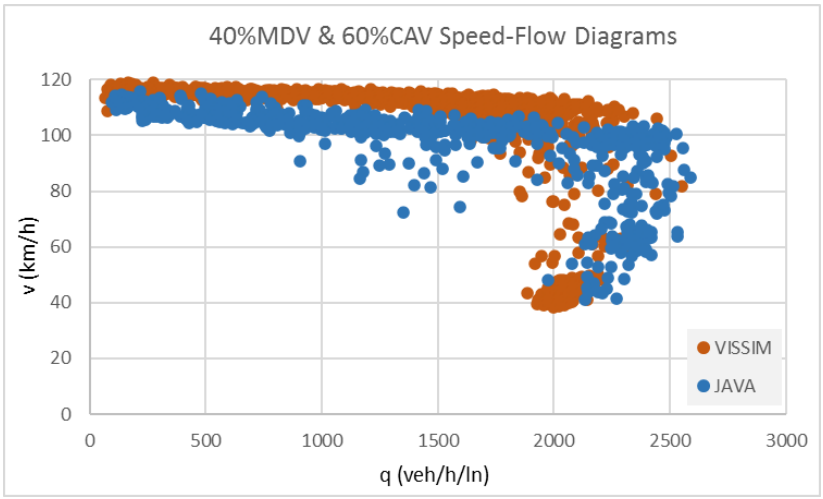

Figure 5-7 Speed-flow diagrams of the downstream traffic in scenario 7

Figure 5-7 also displays the speed-flow diagram in scenario 7 obtained from VISSIM. The shape of the curve appears to be similar to the curve in scenario 6. The capacity of scenario 7 in the VISSIM model was 2,405 veh/h/ln; which increased from the capacity in scenario 6 by 43 veh/h/ln, or 1.8 percent. Furthermore, the overall speed of the traffic in the uncongested flow region in this scenario seems to be slightly higher than the overall speed in the previous scenario.

The capacity and shape of the curves produced by VISSIM and JAVA models are very similar in this scenario. The estimated capacity of scenario 7 in JAVA was found to be greater than the capacity obtained from the VISSIM model by 56 veh/h/ln, or 2.3 percent.

5.1.8 Scenario 8: 30% MDV and 70% CAV Mixed Traffic Scenario

The speed-flow diagrams in scenario 8 and scenario 7 simulated in JAVA appear to show similar shape. Compared to scenario 7, the range of the speed-flow curve in this scenario slightly extends to higher throughputs. Obviously, the overall speed of the datapoints in the uncongested-flow region is slightly higher than the overall speed of the same region in scenario 7. The capacity of the mixed traffic in scenario 8 obtained from the JAVA model was estimated to be 2,490 veh/h/ln; an increase of 29 veh/h/ln, or 1.2 percent from scenario 7. The JAVA model's speed-flow diagram in scenario 8 is presented in Figure 5-8.

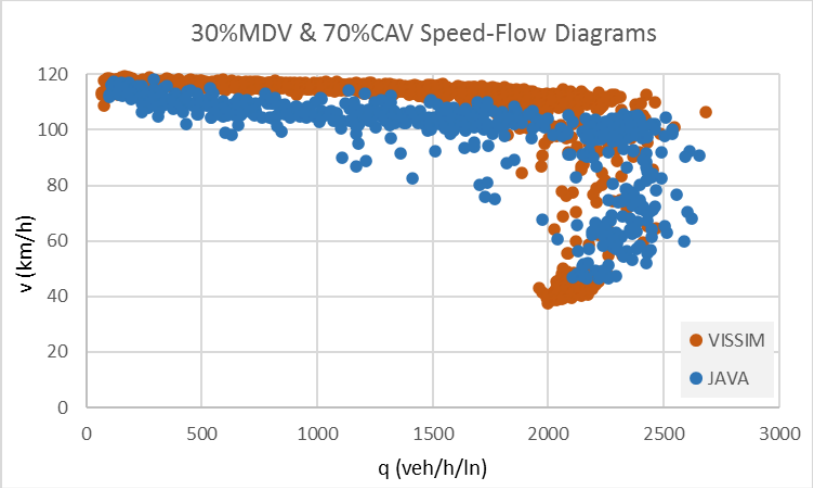

Figure 5-8 Speed-flow diagrams of the downstream traffic in scenario 8

The capacity of the scenario 8 in VISSIM was estimated to be 2,479 veh/h/ln; which was higher than the capacity in scenario 7 by 74 veh/h/ln, or 3.1 percent. The overall speed in the uncongested flow region appears to be slightly higher than the overall speed of the same region in the previous scenario. The speed-flow diagram in scenario 8 generated by VISSIM is presented in Figure 5-8.

The estimated capacity in JAVA was larger than the capacity obtained in VISSIM in this scenario by only 11 veh/h/ln, or 0.4 percent. The shapes of the speed-flow curves obtained from both models appear to be similar.

5.1.9 Scenario 9: 20% MDV and 80% CAV Mixed Traffic Scenario

Compared to scenario 8, the range of the downstream speed-flow diagram obtained from JAVA simulation slightly expands to higher throughputs, while the overall speed of the datapoints in the uncongested flow region is slightly higher than the speed in the previous scenarios. The slope of the JAVA's speed-flow curve of the downstream traffic in scenario 9 appears to be steeper than the angle of the speed-flow curve in scenario 8. The capacity of the mixed traffic scenario 9 simulated in JAVA was estimated to be 2,512 veh/h/ln; which escalated from the capacity in scenario 8 by 22 veh/h/ln, or 0.9 percent. The speed-flow diagram of the downstream traffic in scenario 9 simulated in JAVA is shown in Figure 5-9.

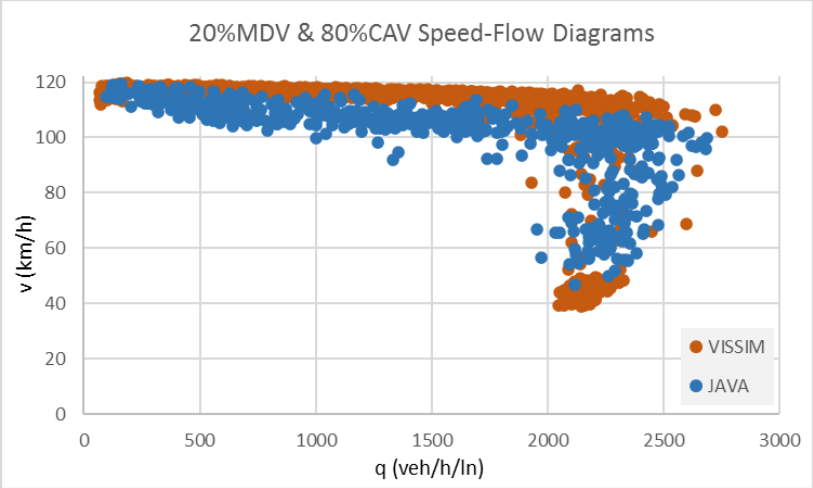

Figure 5-9 Speed-flow diagrams of the downstream traffic in scenario 9

Figure 5-9 also depicts the speed-flow diagram generated by the VISSIM model. The curve in this scenario appears to be similar to the curve in scenario 8; however, the curve in scenario 9 seems to contain fewer datapoints around the boundary between the uncongested and congested flows in the high-flow region compared to scenario 8. Also, the slope of the downstream curve in scenario 9 appears to be slightly flatter than the slope of the curve in the previous scenario. The capacity of scenario 9 in VISSIM was estimated to be 2,507 veh/h/ln; which increased from the capacity simulated in scenario 8 by 28 veh/h/ln, or 1.1 percent. Furthermore, the overall speed in the uncongested flow region in this scenario seems to be slightly higher than the overall speed in the previous scenario.

Similar to scenario 8, the capacity yielded by the JAVA model in scenario 9 was found to be greater than the capacity produced by the VISSIM model by only 5 veh/h/ln, or 0.2 percent. The shapes of the downstream speed-flow curves obtained from both models appear to be similar.

5.1.10 Scenario 10: 10% MDV and 90% CAV Mixed Traffic Scenario

The speed-flow diagrams in scenario 10 and scenario 9 simulated in JAVA show similar shapes. However, the speed in the uncongested-flow region is substantially higher than the speed in scenario 9. In addition, the range of the speed-flow curve in this scenario slightly expands to higher throughputs compared to scenario 9. Also, the slope of the JAVA's speed-flow in scenario 10 appears to be slightly steeper than the angle of the speed-flow curve in scenario 9. The capacity of scenario 10 in the JAVA model was 2,535 veh/h/ln; an increase of 23 veh/h/ln, or 0.9 percent

from scenario 9. The JAVA model's speed-flow diagram in scenario 10 is displayed in Figure 5-10.

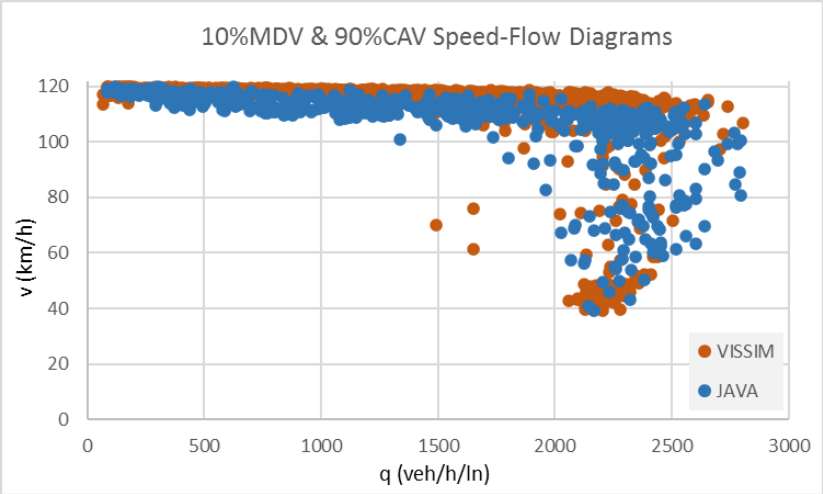

Figure 5-10 Speed-flow diagrams of the downstream traffic in scenario 10

The capacity of scenario 10 in VISSIM was 2,539 veh/h/ln; slightly higher than the capacity in scenario 9 by 32 veh/h/ln, or 1.3 percent. The shapes of the speed-flow diagrams in VISSIM in scenario 10 and scenario 9 appear to be almost identical. The speed during uncongested conditions in this scenario appears to be comparable to the speed in the previous scenario. The speed-flow diagram in scenario 10 generated by VISSIM is shown in Figure 5-10.

The estimated capacity difference between the VISSIM and the Java models is only 4 veh/h/ln, or 0.2 percent. The shapes of the speed-flow curves obtained from both models appear to be very similar. There are more datapoints scattered in the high-flow region at the speed range of 40 - 60 km/h in VISSIM than in JAVA, which implies that less traffic congestion occurred in the JAVA simulation than in the VISSIM simulation in scenario 10.

5.1.11 Scenario 11: 100% CAV Traffic Scenario

The shape of the speed-flow diagram obtained from the JAVA model appears to be different from the speed-flow diagram obtained from the same platform in scenario 10. The range of the speed-flow diagram in JAVA marginally expands to higher throughputs, while the speed during uncongested flows also increased from previous scenarios, with substantially less variations. This means that the traffic of 100% CAV could maintain the highest speed of 120 km/h with less chances of speed disruption, until the throughput of 2,500 veh/h/ln is reached. Also, the

slope of the JAVA's speed-flow curve in scenario 11 appears to be steeper than the slope of the speed-flow curve in scenario 10. The congested part of the speed-flow curve obtained from the JAVA model was substantially smaller than that of scenario 10, with the lowest speed of 85 km/h obtained. Therefore, substantially less congestion occurs in the 100% CAV traffic scenario compared to the previous mixed traffic scenarios. The capacity of the scenario 11 in JAVA was 2,683 veh/h/ln; an increase of 148 veh/h/ln, or 5.8 percent from scenario 10. The speed-flow diagram in scenario 11 simulated in JAVA is shown in Figure 5-11.

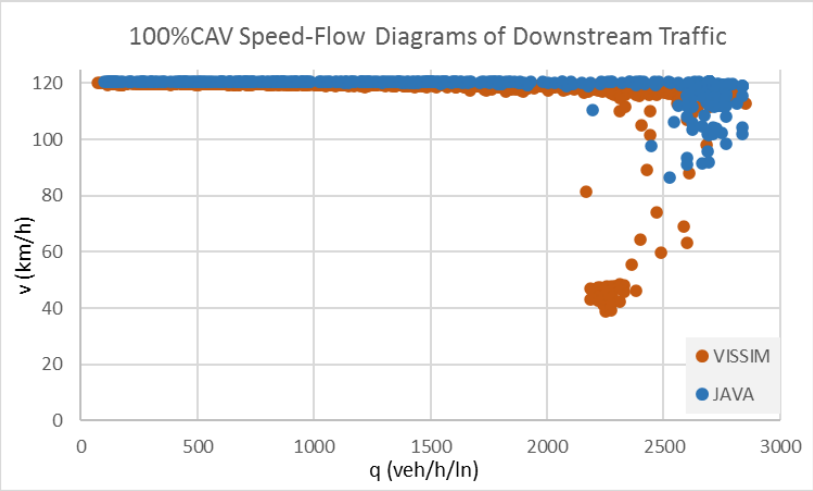

Figure 5-11 Speed-flow diagrams of the downstream traffic in scenario 11

Figure 5-11 also displays the speed-flow diagram generated by the VISSIM model. The shape of the curve in this scenario appears to be marginally different from the curve in scenario 10. The slope of the curve in scenario 11 is steeper than the slope of the curve in the previous scenario. In addition, the speed of the uncongested traffic in this scenario is slightly higher than the speed in the previous scenario. Furthermore, the speed variation was found to be less in this scenario compared to the mixed traffic scenarios. The capacity of scenario 11 in VISSIM was 2,630 veh/h/ln; which increased from the capacity of scenario 10 by 91 veh/h/ln, or 3.6 percent.

Capacity of scenario 11 in JAVA was greater than the VISSIM capacity by 53 veh/h/ln, or 2.0 percent. In contrast to the previous scenarios, the VISSIM model produced longer congestion associated with lower speeds, compared to the JAVA model. As such, there are some congested datapoints in the speed range of 40 - 50 km/h in VISSIM, while the lowest congested speeds in JAVA were around 85 km/h. Also, there are more datapoints scattered within the speed range of 85- 120 km/h in the JAVA model than in VISSIM model. As a result, it can be implied that less

traffic congestion occurred in the JAVA simulation than in the VISSIM simulation in the scenario of 100% CAV and also the queue discharge in JAVA was more efficient than in VISSIM.

5.2 Performance Measures Analysis

Capacity and travel time are the key performance measures that were used to evaluate the performance of the simulated traffic scenarios. The resultant roadway capacities with respect to the changes in CAV penetration rates in both JAVA and VISSIM simulation platforms were analyzed and compared to highlight the trend of the capacity as the proportion of CAVs. In addition, the average total travel time of vehicles in traffic was analyzed based on the variations in CAV penetration rates and demand volumes.

5.2.1 Capacity Analysis

The results showed that the capacity of the simulated traffic on the freeway segment increased with regard to the increase in the CAV penetration rate for both JAVA and VISSIM models, as presented in Figure 5-12.

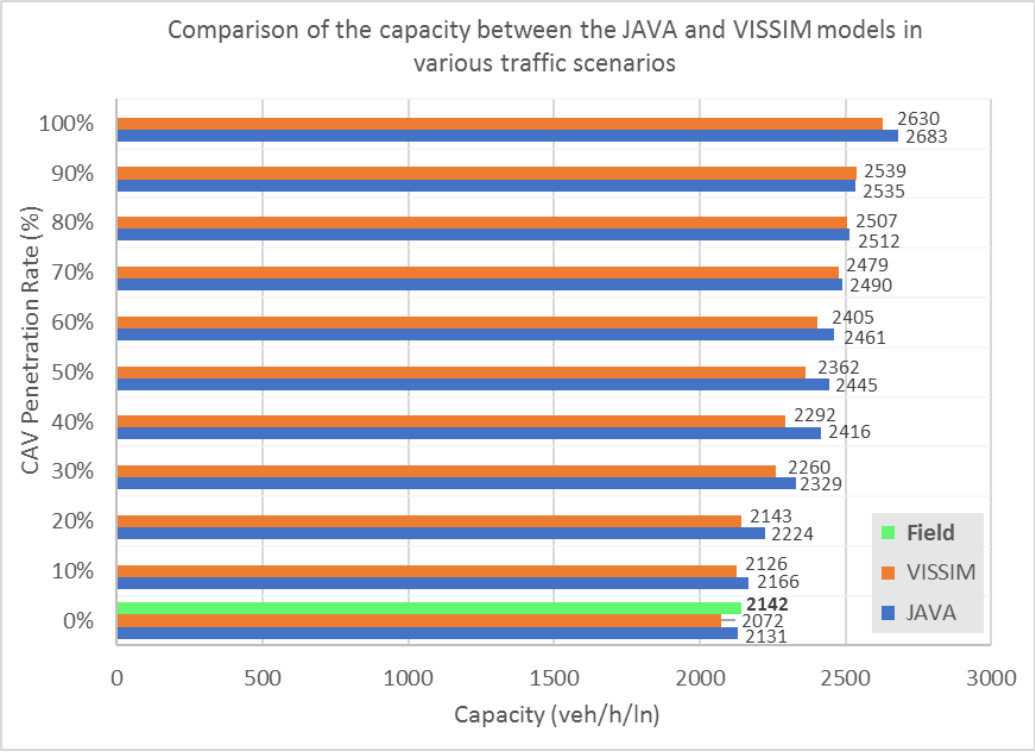

Figure 5-12 Comparison of the capacity between the JAVA and VISSIM models in various traffic scenarios

In conclusion, the results showed increase in capacities in the range of 25.9 – 26.9 percent in both models. According to the results obtained from the JAVA simulation, as the traffic shifted from 100-percent MDV to 100-percent CAV, the capacity increased by 552 veh/h/ln, or 25.9 percent. The VISSIM simulation also suggested the similar results that the capacity would increase by 558 veh/h/ln, or 26.9 percent, as the CAV penetration rate in traffic shifts from 0 to 100 percent (Table 5-1). The results also showed increase in capacities in the range of 14.0 – 14.7 percent in both models as the proportion of CAVs in traffic shifted from 0 percent to 50 percent.

Furthermore, the results also indicated that the capacities obtained from the JAVA and VISSIM models were not significantly different, except in scenarios 5 and 6, according to the two-tailed *t*-test assuming unequal variances at 95 percent confidence level (Table 5-1). The maximum difference between the capacities of these two models occurred in the mixed traffic scenario of 40% CAV, where the difference was 5.4 percent.

Table 5-1 Comparison of the capacity between the JAVA and VISSIM models based on various CAV penetration rates

Scenario	CAV Penetration Rate	Capacity (veh/h/ln)		Difference Between Models		Two-Tailed *t*-test at 95% Confidence Level				
		JAVA Model	VISSIM Model	Vehicles per hour per Lane	%	df	Critical *t*-value	*t* stat	p-value	Diff.
1	0%	2,131	2,072	59	2.8%	11	2.201	1.327	0.211	No
2	10%	2,166	2,126	40	1.9%	15	2.131	0.734	0.474	No
3	20%	2,224	2,143	81	3.8%	11	2.201	1.467	0.170	No
4	30%	2,329	2,260	69	3.1%	13	2.160	1.515	0.154	No
5	40%	2,416	2,292	124	5.4%	16	2.120	2.711	0.015	Sig
6	50%	2,445	2,362	83	3.5%	16	2.120	2.485	0.024	Sig
7	60%	2,461	2,405	56	2.3%	15	2.131	1.459	0.165	No
8	70%	2,490	2,479	11	0.4%	22	2.074	0.243	0.810	No
9	80%	2,512	2,507	5	0.2%	19	2.093	0.106	0.917	No
10	90%	2,535	2,539	-4	-0.2%	13	2.160	0.048	0.963	No
11	100%	2,683	2,630	53	2.0%	10	2.228	0.734	0.480	No

5.2.2 Travel Time Analysis

The JAVA analysis results showed that the average travel time of vehicles in traffic tends to decrease as the CAV penetration rate increases. The average travel time also increased with

respect to the increase in the demand volume. As the CAV penetration rate increases at the high demand volume, the average travel time tends to decrease relatively faster when the proportion of MDVs in traffic is relatively high; while it tends to reduce slower as the proportion of MDVs continues to decline. However, at the low demand volume, the average travel time tends to reduce relatively slower when the proportion of MDVs in traffic is relatively high; whereas it tends to reduce faster as the proportion of MDVs continues to decline. Six levels of demand volume, ranging between 100 veh/h/ln and 1,500 veh/h/ln, in each mixed traffic scenario were used to display the resultant average travel times and construct a 3D profile of the travel time based on the corresponding CAV penetration rate and demand, as illustrated in Figure 5-13.

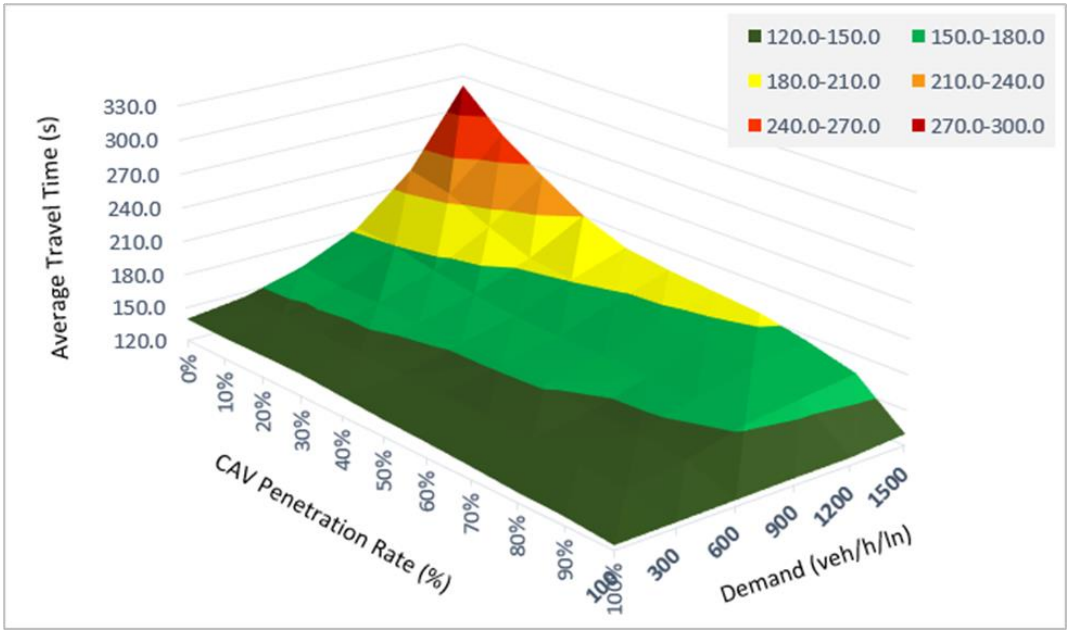

Figure 5-13 Average travel time of vehicles in JAVA with respect to the CAV penetration rate and demand volume

The average travel time appears to reach its peak when the proportion of CAVs in traffic is zero and the demand volume is high, whereas the average travel time reaches its lowest value as the CAV penetration rate reaches 100 percent with the lowest corresponding demand volume. According to the experiment, as the proportion of CAVs in traffic increased from 0 to 50 percent, the average travel time at the demand volume of 1,500 veh/h/ln declined from 291.2 seconds to 190.6 seconds, or reduced by 100.6 seconds; while the average speed for traversing the 4-km freeway segment increased from 49.4 km/h to 75.6 km/h. In addition, as the proportion of CAVs in traffic increased from 0 to 100 percent, the average travel time at the demand volume of 1,500

veh/h/ln decreased from 291.2 seconds to 129.9 seconds, or reduced by 161.3 seconds, and the average speed for traversing the whole 4-km distance increased from 49.4 km/h to 110.9 km/h. However, at the lowest demand volume of 100 veh/h/ln, as the proportion of CAVs in traffic increased from 0 to 100 percent, the average travel time decreased from 139.8 seconds to 124.0 seconds, or reduced by only 15.8 seconds; while the average speed for traversing the whole distance increased from 103.0 km/h to 116.1 km/h. The average travel time and average speed for traversing the 4-km freeway segment based on the variation in CAV penetration rate and demand volume are displayed in Tables 5-2 and 5-3, respectively.

Table 5-2 Average travel time of vehicles for traversing the 4-km freeway segment based on the variation in CAV penetration rate and demand volume

Demand (veh/h/ln)	Average Travel Time (s)										
	CAV Penetration Rate (%)										
	0%	10%	20%	30%	40%	50%	60%	70%	80%	90%	100%
100	139.8	138.9	139.4	139.6	137.2	134.7	133.1	131.1	128.6	127.5	124.0
300	146.0	145.6	143.5	143.9	140.5	140.0	139.6	137.3	135.6	131.9	124.6
600	159.6	156.3	157.5	154.0	152.2	152.2	151.6	145.2	144.4	139.7	125.3
900	182.1	179.8	172.5	166.3	162.3	160.7	160.6	158.7	157.2	152.5	126.0
1200	223.7	215.6	199.2	185.1	180.8	176.2	175.2	173.0	169.7	158.5	126.3
1500	291.2	258.0	233.3	210.6	195.9	190.6	187.2	183.8	175.4	164.2	129.9

Table 5-3 Average speed of vehicles for traversing the 4-km freeway segment based on the average travel time

Demand (veh/h/ln)	Average Speed based on Travel Time (km/h)										
	CAV Penetration Rate (%)										
	0%	10%	20%	30%	40%	50%	60%	70%	80%	90%	100%
100	103.0	103.7	103.3	103.2	104.9	106.9	108.2	109.9	112.0	113.0	116.1
300	98.6	98.9	100.4	100.1	102.5	102.8	103.1	104.9	106.2	109.1	115.6
600	90.2	92.1	91.4	93.5	94.6	94.6	95.0	99.2	99.7	103.1	114.9
900	79.1	80.1	83.5	86.6	88.7	89.6	89.6	90.7	91.6	94.4	114.3
1200	64.4	66.8	72.3	77.8	79.7	81.7	82.2	83.3	84.8	90.9	114.0
1500	49.4	55.8	61.7	68.4	73.5	75.6	76.9	78.3	82.1	87.7	110.9

Therefore, the effect of travel time reduction due to the increase in CAV penetration rate turned to be more substantial at the higher level of demand volume than at the lower level of demand, as shown in Table 5-4.

Table 5-4 Travel time reduction due to the increase in CAV penetration rate

Demand (veh/h/ln)	Travel Time Reduction (%)		
	CAV Proportion Increased from 0% to 50%	CAV Proportion Increased from 0% to 100%	CAV Proportion Increased from 50% to 100%
100	-3.6%	-11.3%	-7.9%
300	-4.1%	-14.7%	-11.1%
600	-4.7%	-21.5%	-17.7%
900	-11.8%	-30.8%	-21.6%
1200	-21.2%	-43.5%	-28.3%
1500	-34.6%	-55.4%	-31.8%

The results showed that at the demand volume of 1,500 veh/h/ln, the average travel time was decreased by 34.6 percent as the CAV penetration rate shifted from 0 to 50 percent, while the average travel time was decreased by 55.4 percent as the proportion of CAVs in traffic shifted from 0 to 100 percent. In addition, for the demand volumes between 100 and 1,200 veh/h/ln, the reduction in travel time appear to be more substantial when the proportion of CAVs increased from 50 to 100 percent rather than from 0 to 50 percent.

5.3 Trajectory Analysis

The vehicular trajectories of the vehicles in a platoon of 10 vehicles in three traffic scenarios: 100-percent MDV traffic, mixed traffic of 50-percent MDVs and 50-percent CAVs, and 100-percent CAV traffic, obtained from the JAVA model, were analyzed to evaluate the effects of CAVs in terms of microscopic traffic flow. All the vehicles were tested by accelerating from standstill to the maximum speed to perceive the vehicular trajectories and speed profiles.

The vehicular trajectories of the 100-percent MDV traffic, in which the vehicles are regulated by the FVD car-following model, were then extracted to observe the longitudinal position (x) versus time (t), as illustrated in Figure 5-14. The velocity profile of the vehicles in a platoon was also plotted to observe the velocities of the vehicles (v) over time (t) in traffic, as presented in Figure 5-15.

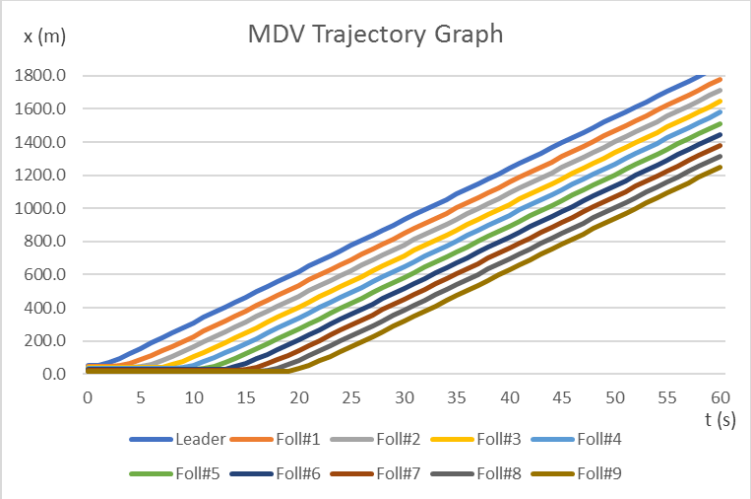

Figure 5-14 Tested vehicular trajectories of vehicles in the 100-percent MDV traffic scenario

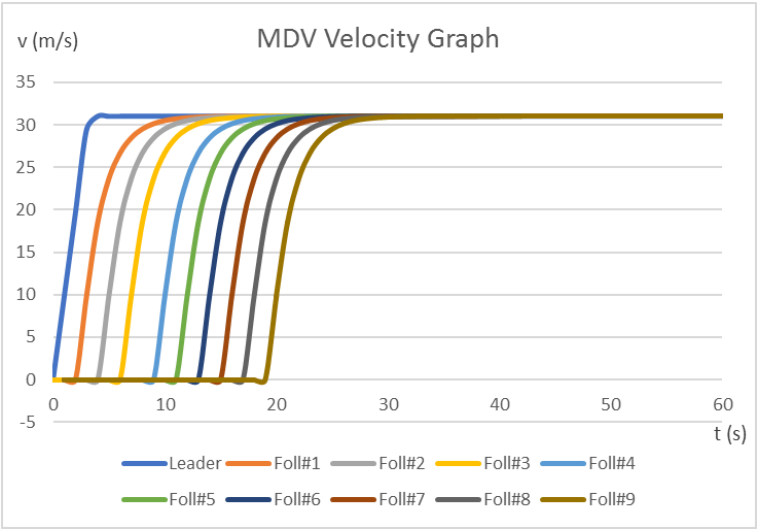

Figure 5-15 Velocity graph of vehicles in the 100-percent MDV traffic scenario

The vehicular trajectories of the 100-percent CAV traffic scenario were then plotted to observe the longitudinal position (x) versus time (t), as illustrated in Figure 5-16. Also, the velocity profile of the vehicles in a platoon was plotted versus time to observe the velocities of the vehicles (v) over time (t) in traffic, as presented in Figure 5-17.

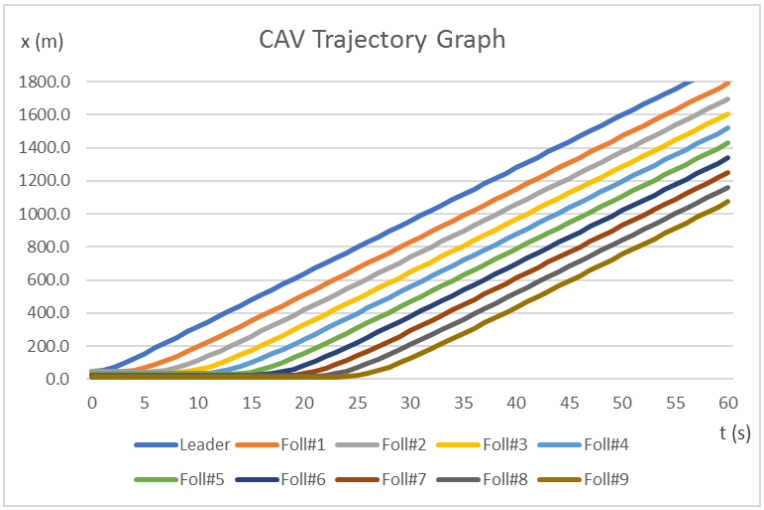

Figure 5-16 Tested vehicular trajectories of vehicles in the 100-percent CAV traffic scenario

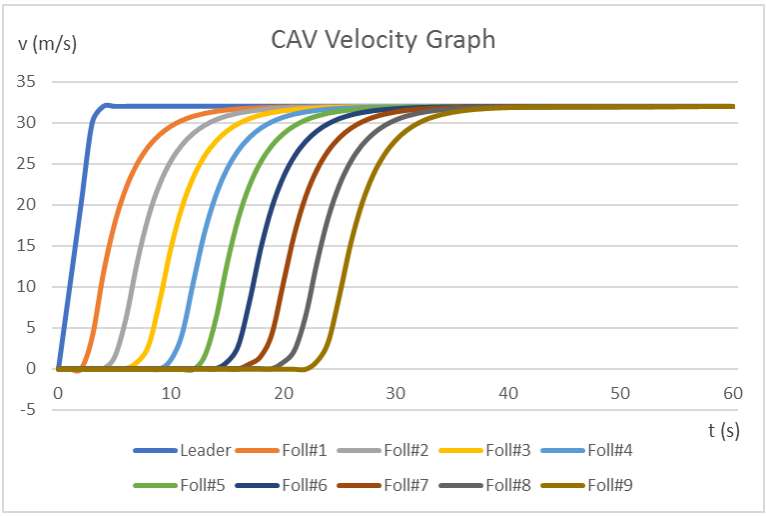

Figure 5-17 Velocity graph of the vehicles in the 100-percent CAV traffic scenario

According to the trajectory plots, the results show that the gaps between CAVs appear to be slightly larger than the gaps between MDVs. To be specific, at the speed of 115 km/h, the average gap between MDVs in the 100-percent MDV platoon turns to be 60 – 65 meters; whereas the average gap between CAVs in the 100-percent CAV platoon turns to be 85 – 90 meters. However, the gap between the leader and the first follower in the 100-percent CAV platoon was found to be greater than the gaps between the followers in the platoon themselves, which is 125 meters at the speed of 115 km/h. However, under congested conditions, the average gap between MDVs in the 100-percent MDV traffic turns to be in the range of 5 – 19 m at the speed of 0 – 40

km/h; while the average gap between CAVs in the 100-percent CAV traffic turns to be 31 – 49 m at the speed of 60 – 80 km/h.

The larger gap between CAVs compared to the gap between MDVs, together with the gap-creation capability of CAVs, allows for more convenient lane-changing maneuvers between CAVs in traffic. Therefore, this leads to smoother traffic flow at the bottleneck, which in turn causes less disruptions due to severe braking and produces increased throughput.

With regard to the velocity profile graphs, the results show that the driving behavior of the leaders in both 100-percent MDV and 100-percent CAV scenarios is indistinguishable. However, it was found that CAVs appear to have milder acceleration rates when behaving as a follower in a platoon, while the acceleration rates of MDVs in a platoon seem to be more severe. The milder acceleration rates conducted by CAVs are due to the omission of the velocity difference function in the CAV algorithm and the smaller value of κ; therefore, the space headway (s) is left as the decisive factor for determining the optimal velocity ($V(s)$) and acceleration rate for CAVs in each time step.

Next, the vehicular trajectories of the 50-percent CAV and 50-percent MDV mixed traffic scenario were also plotted to observe the longitudinal position (x) versus time (t), as illustrated in Figure 5-18. The velocity profile of the vehicles in a platoon was plotted versus time to observe the velocities of the vehicles (v) over time (t) in the mixed traffic, as shown in Figure 5-19.

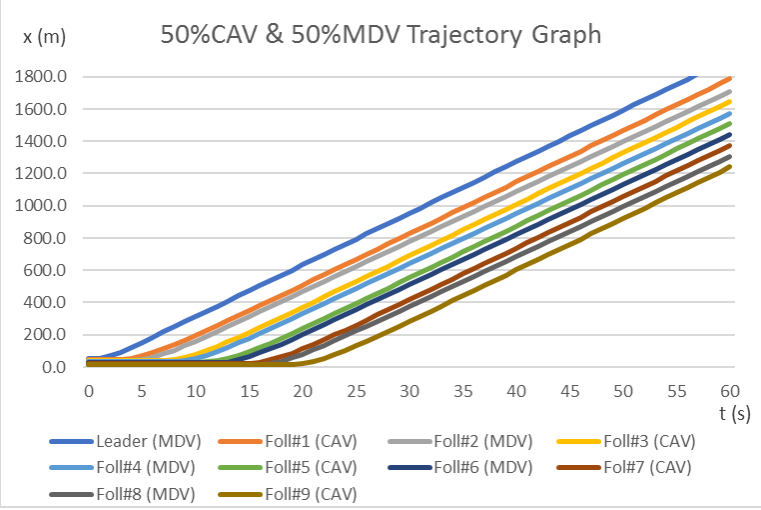

Figure 5-18 Tested vehicular trajectories of vehicles in the 50-percent CAV traffic scenario

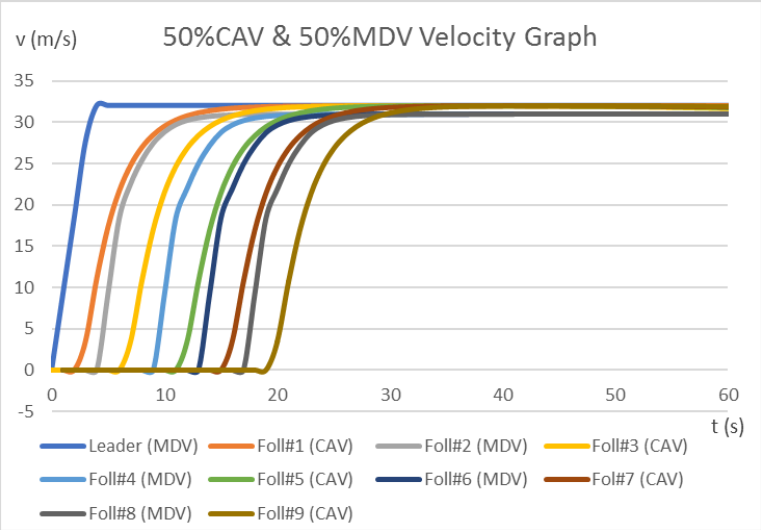

Figure 5-19 Velocity graph of the vehicles in the 50-percent CAV mixed traffic scenario

Based on the trajectory plot of vehicles in the 50-percent CAV mixed traffic scenario, the results show that CAVs still appear to follow their leaders with larger space than MDVs, as found in the scenarios of 100% MDV and 100% CAV traffic. Interestingly, it was found from the velocity profile graph in Figure 5-19 that the acceleration rates of MDVs were milder while following a CAV, compared to following an MDV, especially at higher speeds. In particular, the results indicate that CAVs appear to have an influence on guiding the speed and acceleration rates of MDVs to be smoother, while an MDV is following a CAV in a platoon.

In conclusion, the more cautious behavior of CAVs provided benefits for passengers in terms of safer distance between vehicles in both car-following and lane-changing maneuvers, as well as more comfort for passengers, besides the benefits in terms of throughput and travel time that CAVs offer for the roadway facility. On the other hand, the aggressive driving behavior of MDVs, compelled by the velocity difference function and the greater value of κ in the MDV algorithm, appears to create more adverse impacts on the roadway facility than the benefit in terms of speeding and maintaining closer gap between vehicles.

5.4 Gap Acceptance Comparison

A gap acceptance analysis was performed to compare the gaps accepted by MDVs and CAVs when performing mandatory lane changes at the vicinity of the lane drop by testing the simulation models of 100-percent MDV and 100-percent CAV traffic scenarios at the high-flow

demand volume of 1,500 veh/h/ln. The results obtained from the simulation models showed that the average lag gap accepted by MDVs was 16.4±9.1 m; whereas the average lag gap accepted by CAVs was 32.5±6.8 m, which was approximately twice as large as the average gap accepted by MDVs. In addition, the gap accepted by MDVs in the simulation model was found to range between 4.0 m and 38.3 m, while the gap accepted by CAVs ranged between 17.1 and 65.5 m. The size of the gap accepted by MDVs tends to be more variate, compared to the gap accepted by CAVs, due to the stochasticity of the gap acceptance model and the stochastic desired speed applied in the MDV lane-changing algorithm; while the minimum accepted gap for CAVs was set at 15 m in the CAV lane-changing algorithm for safety reason.

5.5 Summary of Results

This chapter presents the comprehensive analyses on the simulation results. The changes in highway capacity and travel time with respect to the variations in CAV penetration rate were analyzed and compared. The resultant vehicular trajectories were also analyzed to perceive the impact of CAVs on the trajectories and speeds of the interacting vehicles in traffic. Finally, the gap acceptance analysis was conducted to compare the gaps accepted by MDVs and CAVs. The conclusions, recommendations, study limitations, and future research are all presented in the next chapter.

CHAPTER 6 DISCUSSION AND CONCLUSIONS

6.1 Summary

CAVs are expected to be emerged and mixed with MDVs in traffic in the near future; however, the impact of various CAV penetration rates on the performance measures of the mixed traffic is still obscure. Although there are several studies conducted on simulating mixed traffic scenarios, the complex interactions between these types of vehicles in terms of car-following and lane changing has not been studied comprehensively. Also, most of the recent studies were found to merely focus on the longitudinal driving characteristics of CAVs, while the effects of automated lateral vehicular interactions were only taken into account by a few previous studies. In addition, no previous works were found to incorporate the longitudinal and lateral movement functions of vehicles in a traffic simulation model.

This dissertation addresses these limitations by developing realistic mixed traffic simulation models of CAVs and MDVs at the full-spectrum of mixed penetration rates on a freeway segment by integrating the car-following and lane-changing models together via a conditional linkage to investigate the sensitivities in highway capacity and travel time. The car-following models for CAVs and MDVs were modified from the FVD car-following model, while the lane-changing logic was adopted to regulate the lane-changing decisions for both CAVs and MDVs. The desired speeds of each MDVs were determined on the basis of stochasticity to represent various desired speeds taken by human drivers, while the uniform desired speed was employed for CAVs. The stochastic gap acceptance was applied for MDVs to replicate the stochasticity of the gaps accepted by human drivers, whereas the static gap acceptance was adopted to establish the safe decision-making thresholds for CAVs prior to performing lane changes. Two algorithms were proposed separately for governing the movements of CAVs and MDVs in the traffic simulation models. The proposed algorithms, along with a 3-to-2 virtual freeway segment, were coded in JAVA to create a simulation platform, prior to calibrating the default model with the field data. Eleven mixed traffic scenarios were simulated in the developed platform, along with the parallel simulation in VISSIM, to generate and validate the resultant speed-flow diagrams.

The results were then analyzed and compared to determine the changes in highway capacity and travel time with respect to the variations in CAV penetration rate. The resultant vehicular trajectories in the scenarios of interest were also analyzed to perceive the impact of CAVs on the trajectories and speeds of the interacting vehicles in traffic.

6.2 Conclusions

The analysis showed that the capacity of the simulated traffic on the freeway segment increased with respect to the increase in the CAV penetration rate for both models simulated in JAVA and VISSIM. The simulation results obtained from both models showed increase in capacities in the range of 25.9 – 26.9 percent as the traffic shifted from the traffic of 100-percent conventional vehicles to the traffic of 100-percent CAVs. The predicted capacity improvement in this dissertation is relatively conservative compared to increased capacity of 34 – 200 percent, as suggested in the literatures, due to the larger headway of CAVs applied for safety and passenger comfort reasons. The simulation results also showed increase in capacities in the range of 14.0 – 14.7 percent in both models as the proportion of CAVs in traffic shifted from 0 percent to 50 percent.

Lane change rates were adopted in the previous studies to randomly assign vehicles for making lane changes in simulation models. However, the proposed JAVA model applies the conditional linkage to determine the lane-changing demand of each vehicle based on its desired speed, the perceived average speed of the lanes, and the speed margin between the interacting vehicles. Besides, this linkage is not applied in VISSIM. In addition, the gap-creation model is attached in the JAVA model to enhance the lane-changing cooperation between CAVs; however, this feature is also not applicable for CAVs in VISSIM.

The analysis also indicated that the differences between the capacities obtained from the JAVA and VISSIM models in most of the simulated traffic scenario were not statistically significant; except in scenarios 5 and 6, in which the capacities in JAVA models were significantly greater than VISSIM models, according to the *t*-test.

The analysis also shows that the average travel time of vehicles in traffic tends to decrease with respect to the increase in CAV penetration rate, as well as the increase in the demand volume.

Also, the effect of travel time reduction due to the increase in CAV penetration rate turns to be more substantial at the higher level of demand volume than at the lower level of demand.

As the CAV penetration rate increments at the high demand volume, the average travel time tends to decrease at a relatively great rate when the proportion of MDVs in traffic is relatively high; while it tends to decrease at a relatively mild rate as the proportion of MDVs continues to decline. However, at a low demand volume, the average travel time tends to reduce relatively slower when the proportion of MDVs in traffic is relatively high, whereas it tends to reduce at a greater rate as the proportion of MDVs continues to decline.

The analysis showed that CAVs appear to have milder acceleration rates when behaving as followers in a platoon, while the acceleration rates of MDVs in a platoon seem to be greater. The milder acceleration rates conducted by CAVs was found to be caused by the smaller value of κ and the omission of the velocity difference function in the FVD car-following model; therefore, the space headway (s) is left as the decisive factor for determining the optimal velocity ($V(s)$) and acceleration rate for CAVs in each time step.

The larger gap between CAVs compared to the gap between MDVs, together with the gap-creation capability of CAVs, allows for more convenient lane-changing maneuvers between CAVs in traffic. This, therefore, leads to the smoother traffic flow at the bottleneck, which in turn causes less stream disruptions due to severe braking, and yields the higher level of throughput. The analysis also indicates that CAVs appear to have an influence on guiding the speed and acceleration rates of MDVs to be smoother while an MDV is following a CAV in a platoon.

The more cautious driving characteristics of CAVs were found to provide benefits for passengers in terms of safer distance between vehicles in both car-following and lane-changing maneuvers, as well as more comfort for passengers in motion, besides the benefits in terms of throughput and travel time that CAVs offer for the roadway facility. On the other hand, it can be implied that the more aggressive driving characteristic of MDVs, compelled by the greater value of κ and the velocity difference function in the MDV algorithm, appears to create more adverse impacts on the roadway facility than the benefit in terms of speeding and maintaining closer gap between vehicles.

The results obtained from the simulation models showed that the average lag gap accepted by MDVs was 16.4±9.1 m; whereas the average lag gap accepted by CAVs was 32.5±6.8 m, which was approximately twice as large as the average gap accepted by MDVs.

Consequently, this study suggests that minimizing headway does not maximize capacity at a lane drop since the small gaps can create adverse impacts on lane-changing maneuvers of the vehicles in the dropping lane. As a result, there should be an optimal headway that maximizes the capacity at a lane drop.

6.3 Recommendations

The developed simulation model can be applied to estimate the capacity and travel time of the mixed traffic scenarios on freeways by taking into account the impact of both car-following and lane-changing behavior of vehicles. Ultimately, the integrated car-following and lane-changing model via the conditional linkage, considering the speed difference and displacement margin between the interacting vehicles in traffic, can be applied as a basis to improve the traffic simulation models in the future.

The study suggests that the emerging CAV technology should consider maintaining a sizeable gap between vehicles in a platoon and attaching the gap creation capability in the algorithm for the purposes of providing convenient lane-changing maneuvers in traffic and assuring safe braking distance between vehicles.

In addition, the aggressive speeding characteristic should not be adopted for governing the movements of the emerging CAVs since such characteristic could cause instability in traffic streams and make lane-changing maneuvers more difficult; which eventually leads to the reduction in the overall capacity of the traffic flow, as well as worsens the passenger comfort. Consequently, the study suggests that the CAV algorithm had better enable the fairly mild acceleration and deceleration rates to maintain smooth flow; which can increase stability of the traffic flow and make room for increasing the capacity of the roadway facility, as well as providing safety and comfort benefits for passengers.

6.4 Study Limitations

First of all, limited aspects of the geometric design of the traffic facility are taken into account in the simulation. The study assumed a 3-to-2 tangent freeway segment with 0% grade as a test network, where the lane width of 3.66 m (12 ft) was assigned. However, the effects of the lateral clearance, grade, and degree of curvature of the freeway segment, as well as the weather conditions, were neglected in this study due to the limitation of the models used.

In addition, since the FVD model was adopted as a basis for developing the proposed CAV and MDV algorithms, the time step of one second was automatically applied in the JAVA model, as limited by the FVD model. On the other hand, the default time step for simulating the traffic scenarios in VISSIM is 0.1 second, which can determine the movements of the vehicles in simulation more precisely.

Also, the acceleration rate determined by the proposed model is uniform throughout the vehicles in traffic for a specific situation at lower speeds, and it only varies with the desired speed of each vehicle at higher speeds. However, in real life, the acceleration rate is more randomized based on the variations in type of automobile, engine capacity, engine power, perception-reaction time, and driving behavior.

The present study does not account for the impact of vehicle automation on driver reaction time, or the effect of activation/deactivation of the automated features, but rather, it assumes that CAVs drive in high automation modes (level 4-5) and driver interventions are not needed.

6.5 Future Research

Several research extensions can be attempted to improve the presented work. Firstly, the proposed JAVA model can be improved by converting and modifying all the equations used in the current model to be based on the time step of 0.1 second to improve the precision of the model. Secondly, the broader range of the freeway configurations can be added to increase the capability of the model in simulating traffic on various types of freeway facilities; therefore, the following elements can be added to the current simulation platform: on-ramp, off-ramp, and customizable number of lanes. Thirdly, additional aspects of the roadway geometry that affect the movements of vehicles can be quantified and included in the future work; such as lateral clearance, grade, and degree of curvature of the roadway facilities. Various acceleration characteristics which represent

variations in type of vehicle, engine capacity, engine power, perception-reaction time, and driving behaviors can be taken into account to increase the level of stochasticity of the model. Lastly, the developed algorithms could improve by introducing varying levels of automation and by considering other combinations of connectivity and automation, such as CVs and AVs in the vehicle mix.

Bibliography

Ahmed, K. I. (1999). Modeling drivers' acceleration and lane changing behavior. Doctoral dissertation. Massachusetts Institute of Technology, USA.

Asplund, M., Manzoor, A., Bouroche, M., Clarke, S., & Cahill, V. (2012). A formal approach to autonomous vehicle coordination. International Symposium on Formal Methods (pp. 52-67). Springer, Berlin, Heidelberg.

Bando, M., Hasebe, K., Nakayama, A., Shibata, A., & Sugiyama, Y. (1995). Dynamical model of traffic congestion and numerical simulation. Physical Review E, 51(2), 1035.

Bando, M., Hasebe, K., Nakanishi, K., & Nakayama, A. (1998). Analysis of optimal velocity model with explicit delay. Physical Review E, 58(5), 5429.

Behrisch, M., Bieker, L., Erdmann, J., & Krajzewicz, D. (2011). SUMO–simulation of urban mobility: an overview. The Third International Conference on Advances in System Simulation.

Bekiaris-Liberis, N., Roncoli, C., & Papageorgiou, M. (2016). Highway traffic state estimation with mixed connected and conventional vehicles. IEEE Transactions on Intelligent Transportation Systems, 17(12), 3484-3497.

Ben-Akiva, M. E., Choudhury, C., & Toledo, T. (2006). Lane changing models. Proceedings of the International Symposium of Transport Simulation.

Bierstedt, J., Gooze, A., Gray, C., Peterman, J., Raykin, L., & Walters, J. (2014). Effects of next-generation vehicles on travel demand and highway capacity. FP Think Working Group, 10-11.

Bose, A. & Ioannou, P. (2003). Mixed manual/semi-automated traffic: a macroscopic analysis. Transportation Research Part C: Emerging Technologies, 11(6), 439-462.

Brackstone, M. & McDonald, M. (1999). Car-following: a historical review. Transportation Research Part F: Traffic Psychology and Behaviour, 2(4), 181-196.

Brilon, W., Geistefeldt, J., & Regler, M. (2005). Reliability of freeway traffic flow: a stochastic concept of capacity. Proceedings of the 16th International Symposium on Transportation and Traffic Theory, Vol. 125143, College Park Maryland.

Chandler, R. E., Herman, R., & Montroll, E. W. (1958). Traffic dynamics: studies in car following. Operations Research, 6(2), (pp. 165-184).

Chen, D., Ahn, S., Chitturi, M., & Noyce, D. A. (2017). Towards vehicle automation: Roadway capacity formulation for traffic mixed with regular and automated vehicles. Transportation Research Part B: Methodological, 100, (pp. 196-221).

Devore, J. (2019). "Making it happen: A pilot test on SB I-35W in Minneapolis puts connected vehicles out front"; at https://www.roadsbridges.com/making-it-happen

Dimitrakopoulos, G. (2011). Intelligent transportation systems based on internet-connected vehicles: Fundamental research areas and challenges. 11th IEEE International Conference on ITS Telecommunications (ITST), 2011 (pp. 145-151).

Fan, W. & Liu, P. (2019). Impact of connected and automated vehicles on freeway capacity.

Fernandes, P., & Nunes, U. (2010). Platooning of autonomous vehicles with intervehicle communications in SUMO traffic simulator. Intelligent Transportation Systems (ITSC), 2010, 13th International IEEE Conference (pp. 1313-1318).

FHWA (2008). The Next Generation Simulation (NGSIM); at https://ops.fhwa.dot.gov/trafficanalysistools/ngsim.htm

Fiosins, M., Fiosina, J., Müller, J. P., & Görmer, J. (2011). Agent-based integrated decision making for autonomous vehicles in urban traffic. Advances on Practical Applications of Agents and Multi-Agent Systems (pp. 173-178).

Fountoulakis, M., Bekiaris-Liberis, N., Roncoli, C., Papamichail, I., & Papageorgiou, M. (2017). Highway traffic state estimation with mixed connected and conventional vehicles: Microscopic simulation-based testing. Transportation Research Part C: Emerging Technologies, 78, 13-33.

Ghiasi, A., Hussain, O., Qian, Z. S., & Li, X. (2017). A mixed traffic capacity analysis and lane management model for connected automated vehicles: A Markov chain method. Transportation Research Part B: Methodological, 106, 266-292.

Gipps, P. G. (1981). A behavioural car-following model for computer simulation. Transportation Research Part B: Methodological, 15(2), 105-111.

Gong, S., Shen, J., & Du, L. (2016). Constrained optimization and distributed computation based car following control of a connected and autonomous vehicle platoon. Transportation Research Part B: Methodological, 94, 314-334.

Gurupackiam, S., & Jones Jr, S. L. (2012). Empirical study of accepted gap and lane change duration within arterial traffic under recurrent and non-recurrent congestion. International Journal for Traffic & Transport Engineering, 2(4): 306 – 322.

Hill, C., Elefteriadou, L., & Kondyli, A. (2015). Exploratory analysis of lane changing on freeways based on driver behavior. Journal of Transportation Engineering 141.4 (2014): 04014090.

Helbing, D., & Tilch, B. (1998). Generalized force model of traffic dynamics. Physical Review E, 58(1), 133.

Herman, R. (1961). Theory of traffic flow; proceedings of the Symposium on the Theory of Traffic Flow, held at the General Motors Research Laboratories, Warren, Michigan, 1959. International Symposium on the Theory of Traffic Flow, 1st, 1959, Warren, Michigan, USA.

Highway Capacity Manual (2010). Transportation Research Board.

Hollander, Y., & Liu, R. (2008). The Principles of Calibrating Traffic Microsimulation Models. Transportation, 35(3), 347-362.

Hoogendoorn, R., van Arem, B., & Hoogendoorn, S. (2014). Automated driving, traffic flow efficiency, and human factors: Literature review. Transportation Research Record: Journal of the Transportation Research Board, (2422), 113-120.

Hwang, S. Y., & Park, C. H. (2005). Modeling of the gap acceptance behavior at a merging section of urban freeway. In Proceedings of the Eastern Asia Society for Transportation Studies (Vol. 5, No. 1641, p. e1656). Tokyo: Eastern Asia Society for Transportation (EASTS).

Ioannou, P. A., & Stefanovic, M. (2005). Evaluation of ACC vehicles in mixed traffic: Lane change effects and sensitivity analysis. IEEE Transactions on Intelligent Transportation Systems, 6(1), 79-89.

Jiang, R., Wu, Q., & Zhu, Z. (2001). Full velocity difference model for a car-following theory. Physical Review E, 64(1), 017101.

Knorr, F., & Schreckenberg, M. (2012). Influence of inter-vehicle communication on peak hour traffic flow. Physica A: Statistical Mechanics and its Applications, 391(6), 2225-2231.

Kondyli, A., & Elefteriadou, L. (2011). Modeling driver behavior at freeway-ramp merges. Transportation Research Record: Journal of the Transportation Research Board, (2249), 29-37.

Le Vine, S., Zolfaghari, A., & Polak, J. (2015). Autonomous cars: The tension between occupant experience and intersection capacity. Transportation Research Part C: Emerging Technologies, 52, 1-14.

Lee, G. (2006). Modeling gap acceptance at freeway merges. MS Thesis. Massachusetts Institute of Technology, USA.

Lefèvre, S., Carvalho, A., & Borrelli, F. (2015). Autonomous car following: A learning-based approach. Intelligent Vehicles Symposium (IV), 2015. pp. 920-926.

Levin, M. W., & Boyles, S. D. (2016). A multiclass cell transmission model for shared human and autonomous vehicle roads. Transportation Research Part C: Emerging Technologies, 62, 103-116.

Letter, C., & Elefteriadou, L. (2017). Efficient control of fully automated connected vehicles at freeway merge segments. Transportation Research Part C: Emerging Technologies, 80, 190-205.

Li, S. E., Deng, K., Zheng, Y., & Peng, H. (2015). Effect of pulse-and-glide strategy on traffic flow for a platoon of mixed automated and manually driven vehicles. Computer-Aided Civil and Infrastructure Engineering, 30(11), 892-905.

Li, Y., Zhang, L., Peeta, S., He, X., Zheng, T., & Li, Y. (2016). A car-following model considering the effect of electronic throttle opening angle under connected environment. Nonlinear Dynamics, 85(4), 2115-2125.

Li, Z., Chitturi, M., Zheng, D., Bill, A., & Noyce, D. (2013). Modeling reservation-based autonomous intersection control in VISSIM. Transportation Research Record: Journal of the Transportation Research Board, (2381), 81-90.

Litman, T. (2018). Autonomous vehicle implementation predictions. Victoria Transport Policy Institute.

Luettel, T., Himmelsbach, M., & Wuensche, H. J. (2012). Autonomous ground vehicles—Concepts and a path to the future. Proceedings of the IEEE, 100 (Special Centennial Issue), 1831-1839.

Lv, W., Song, W. G., Liu, X. D., & Ma, J. (2013). A microscopic lane changing process model for multilane traffic. Physica A: Statistical Mechanics and its Applications, 392(5), 1142-1152.

Markus, F., Brantley, B., & Lutz, C. (2017). "A Closer Look at the 2017 Tesla Model S P100D's Ludicrous Acceleration Run"; at https://www.motortrend.com/news/a-closer-look-at-the-2017-tesla-model-s-p100d-ludicrous-acceleration-run/

Michael, J. B., Godbole, D. N., Lygeros, J., & Sengupta, R. (1998). Capacity analysis of traffic flow over a single-lane automated highway system. Journal of Intelligent Transportation System, 4(1-2), 49-80.

Milanés, V., Godoy, J., Villagrá, J., & Pérez, J. (2011). Automated on-ramp merging system for congested traffic situations. IEEE Transactions on Intelligent Transportation Systems, 12(2), 500-508.

Morgan, A., Cesme, B., & Schroeder, B. (2019). "How connected & automated vehicles may change freeway capacities". Kittelson & Associates; at https://www.kittelson.com/ideas/how-connected-automated-vehicles-may-change-freeway-capacities/

Murphy, J. T., & Smoot, R. C. (1982). Physics: Principles and problems. Charles E. Merrill.

National Conference of State Legislature (2019). Autonomous vehicles. Self-driving vehicles enacted legislation; at http://www.ncsl.org/research/transportation/autonomous-vehicles-self-driving-vehicles-enacted-legislation.aspx.

Naumann, R., Rasche, R., & Tacken, J. (1998). Managing autonomous vehicles at intersections. IEEE Intelligent Systems and Their Applications, 13(3), 82-86.

Olia, A., Razavi, S., Abdulhai, B., & Abdelgawad, H. (2018). Traffic capacity implications of automated vehicles mixed with regular vehicles. Journal of Intelligent Transportation Systems, 22(3), 244-262.

Patel, R. H., Harri, J., & Bonnet, C. (2017). Impact of localization errors on automated vehicle control strategies. IEEE Vehicular Networking Conference (VNC). Torino, Italy.

PTV (2016). PTV VISSIM & Connected autonomous vehicles. Karlsruhe, Germany.

PTV (2018). PTV VISSIM Driver model DLL interface documentation. Karlsruhe, Germany.

Qu, X., Zhen, L., Howlett, R. J., & Jain, L. C. (2019). Smart Transportation Systems 2019 (Vol. 149). Springer.

Ramezani, M., Machado, J. A., Skabardonis, A., & Geroliminis, N. (2017). Capacity and delay analysis of arterials with mixed autonomous and human-driven vehicles. 5th IEEE International Conference on Models and Technologies for Intelligent Transportation Systems (MT-ITS), 2017 (pp. 280-284).

Rios-Torres, J., & Malikopoulos, A. A. (2017). Automated and cooperative vehicle merging at highway on-ramps. IEEE Transactions on Intelligent Transportation Systems, 18(4), 780-789.

Roess, R. P., Prassas, E. S., & McShane, W. R. (2011). Traffic engineering – Fourth Edition. Pearson/Prentice Hall.

Rohatgi, A. (2019). WebPlotDigitizer Version 4.2; at https://automeris.io/WebPlotDigitizer/.

SAE (2014), Levels of driving automation are defined in new SAE international standard J3016, Society of Automotive Engineers (www.sae.org); at www.sae.org/misc/pdfs/automated_driving.pdf.

Schubert, R., Schulze, K., & Wanielik, G. (2010). Situation assessment for automatic lane-change maneuvers. IEEE Transactions on Intelligent Transportation Systems, 11(3), 607-616.

Shi, L., & Prevedouros, P. (2016). Autonomous and connected cars: HCM estimates for freeways with various market penetration rates. Transportation Research Procedia, 15, 389-402.

Shi, L., & Prevedouros, P. D. (2017). Operational analysis of a single-lane roundabout with a mix of driverless vehicles. Transportation Research Record: Journal of the Transportation Research Board, (2615), 123-131.

Songchitruksa, P., Bibeka, A., Lin, L. I., & Zhang, Y. (2016). Incorporating driver behaviors into connected and automated vehicle simulation (No. ATLAS-2016-13). Center for Advancing Transportation Leadership and Safety (ATLAS Center).

Sun, D. J., & Elefteriadou, L. (2010). Research and implementation of lane-changing model based on driver behavior. Transportation Research Record: Journal of the Transportation Research Board, (2161), 1-10.

Sun, D. J., & Kondyli, A. (2010). Modeling vehicle interactions during lane-changing behavior on arterial streets. Computer-Aided Civil and Infrastructure Engineering, 25(8), 557-571.

Talebpour, A., Mahmassani, H. S., & Hamdar, S. H. (2015). Modeling lane-changing behavior in a connected environment: A game theory approach. Transportation Research Part C: Emerging Technologies, 59, 216-232.

Talebpour, A. & Mahmassani, H.S. (2016), Influence of connected and autonomous vehicles on traffic flow stability and throughput, Transportation Research Part C: Emerging Technologies, 71, pp.143-163.

Tang, T., Shi, W., Shang, H., & Wang, Y. (2014a). A new car-following model with consideration of inter-vehicle communication. Nonlinear Dynamics, 76(4), 2017-2023.

Tang, T., Shi, W. F., Shang, H. Y., & Wang, Y. P. (2014b). An extended car-following model with consideration of the reliability of inter-vehicle communication. Measurement, 58, 286-293.

Tientrakool, P., Ho, Y. C., & Maxemchuk, N. F. (2011). Highway capacity benefits from using vehicle-to-vehicle communication and sensors for collision avoidance. IEEE Vehicular Technology Conference (VTC Fall), 2011. (pp. 1-5).

Treiber, M., Hennecke, A., & Helbing, D. (1999). Derivation, properties, and simulation of a gas-kinetic-based, nonlocal traffic model. Physical Review E, 59(1), 239.

UK Department for Transport (2016), Research on the impacts of connected and autonomous vehicles (CAVs) on traffic flow, Summary Report, Department for Transport, UK.

USDOT (2019), Automated Vehicle Research; at https://www.its.dot.gov/automated_vehicle/index.htm.

Wang, J., Ni, D., & Li, K. (2014). RFID-based vehicle positioning and its applications in connected vehicles. Sensors, 14(3), 4225-4238.

Wang, M., Hoogendoorn, S. P., Daamen, W., van Arem, B., & Happee, R. (2015). Game theoretic approach for predictive lane-changing and car-following control. Transportation Research Part C: Emerging Technologies, 58, 73-92.

Wang, M., Daamen, W., Hoogendoorn, S. P., & Van Arem, B. (2016). Connected variable speed limits control and car-following control with vehicle-infrastructure communication to resolve stop-and-go waves. Journal of Intelligent Transportation Systems, 20(6), 559-572.

Wang, M., Daamen, W., Hoogendoorn, S. P., & van Arem, B. (2016). Cooperative car-following control: Distributed algorithm and impact on moving jam features. IEEE Transactions on Intelligent Transportation Systems, 17(5), 1459-1471.

Winston, W. L., & Goldberg, J. B. (2004). Operations research: applications and algorithms (Vol. 3). Belmont, CA: Thomson/Brooks/Cole.

Wojdyla, B. (2011). "7 Cars That Could Win a Drag Race Against Gravity"; at https://www.popularmechanics.com/cars/g560/7-cars-that-could-win-a-drag-race-against-gravity/?slide=6

Xie, Y., Zhang, H., Gartner, N., & Arsava, T. (2014). Collaborative merging behaviors and their impacts on freeway ramp operations under connected vehicle environment. Symposium Celebrating 50 Years of Traffic Flow Theory, 392.

You, F., Zhang, R., Lie, G., Wang, H., Wen, H., & Xu, J. (2015). Trajectory planning and tracking control for autonomous lane change maneuver based on the cooperative vehicle infrastructure system. Expert Systems with Applications, 42(14), 5932-5946.

Yu, Y., Jiang, R., & Qu, X. (2019). A modified full velocity difference model with acceleration and deceleration confinement: calibrations, validations, and scenario analyses. IEEE Intelligent Transportation Systems Magazine.

Zhang, Y. J., Malikopoulos, A. A., & Cassandras, C. G. (2016). Optimal control and coordination of connected and automated vehicles at urban traffic intersections. IEEE American Control Conference (ACC), 2016 (pp. 6227-6232).

Zhao, L., & Sun, J. (2013). Simulation framework for vehicle platooning and car-following behaviors under connected-vehicle environment. Procedia-Social and Behavioral Sciences, 96, 914-924.